



**HAL**  
open science

# Identification of a novel domain within the CIL regulates egress of IFITM3 from the Golgi and prevents its deleterious accumulation in this apparatus

Li Zhong

## ► To cite this version:

Li Zhong. Identification of a novel domain within the CIL regulates egress of IFITM3 from the Golgi and prevents its deleterious accumulation in this apparatus. Biochemistry, Molecular Biology. Université de Lyon, 2021. English. NNT : 2021LYSEN056 . tel-03881726

**HAL Id: tel-03881726**

**<https://theses.hal.science/tel-03881726v1>**

Submitted on 2 Dec 2022

**HAL** is a multi-disciplinary open access archive for the deposit and dissemination of scientific research documents, whether they are published or not. The documents may come from teaching and research institutions in France or abroad, or from public or private research centers.

L'archive ouverte pluridisciplinaire **HAL**, est destinée au dépôt et à la diffusion de documents scientifiques de niveau recherche, publiés ou non, émanant des établissements d'enseignement et de recherche français ou étrangers, des laboratoires publics ou privés.



Numéro National de Thèse : 2021LYSEN056

## **THESE DE DOCTORAT DE L'UNIVERSITE DE LYON**

opérée par

**l'Ecole Normale Supérieure de Lyon**

**Ecole Doctorale N° 340**

**Biologie Moléculaire, Intégrative et Cellulaire (BMIC)**

**Discipline : Sciences de la vie et de la santé**

Soutenue publiquement le 30/09/2021, par :

**Li ZHONG**

---

**Identification of a novel domain within the CIL regulates egress of IFITM3 from the Golgi and prevents its deleterious accumulation in this apparatus**

Identification d'un nouveau domaine régulant la sortie d'IFITM3 du Golgi et empêchant son accumulation délétère dans cet appareil

---

Devant le jury composé de :

Dr Katy JANVIER

CR CNRS Institut Cochin

Rapporteure

Dr Stéphanie MISEREY-LENKEI

DR CNRS Institut Curie

Rapporteure

Dr Delphine MURIAUX

DR CNRS IRIM

Examinatrice

Dr Andrea CIMARELLI

DR CNRS ENS de Lyon

Directeur de Thèse



## **Abstract**

The InterFeron-Induced TransMembrane proteins (IFITMs) are broad viral inhibitors that protect cells by preventing viral-to-cellular membrane fusion and they belong to the dispanin/CD225 family that includes vesicle trafficking regulators and proteins of unknown functions into four subfamilies (A-D). In this study, we uncover a novel domain that regulates the egress of IFITM3 from the Golgi and that is required to prevent IFITM3-driven v- to t-SNAREs membrane fusion inhibition and Golgi dysfunctions.

The Golgi egress domain is conserved among vertebrate members of the dispanin/CD225 A subfamily that regroups all IFITMs and through the study of mutations identified in patients affected by paroxysmal kinesigenic dyskinesia (PKD), we determine that it is functionally conserved also in PRRT2, member of the B subfamily.

Overall, our study defines a novel domain that regulates the egress of dispanin/CD225 members from the Golgi and stresses the importance that regulation of this process bears to preserve the functions of this apparatus.

**Key words:** IFITM3, Interferon, HIV, Golgi, Traccking, PRRT2

## Résumé

Les protéines transmembranaires induites par l'interféron (IFITM) sont une famille de protéines antivirales capables d'inhiber la réplication de nombreux virus en empêchant la fusion des membranes virales et cellulaires. Plus largement, les IFITM appartiennent à la plus grande famille des dispanines/CD225 qui comprend des régulateurs de trafic vésiculaire ainsi que des protéines dont les fonctions demeurent inconnues. Dans cette étude, nous avons identifié un nouveau domaine qui régule la sortie d'IFITM3 du Golgi et qui est nécessaire pour prévenir l'inhibition de la fusion membranaire v- à t-SNAREs induite par IFITM3 et les dysfonctionnements de l'appareil de Golgi.

Le domaine de sortie de Golgi est conservé chez les vertébrés membres de la sous-famille dispanine/CD225 A qui regroupe tous les IFITM et grâce à l'étude des mutations identifiées chez les patients atteints de dyskinésie kinésigénique paroxystique (PKD), nous montrons qu'il est fonctionnellement conservé également dans PRRT2, membre de la sous-famille B.

Dans son ensemble, notre étude définit un nouveau domaine qui régule la sortie des membres de la dispanine/CD225 du Golgi et souligne l'importance de la régulation de ce processus pour préserver les fonctions de cet appareil.

Mots-clés: IFITM3, Interféron, HIV, Golgi, Trafic, PRRT2

## Contents

<b>Abstract</b> .....	3
<b>Contents</b> .....	4
<b>Acknowledgement</b> .....	7
<b>Introduction</b> .....	8
1. The “InterFeron Induced TransMembrane proteins” .....	9
1.1 <i>Discovery and presentation of the different members of the dispanin/CD225 family</i> .....	9
1.2 <i>Structure and topology</i> .....	12
1.3 <i>Intracellular traffic and post-translational modifications</i> .....	14
2. Antiviral role(s) of IFITMs .....	18
2.1 <i>Discovery of the antiviral properties of IFITMs</i> .....	18
2.2 <i>Effect of IFITMs in animal mouse models</i> .....	19
2.3 <i>Antiviral function of IFITMs</i> .....	20
2.4 <i>Dual inhibition by IFITM3</i> .....	23
2.5 <i>Mechanism of membrane fusion inhibition by IFITMs</i> .....	31
3. Other physiological roles of IFITM proteins .....	34
3.1 <i>Involvement in placental formation</i> .....	34
3.2 <i>Regulation of immune responses</i> .....	34
3.3 <i>Involvement in carcinogenesis, migration of primordial germ cells and osteogenesis</i> .....	36
4. IFITM polymorphisms in humans .....	37
5. The ER-Golgi secretory pathway .....	40
5.1 <i>ER and Golgi organelles</i> .....	40
5.2 <i>Anterograde and Retrograde transport</i> .....	44
<b>Objectives</b> .....	47
<b>Results</b> .....	49
<i>Identification of a mutation in the CIL loop of IFITM3 that modifies glycoprotein trafficking through Golgi.</i> .....	50
<i>The 85-90 IFITM3 mutant accumulates in the cis-Golgi and leads to structural changes in the Golgi apparatus.</i> .....	53
<i>The 85-90 mutation defines a domain in CIL that regulates the exit of wild-type IFITM3 from the Golgi.</i> .....	60
<i>Identification of the amino acids in the CIL that mediate the retention of IFITM3 in the Golgi.</i> .	62
<i>The Golgi egress domain identified in IFITM3 seems conserved in other members of the dispanin subfamily.</i> .....	63
<b>Discussion</b> .....	71
<b>Material and Methods</b> .....	76
<b>References</b> .....	82

**Annexes (publications and list of abstracts) ..... 91**

- 1) *A novel domain within the CIL regulates egress of IFITM3 from the Golgi and prevents its deleterious accumulation in this apparatus (First author, manuscript submitted to Biorxiv)*
- 2) *Functional mapping of regions involved in the negative imprinting of virion particles infectivity and in target cell protection by the Interferon-Induced Transmembrane Protein 3 (IFITM3) against HIV-1. R. Appourchaux, M. Delpeuch, L. Zhong, J. Burlaud Gaillard, K. Tartour, G. Savidis, A. Brass, L. Etienne, P. Roingeard, A. Cimorelli. J Virol. Jan 4;93(2). pii: e01716-18. doi: 10.1128/JVI.01716-18. (2019). (Third author, first page only)*
- 3) *Dahoui C, Picard L, Wcislo M, Legrand A, Pillon M, Allatif O, Zhong L, Cimorelli A, Guéguen L, Etienne L. (2020) Identification of a primate gene family modulating lentiviral/HIV replication, using the DGINN pipeline to Detect Genetic INNOvations in combination with functional assays. Cold Spring Harbor Laboratory Meetings on Retroviruses, NYC Virtual, 05/2020. Selected talk (Abstract)*
- 4) *Picard L, Wcislo M, Ganivet Q, Dahoui C, Pillon M, Zhong L, Cimorelli A, Guéguen L, Etienne L (2019) Discovery of evolutionary-relevant virus-host protein interfaces, through a novel automated method detecting genetic innovations (DGINN) combined with virus-host experimental assays. Jacques Monod Conference: Virus Evolution, Roscoff, 10/2019. Poster (Abstract)*
- 5) *Dahoui C, Picard L, Legrand A, Wcislo M, Pillon M, Zhong L, Cimorelli A, Guéguen L, Etienne L. (2021) Identification of a primate genes modulating lentiviral/HIV replication, using the DGINN pipeline to Detect Genetic INNOvations in combination with functional assays. ANRS AC41, Work In Progress (WIP) meeting, Paris (Virtual), 18-19/05/2021. Selected Talk (Abstract)*

## **Acknowledgement**

During my four years PhD, I gained both scientific progress and had also a nice experience living in France. First of all, I would like to thank the members of the jury: Doctor Katy Janvier and Stéphanie Miserey-Lenkei, who agreed to be my rapporteurs and Doctor Delphine Muriaux to be the president of the jury. Thanks to them for judging my thesis work.

From a scientific point of view, I would like to thank my thesis director sincerely, Andrea Cimarelli for helping me with the application of CSC scholarship, for helping me with the design of the subject and the guidance in the experiment and writing. His rigor and enthusiasm for scientific research inspired me to continue in the field of scientific research.

I would thank Chloé Journo and Delphine Muriaux for being members of my thesis monitoring committee. Thanks for the kind advice on the experiments and also concerns for my daily life which helped me running smoothly of the thesis work.

I would like to thank all the members of the team that I worked with during my thesis: Lucie, Xuan-Nhi, Mégane, Léa, Stéphanie, Fabien, Véro, Anuj, Mathilde, Yuxin, Clara, Federico, Alexandre, Florent, Severine, Giulia, Julie and Amandine. Thanks for the daily company and the advice in experiments.

Finally, I would like to thank all the people from the CIRI, the ENS, the Platim and the surrounding laboratories (OR, TEV, EBV and EVIR) for the help during my thesis.

From a personal point of view, I want to thank my parents, my sister and brother who make me feel free to study abroad. I thank all my friends for their company and the cherished experiences during vacations in these four years. I would like to thank the China government for the fellowship support and official aid during the Covid19 restrictions which allows me to continue my studies.

## **Introduction**

## **1. The “InterFeron Induced TransMembrane proteins”**

### **1.1. Discovery and presentation of the different family members**

IFITM proteins were identified as the first transmembrane proteins the expression of which was upregulated by interferon in 1984 (Friedman et al., 1984). Later studies indicated that IFITM proteins are part of a larger family of proteins termed dispanins or CD225 containing structurally related proteins characterized by the presence of an intramembrane domain, IMD) as well as of a trans-membrane domain (TMD) separated by an intracellular cytoplasmic loop (CIL, Figure 1A). The dispanin family is subdivided into four subfamilies (A through D) that include proteins of known functions in endosomal/vesicular trafficking as well as proteins of unknown functions. IFITMs are regrouped in the A subfamily which in humans comprise five distinct members: IFITM1,2,3,5 and 10 (Hickford et al., 2012). IFITM1, 2 and 3 proteins are strongly upregulated after stimulation by type I interferons and are essentially studied in the context of viral infection, while expression of IFITM5 is independent of interferon and restricted to bone tissue. Expression pattern as well as functions are currently unknown for IFITM10.

The evolutionary history of IFITMs proteins is complex. Generally, the gene sequences can segregate into three phylogenetic groups: a first group containing IFITMs whose functions are linked to immunity (as IFITM1, 2 and 3 in humans), a second group with IFITM5 and a third with IFITM10, with the latest two members that appear to have originated from an ancestor common to vertebrates. As a result, IFITM1, 2 and 3 are closer to each other than other IFITMs with IFITM2 and IFITM3 that display 90% similarity at the amino acids level with each other and about 60% identity between themselves and IFITM1 mainly due to the fact that this member exhibits a shorter N terminus of 21 amino acids (Figure 1B).

A



B

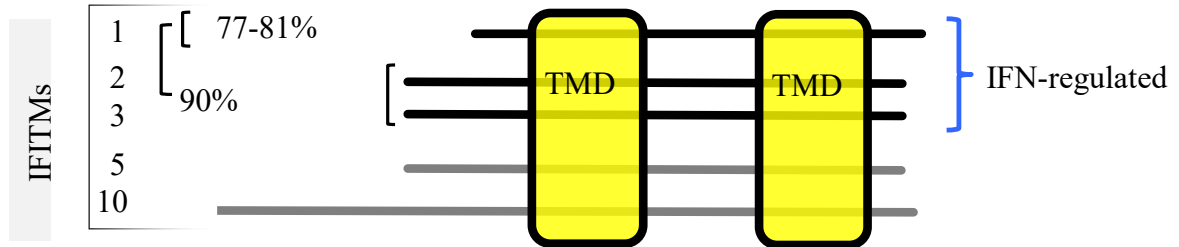


**Figure 1. Presentation of human IFITM proteins.** A) Schematic representation of the structural features of a prototypical IFITM protein. N and C, N and C terminus, respectively; IMD and TMD, intra- and trans-membrane domains, respectively. CIL, cytoplasmic intracellular loop. B) Schematic representation of the five IFITM members in humans.

The number of *ifitm* genes varies from one species to another and have been subjected to several duplication events, resulting in unique repertoires according to the animal species considered. For example, mouse possesses seven *ifitm* genes and several copies are also present in primates that may represent either functional copies or pseudogenes. Sequences with similarities to animal *ifitm* genes have also been identified in bacteria, suggesting that they may have originated from horizontal transfer from bacteria to eukaryotes (Melvin et al., 2015; Sällman Almén et al., 2012).

As said above, IFITMs constitute a subfamily within the larger family of transmembrane (TM) proteins termed Dispanins, which contains four subfamilies (A through D, Figure 1C). In addition to IFITMs, the family is composed of ten additional human genes: PRRT2, TUSC5, TMEM233,

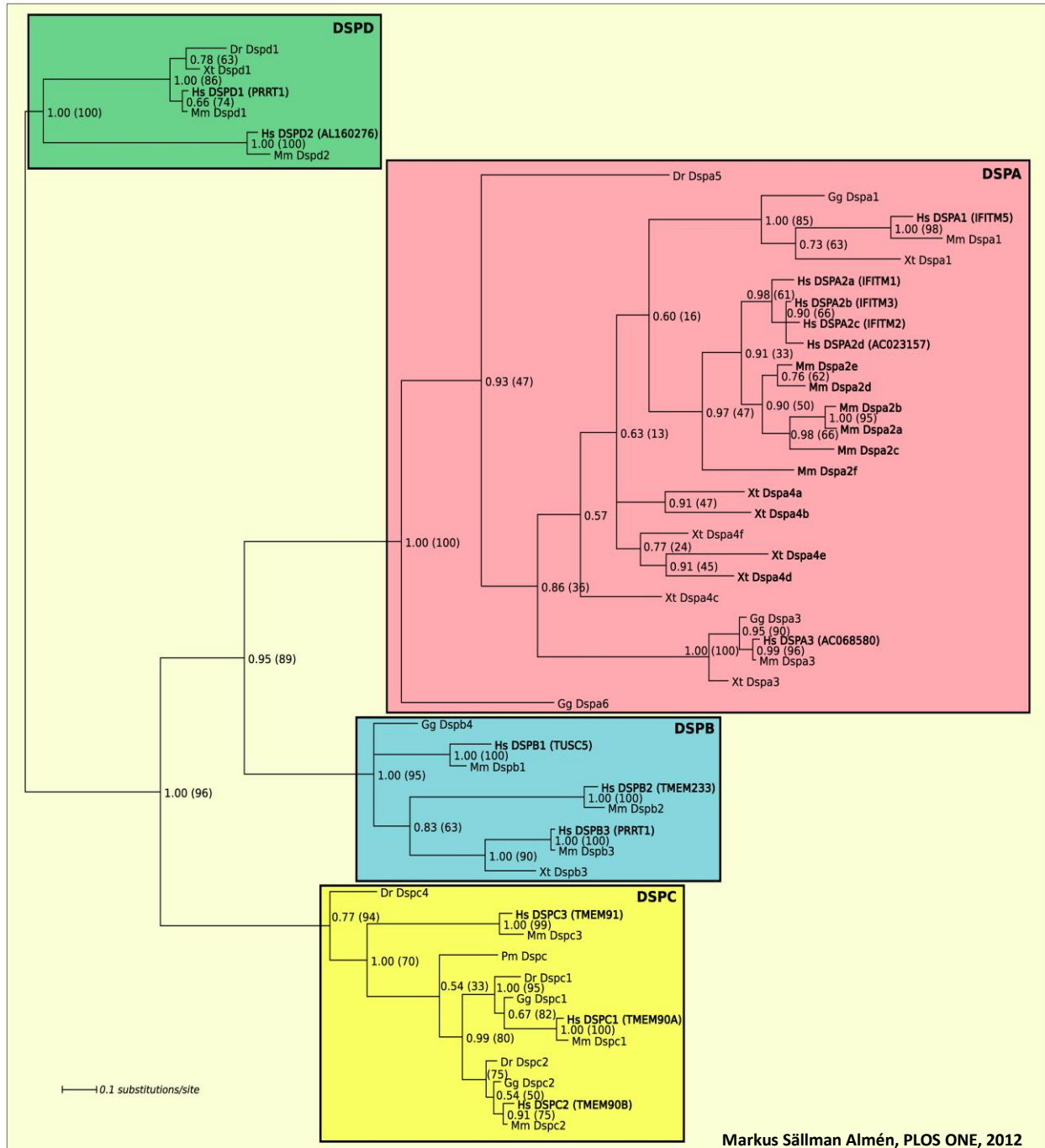


**Figure 1, continued. C) The phylogeny of the vertebrate Dispanins.** The dispanin family can be divided into four subfamilies (A–D) marked with colors. In addition to IFITM genes, other human genes, known as TUSC5, TMEM233, PRRT2, TMEM90A, DSPC2, TMEM90B, TMEM91, AC023157, AL160276 and AC068580, together form a novel gene family that we call the Dispanins, which refers to the 2TM membrane topology that is common to all identified members.

TMEM90A, DSPC2, TMEM90B, TMEM91, AC023157, AL160276 and AC068580. While the functions of most of the members of this family is unknown, PRRT2, TUSC5 and TMEM90s appear to be involved in vesicular regulation. However, overall members of this family are likely to exert different functions as little homology is present outside the TM-CIL domains. Of note, this family is the second largest 2TM family in the human genome, superseded only by the Inwardly rectifying potassium channel family (IRK) that contains 15 members. Among the dispanin members, the proline-rich transmembrane protein 2 is a protein that in humans is encoded by the PRRT2 gene. PRRT2 is associated with a number of movement disorders, most commonly paroxysmal kinesigenic dyskinesia where approximately 1/3 of cases were harboring mutations in PRRT2. Mutations in this protein have also been associated with episodic ataxias, and in particular in combination with various types of epilepsy.

By virtue of their immune and in particular antiviral functions which will be detailed below, the IFITM1, 2 and 3 proteins are the most studied and will be grouped together under the term IFITMs in the rest of this introduction. The specificities of individual IFITM members will be detailed when relevant.

## **1.2. Structure and topology**

IFITMs are membrane proteins that have a relatively long N-terminus compared to the C-terminus, two hydrophobic domains (also called intra and trans-membrane domains) separated by a cytoplasmic loop (CIL). The association of the first intramembrane domain and the cytosolic loop is referred to as the CD225 domain which is shared by all members of the dispanin family (John et al., 2013). The N and the C terminus of IFITMs exert regulatory functions. The N-terminus is

longer for IFITM2 and 3 than for IFITM1 (IFITM1 lacks the first 21 amino acids that are instead present in IFITM2/3) and reciprocally for the C-terminus. The exact topology of IFITMs on membranes has been the subject of several studies with no clear consensus reached as yet (Figure 2).

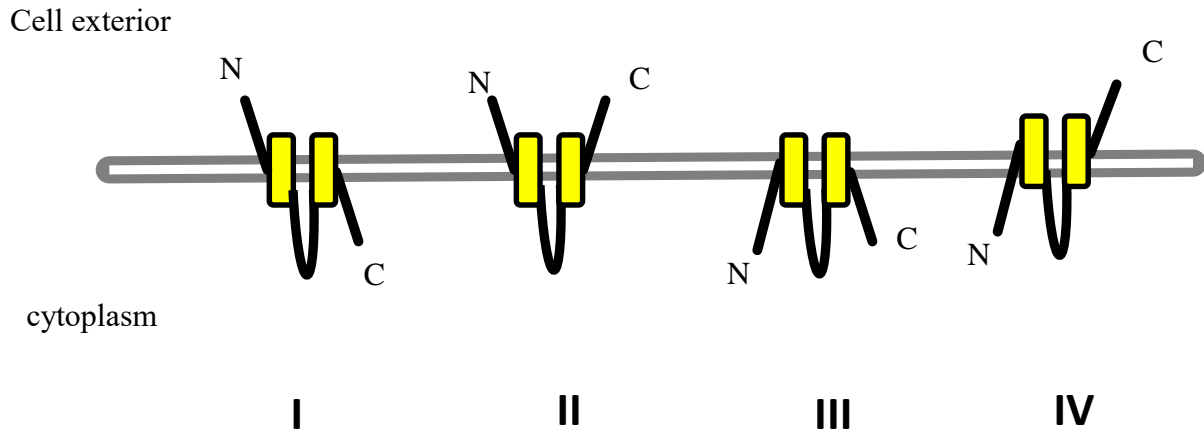


**Figure 2. Possible topological conformations of a typical IFITM on cellular membranes.** The IMD and TMD are represented in yellow. The conformation number IV is currently thought to be the most plausible, although evidence of exposure of the N terminus to the exterior of the cell is present in the literature, comprised from data obtained from our laboratory.

The initially predicted topology of IFITMs was the one with both N-ter and C-ter exposed in the extracellular medium (Brass et al., 2009; Chen et al., 1984; Weidner et al., 2010; Yount et al., 2010), which was supported by the fact that antibodies directed against epitope tags inserted at the N-ter and the C-ter were recognized by antibodies without the need to permeabilize the cell.

Subsequent studies however reported that tag insertions at the C-ter of IFITMs affected their functions, suggesting the existence of potential artefacts (Jia et al., 2012; Yount et al., 2012).

Later, using antibodies directed against specific portions of the protein, a new type topology was proposed for IFITMs by two teams (Bailey et al., 2013; Weston et al., 2014). In this model, the C-ter was located in the extracellular portion, while the N-ter and the CIL were instead oriented towards the cytoplasm, in line with the fact that such regions are heavily modified post-translationally by numerous cytoplasmic proteins and also in line with the fact that the C-terminal end of IFITMs could be degraded by lysosomal enzymes which requires the insertion of this portion of the protein within the lumen of lysosomes.

Although this appears at the moment a plausible model, it must be remembered that data from our lab indicated the presence of the N-ter of IFITM3 also at the exterior of the cell in primary cells stimulated with IFN, indicating that different topologies are likely to coexist in cells expressing IFITM proteins.

### **1.3 Intracellular traffic and post-translational modifications**

At steady-state, IFITM proteins exhibit different enrichments in specific cellular compartments and in particular, IFITM1 is mostly concentrated at the plasma membrane, while IFITM2 and IFITM3 are mostly concentrated in endo-lysosomal membranes (Feeley et al., 2011). These differences are specified by post-translational modification that take place at the N and C terminal regions of the different IFITM proteins.

After translation from endoplasmic reticulum-associated ribosomes, IFITMs pass through the Golgi apparatus to reach the plasma membrane. Thanks to specific docking sequences present in their longer N-terminal regions, IFITM2 and IFITM3 can be re-endocytosed from the plasma membrane to concentrate essentially, albeit not exclusively, in late endosomes and lysosomes,

while the shorter N-term of IFITM1 lacks endocytosis-related domains and thus remains essentially at the plasma membrane (Figure 3).

Several juxtaposed sequences at the amino-terminal end of IFITM2 and IFITM3 are involved in this behavior within this region: PPxYEML (Chesarino et al., 2014a; Jia et al., 2014; Yount et al., 2012). The YEML domain represents the Yxx $\Phi$  recognition pattern known to associate to the subunit  $\mu$ 2 of the endocytosis machinery AP2 ("adapter complex 2"), while the PPxY sequence is recognized by the ubiquitin ligase E3 NEDD4 that mono and polyubiquitinates four lysines (in position 24, 83, 88 and 104 in IFITM3) (Yount et al., 2012), leading on one hand to lower levels of IFITM3 but on the other, also contributing itself to the protein re-localization in endo-lysosomal membranes.

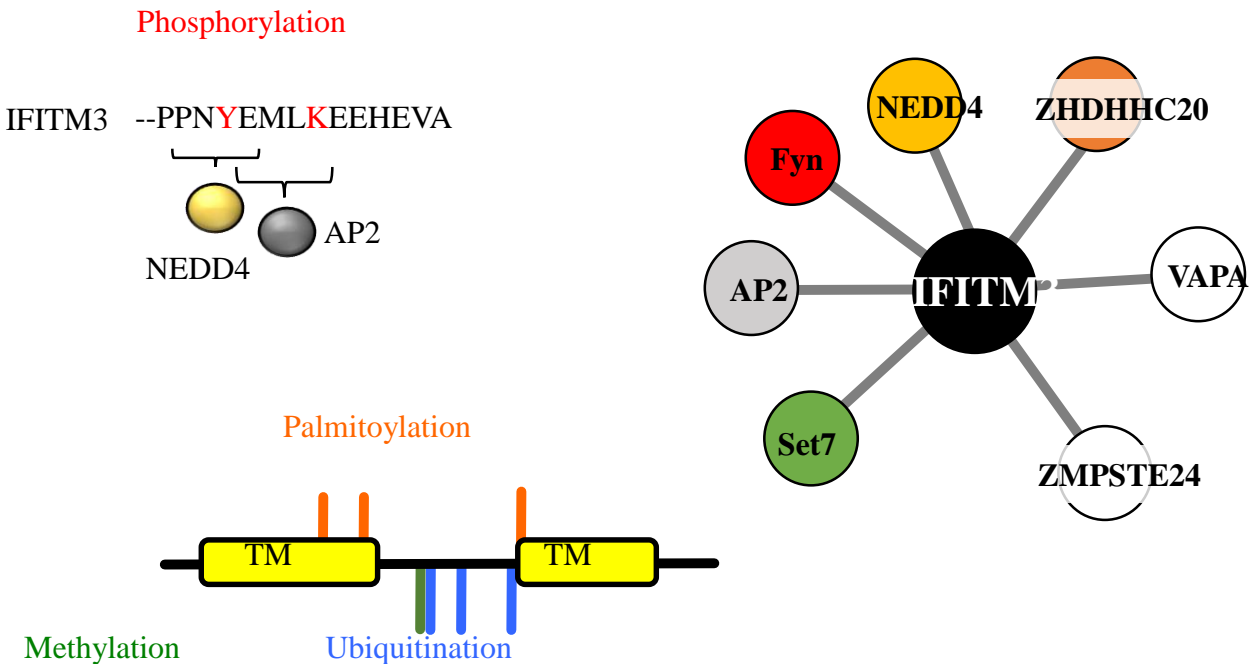


**Figure 3. Post-translational modifications described in the literature for human IFITM3.** Representation of the amino acids at the N-terminus of the IFITM3 protein that act in the recruitment of the  $\mu$ 2 subunit of the AP2 complex and of the E3 NEDD4 ubiquitin ligase. Below is a schematic representation of the other cellular proteins described to interact with IFITM3. In some cases, the functional relevance of these interactions remains to be formally demonstrated.

Interestingly, IFITM3 can be phosphorylated on the tyrosine at position 20 by the tyrosine kinase Fyn (Chesarino et al., 2014a; Jia et al., 2014). While the docking domain on IFITMs responsible for the recruitment of this kinase is unknown, phosphorylation greatly influences both intracellular localization and antiviral activity of IFITM3. Indeed, when this residue is mutated and its phosphorylation is prevented, IFITM3 is retained at the plasma membrane indicating this modification as important in the regulation of AP2-driven endocytosis from the plasma membrane as well as in the regulation of its ubiquitination pattern (as docking of NEDD4 is also prevented). Given that phosphorylation is a dynamic process and also given the fact that IFITMs exhibit a dynamic behavior and heterogeneous distributions in cellular membranes, it is likely that phosphorylation provides the mean to finely regulate the intracellular dynamics of IFITM proteins linking this process to the activation status of the cell itself (Chesarino et al., 2014b). The above-mentioned regions are not present in the shorter N-terminus of IFITM1 which as a result cannot dock either NEDD4, AP2 or Fyn.

While the lysine residue 88 (in IFITM3) can be ubiquitinated (Figure 3), a recent study indicated that this same residue can also be dynamically monomethylated by the lysine methyltransferase **Su(var)3-9**, **Enhancer-of-zeste** and **Trithorax** (SET) domain-containing protein 7 (Set7) (Shan et al., 2013). Methylation at this residue decreases the antiviral restriction of IFITM3 against the Vesicular Stomatitis and Influenza viruses (VSV and Flu, respectively). It is not known whether this methylation leads to changes in the intracellular distribution of IFITM3 and the weight of the modification in this residue remains debated because lysine 88 mutations do not modify the activity of IFITM3 against these viruses in other studies (John et al., 2013). However, a subsequent study indicated that monomethylation could be reversibly removed by the Lysine-specific histone

demethylase 1 (LSD1), raising the possibility of an intricately cross-regulatory network between ubiquitination, mono-methylation and demethylation in the CIL (Shan et al., 2017).

Lastly, it has been shown that IFITM3 can be S-palmitoylated on three cysteines at positions 71, 72 and 104 (Yount et al., 2010), that are conserved across all IFITM members. Palmitoylation involves the addition of a fatty acid to a cysteine residue and this modification is generally described as modulating the binding of modified proteins to the lipid bilayer, suggesting therefore that it could also contribute to finely tune the association of IFITMs to membranes (Chesarino et al., 2014b). This modification increases the affinity for the membranes. It is important for the membrane localization of IFITM3 and allows the formation of IFITM3 clusters at the membrane. Indeed, cell fractionation experiments have shown for the wild-type IFITM3 protein that the majority of the proteins were membrane-bound even if there was a minor fraction of the cytoplasmic IFITM3 protein despite the presence of the two hydrophobic domains (Yount et al., 2012). A mutant of the three cysteines gives a more diffuse localization of the protein in fluorescence microscopy and an increase in the cytosolic fraction of IFITM3. This mutant also loses its antiviral activity against the Influenza A virus (Yount et al., 2010), indicating that S-palmitoylation of IFITM3 is crucial for its activity against virus infection.

## **2 Antiviral role of IFITMs**

### **2.1 Discovery of antiviral effect**

The antiviral activity of IFITM3 was first discovered in 1984, but it was not until 2009 that the antiviral role of IFITMs was finally identified (Brass et al., 2009). An siRNA interference screen showed that IFITMs displayed an antiviral effect by restrict an early step in replication against several viruses and in particular Influenza, West Nile and Dengue viruses. Following this study, numerous studies from different laboratories, including ours, indicated IFITMs as antiviral factors capable of broad inhibition, i.e. of interfering with the replication of a large spectrum of enveloped viruses, as diverse as Ebola virus and the human immunodeficiency type I virus (HIV-1).

We now know that IFITMs can interfere with viral replication at two distinct stages of the viral life cycle: in target cells, where IFITMs inhibit viral entry by blocking the fusion of viral and cell membranes in endosomes; in infected cells undergoing the production of novel virion particles, where IFITMs lead to the production of novel particles of diminished infectivity, also due to a membrane fusogenicity defect. The first case is more occurred in several classes of viruses (Tartour and Cimorelli, 2015). In this latter case, that our laboratory described in 2014 in the case of HIV-1 and later extended to other viruses, IFITMs are recruited, or are found, at the assembly site of the virus, are incorporated into virion particles, and lead to virions of apparently normal morphology but lower infectivity, property that we defined as negative imprinting of virion particles infectivity (Compton et al., 2014; Tartour et al., 2014).

Overall, regardless of the configuration studied in the target cell or in the virus-producing cell, the molecular mechanisms used by IFITMs to interfere with the viral cycle appear to focus on membrane fusion through mechanisms that are not yet well understood.

## 2.2 Effect of IFITMs in animal mouse models

The importance of IFITMs in combating viral infections has been demonstrated *in vivo* in mice lacking either the *ifitm3* gene or the entire *ifitm* locus (*ifitm1*, 2, 3, 5 and 10). These mice do not exhibit any particular developmental phenotype (Lange et al., 2008), although recent studies indicated them as more obese than their WT counterpart. On the other hand, these mice were more susceptible to infection with different viruses such as Influenza A virus and the respiratory syncytial virus (RSV) (Bailey et al., 2012; Everitt et al., 2013). Knockout mice for the entire *ifitm* locus exhibit the same phenotype as knockout mice for *ifitm3* (Bailey et al., 2012), indicating this latter as the main antiviral member of the IFITM family in mice. This result is also interesting because RSV is a virus which, as HIV-1, is thought to fuse at the plasma membrane and that does not require the endosomal route, again suggesting that the dynamic behavior of IFITM3 and IFITMs more in general distributes them across most cellular membranes facilitating their encounter with viruses that enter, or exit the cell, at different locations.

Interestingly, knockout mice for *ifitm3* were also used to try to define bacterial susceptibility to IFITM3 (Everitt et al., 2013). In particular, they used different types of bacterial pathogens (*Salmonella typhimurium*, *Citrobacter rodentium*, *Mycobacterium tuberculosis*) with different replication niches and different pathways into cells and a parasite (*Plasmodium berghei*). However, the authors found no significant differences between wild-type and *ifitm3* knockout mice following infections with these pathogens, suggesting that the main functions of IFITMs are essentially directed against viruses.

### 2.3 Antiviral function of IFITMs

The original study which discovered the antiviral effect of IFITMs showed that they were able to inhibit the replication of influenza A, West Nile and dengue viruses (Brass et al., 2009). The following studies have shown that they are able to inhibit the entry of viruses from several different viral families in vitro (Table I). When expressed in target cells, IFITMs have been shown to inhibit the entry of influenza A and B viruses (*Orthomyxoviridae*), HIV-1, HIV-2 and various SIVs (*Retroviridae*), dengue, zika, hepatitis C and West Nile (*Flaviviridae*), Marburg and

<i>Family</i>	<i>Viruses</i>	<i>Genome</i>	<i>pH</i> <i>dependency</i>	<i>Envelope</i>
RNA viruses				
Orthomyxoviridae	Influenza A and B viruses	RNA (-)	**	Yes
Flaviviridae	West Nile virus	RNA (+)	*	Yes
	Dengue virus	RNA (+)	**	Yes
	Hepatitis C virus	RNA (+)	**	Yes
	Avian tembusu virus	RNA (+)	**	Yes
	Zika virus	RNA (+)	**	Yes
Rhabdoviridae	Vesicular stomatitis virus	RNA (-)	*	Yes
	Rabies virus	RNA (-)	**	Yes
	Lagos Bat virus	RNA (-)	**	Yes
Bunyaviridae	La Crosse virus	RNA (-)	**	Yes
	Hantaan virus	RNA (-)	**	Yes

	Andes Virus	RNA (-)	**	Yes
	Rift valley fever	RNA (-)	**	Yes
Filoviridae	Ebola virus	RNA (-)	*	Yes
	Marburg virus	RNA (-)	*	Yes
Alphaviridae	Sindbis and Semliki Forest Virus	RNA (+)	*	Yes
Coronaviridae	SARS Corona virus	RNA (+)	**	Yes
Retroviridae	HIV-1	RNA (+)	no	Yes
	Jaagsiekte sheep retrovirus (JSRV)	RNA (+)	**	Yes
Reoviruses	Reovirus	RNA double	**	no
DNA viruses				
Asfarviridae	African swine fever virus	DNA double	**	Yes
Poxviridae	Vaccinia virus	DNA double	**	Yes
Iridoviridae	Rana grylio virus	DNA double	**	Yes

**Table I. Summary of antiviral activity of IFITMs.** \* low pH dependence; \*\* strong dependence on pH.

Ebola viruses (*Filoviridae*), coronavirus (*Coronaviridae*), Semliki and Sindbis forest viruses (*Alphaviridae*), reoviruses (*Reoviridae*), vesicular stomatitis, rabies and Lagos bat virus (*Rhabdoviridae*), respiratory syncytial virus (*Paramyxoviridae*), African swine fever virus (*Asfarviridae*) and Rift Valley fever viruses (*Bunyaviridae*) (Anafu et al., 2013; Brass et al., 2009; Huang et al., 2011; Jiang et al., 2010; Lu et al., 2011; Muñoz-Moreno et al., 2016; Narayana et al., 2015; Qian et al., 2015; Savidis et al., 2016; Schoggins, 2014; Wrensch et al., 2014; Xu-Yang et al., 2016). This list is not exhaustive and it includes the main viruses impacted by human IFITMs. Numerous studies also show that IFITMs from other species (fish, mycobacteria, mouse, duck, chicken or monkey) have an antiviral effect on cognate viruses of their own species (Blyth et al., 2016; Huang et al., 2011; Melvin et al., 2015; Qian et al., 2015; Smith et al., 2013; Wilkins et al., 2016; Winkler et al., 2017; Zhu et al., 2013). These studies show that the antiviral action spectrum of IFITMs is wide and that their functions are preserved across different animal species. Viral inhibition by IFITMs occurs with both DNA and RNA viruses that enter the cell at either plasma membrane or endosomal vesicles. The inhibition efficiency is variable and depends on the virus studied, the cell type, the IFITM protein involved, as well as the experimental setting used.

A certain number of viruses are instead resistant to IFITMs: Lassa, Machupo and lymphocytic choriomeningitis viruses (*Arenaviridae*), Congo hemorrhagic fever virus (*Bunyaviridae*), human papilloma virus 16 (*Papillomaviridae*), cytomegalovirus (*Herpesviridae*) and adenovirus 5 (*Adenoviridae*) (Brass et al., 2009; Mudhasani et al., 2013; Warren et al., 2014). A few viruses seem instead to be favored by IFITMs, although the underlying mechanisms remain unclear: the OC43 coronavirus that seem to use IFITMs as a factor promoting cell entry (Zhao et al., 2014). In the case of HIV-1, sensitivity to IFITMs seems also to be modulated by the viral envelope, although how this may occur remains a subject of investigation (Wrensch et al., 2017).

## **2.4 Dual inhibition by IFITM3**

IFITMs have been shown to be able to inhibit viral replication at two distinct phases of the viral life cycle: in target cells, IFITM3 blocks incoming virions in endosomal vesicles, protecting target cells from infection (Figure 4, while a more detailed overview of the HIV-1 life cycle and of some host factors is provided in Figure 5). In the case of HIV-1, we and others reported the existence of an additional antiviral mechanism through which IFITMs lead to the production of virions of reduced infectivity (Tartour et al., 2014). In infected cells undergoing the production of novel virion particles, IFITMs lead to the production of novel particles of diminished infectivity. All of these establishes IFITMs as a paradigm of restriction factor capable of interfering with two distinct phases of a virus life cycle.

### ***(1) Target cell protection (viral inhibition during viral entry into the cell)***

To deliver their content into the cytoplasm of the target cell, viral membranes must first fuse with the membrane of the target cell. According to the nature of the viral glycoprotein, this step can occur directly at the plasma membrane (as in the case of HIV-1 that is a pH-independent entry mechanisms), or after internalization into endosomes in which the acidic pH triggers a structural conformation of the viral glycoproteins that results in viral-to-cellular membrane fusion (as in the case of Influenza virus, referred to as a pH-dependent entry mechanism). After the engagement between the viral glycoprotein and the cellular receptor, the viral and cellular membranes get in close proximity and first hemifuse (one leaflet fused) before fusion of both leaflets and formation

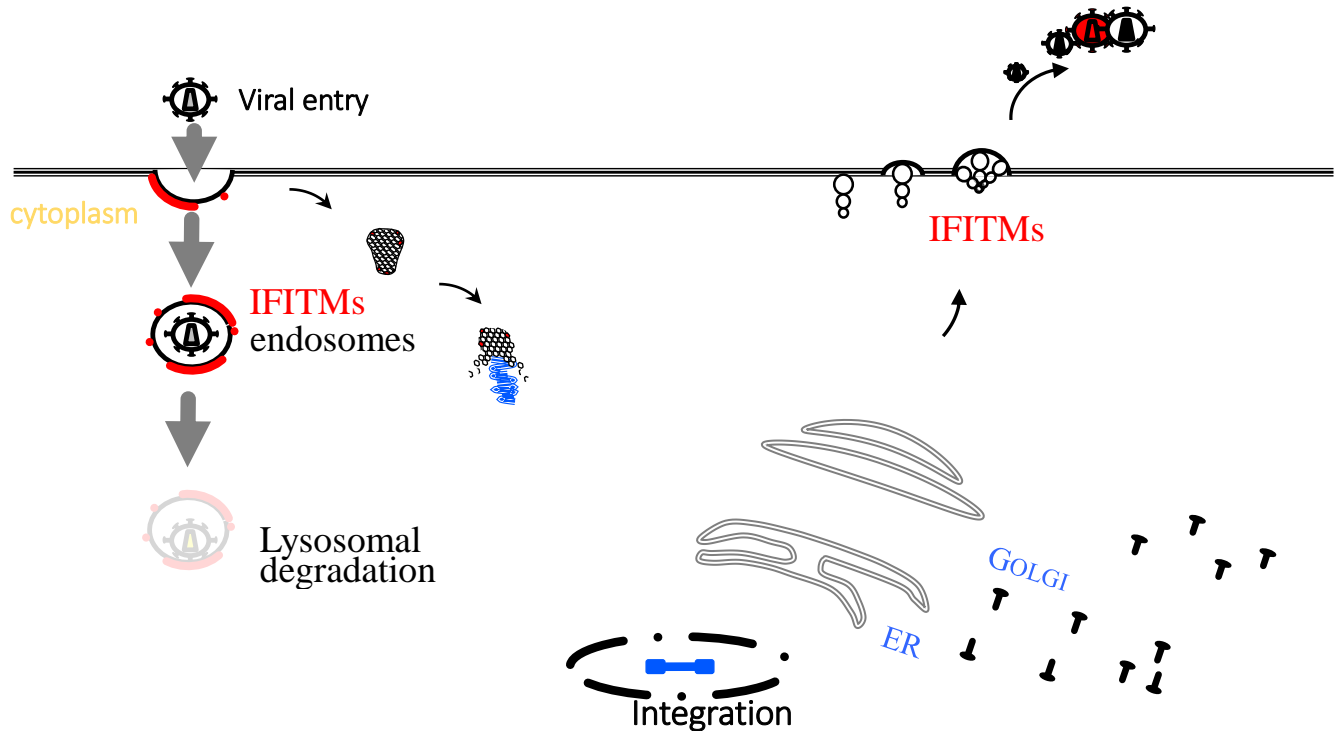


**Figure 4. IFITM3-mediated inhibition of HIV-1.** In target cells, IFITMs arrest incoming virion particles in endosomes, leading to their subsequent degradation. In virion-producing cells, IFITMs coalesce with viral structural proteins at sites of assembly, leading to the production of virion particles that package IFITMs and display reduced infectivity.

of a pore that allows access of the viral content into the cell (full fusion). A first study concluded that IFITMs affected the transition between hemifusion and full fusion (Desai et al., 2014; Li et al., 2013). The blocked viruses were then degraded in the endosomal environment (after endocytosis for viruses blocked at the plasma membrane) (Feeley et al., 2011) (Lin et al., 2013). In agreement with this model, the IFITM3 protein which is considered the model of this family and is widely

used to study the mechanism of inhibition of IFITMs strongly co-localizes with endosomal and lysosomal vesicles.

One study suggested that IFITM3 could affect the pH of these compartments thus affecting viral entry also indirectly, but such findings have not been confirmed (Amini-Bavil-Olyaei et al., 2013; Feeley et al., 2011; Huang et al., 2011; Muñoz-Moreno et al., 2016; Wee et al., 2012; Yount et al., 2012). In addition, an expansion of endo-lysosomal compartment (because it contains both endosomal and lysosomal markers) and multivesicular bodies also positive for the LC3 autophagosome marker (Feeley et al., 2011; Yount et al., 2012) is often associated to IFITM3 expression (Amini-Bavil-Olyaei et al., 2013; Chesarino et al., 2014b).

Several mechanisms have been proposed to explain the inhibition of the fusion of the viral membrane with the cell membrane. This mechanism of viral inhibition was described more recently by our laboratory together with the Schwartz's laboratory in the inhibition of HIV-1 and was later on extended to other viruses by our lab (Tartour et al., 2014).

In the study where the antiviral role of IFITMs was discovered, preliminary experiments did not show any effect of IFITMs on HIV (Brass et al., 2009), but different screens on the antiviral effect of genes stimulated with interferon revealed an effect of IFITMs on HIV-1 infection (Kane et al., 2016; Lu et al., 2011; Schoggins et al., 2011). Further studies subsequently showed that IFITMs did indeed have an effect on HIV-1 replication (Lu et al., 2011). They showed that IFITM2 and 3 were able to reduce the entry of HIV-1 but not IFITM1. A more recent study showed that IFITM1 was also able to inhibit the entry of HIV-1 (Foster et al., 2016). It actually depends on the coreceptor used by the strain of HIV-1 that is used for infection.

The strains which use the CCR5 coreceptor are more sensitive to IFITM1 whereas the strains which use CXCR4 are more sensitive to IFITM2 and 3. IFITM2 and 3 being mainly localized in the endosomes, this implies that the strains using CXCR4 fuse to the endosomal membrane. This study also showed that the viruses causing a new infection ("transmitted founder") were resistant to IFITMs. Susceptibility develops over the months of infection. It is due to mutations in the envelope protein that the virus acquires to escape neutralizing antibodies but which make them susceptible to IFITMs. Human IFITMs have also been shown to have an effect on the entry of HIV-2 and on different strains of SIVs (Qian et al., 2015). In addition, this antiviral property is retained in IFITMs of primate species (Wilkins et al., 2016).

Despite the fact that HIV-1 has been shown to be inhibited more efficiently by IFITM1 rather than IFITM3 (IFITM1 is mostly at the plasma membrane while IFITM3 is mostly in endosomal membranes), this finding is debated and inhibition by IFITM3 is commonly observed in HIV studies. This is intriguing because contrarily to other viruses that require the passage through the acidic pH of endosomes to become competent for membrane fusion and to infect cells, HIV-1 infection is thought to occur exclusively at the plasma membrane. Two possibilities can explain HIV inhibition by IFITM3: first, a fraction of IFITM3 is also localized at the plasma membrane and the dynamics of membrane recycling are likely to move this protein continuously to and from the plasma membrane; 2) HIV-1 can borrow a functional endosomal entry pathway (Chauhan and Khandkar, 2015; Fackler and Peterlin, 2000; Miyauchi et al., 2009; Sloan et al., 2013). Although this finding remains debated the possibility that a portion of HIV virion particles enters cells through endosomes (although without need for an acidic pH switch) can explain why HIV-1 is susceptible to all IFITMs despite intracellular distribution differences.

***(2) Effect on the late stages of HIV-1 life cycle and mechanisms***

Early studies showed that IFITMs influenced HIV-1 replication and virus entry by blocking the fusion step. The possible effect on the late stages of HIV-1 (after integration) has been studied more and more detailed during these recent years. It had just been observed that the presence of IFITMs decreased viral production by reducing the amount of Gag in the producer cell (Chutiwitoonchai et al., 2013; Lu et al., 2011). It has been suggested that IFITMs may interfere with the export of Rev-dependent viral RNAs and the activation of transcription of Tat-dependent viral genes (Chutiwitoonchai et al., 2013). At the previous study of my lab, results showed the presence of the three IFITMs during the late phases had an effect on HIV-1 (Tartour et al., 2014). It pointed out the importance of IFITM3 in the late phases of virus infection and their presence during the late phases mainly allows two things: a decrease in the infectivity of the new viruses produced and the incorporation of IFITMs into the viral membrane lipid. These results were confirmed by those of two other independent teams of ours (Compton et al., 2014; Yu et al., 2015). The latter notably showed that the antiviral effect of IFITMs against HIV-1 was stronger when they were present in the producer cell than in the target cell. Viruses produced in the presence of IFITMs show a defect in entry and membrane fusion during a new infection. The decrease in infectivity of HIV and SIV is a conserved property of IFITMs from different primate species (Wilkins et al., 2016). The defect in infectivity varies depending on the IFITM studied and the virus strain used. The mechanisms leading to this defect in infectivity are not well understood. Several questions are still unanswered. It was reported that it was the IFITM2 and 3 proteins, but not IFITM1, that interact with the envelope protein in the target cell, which leads to its maturation by cellular Furin being reduced (Yu et al., 2015).

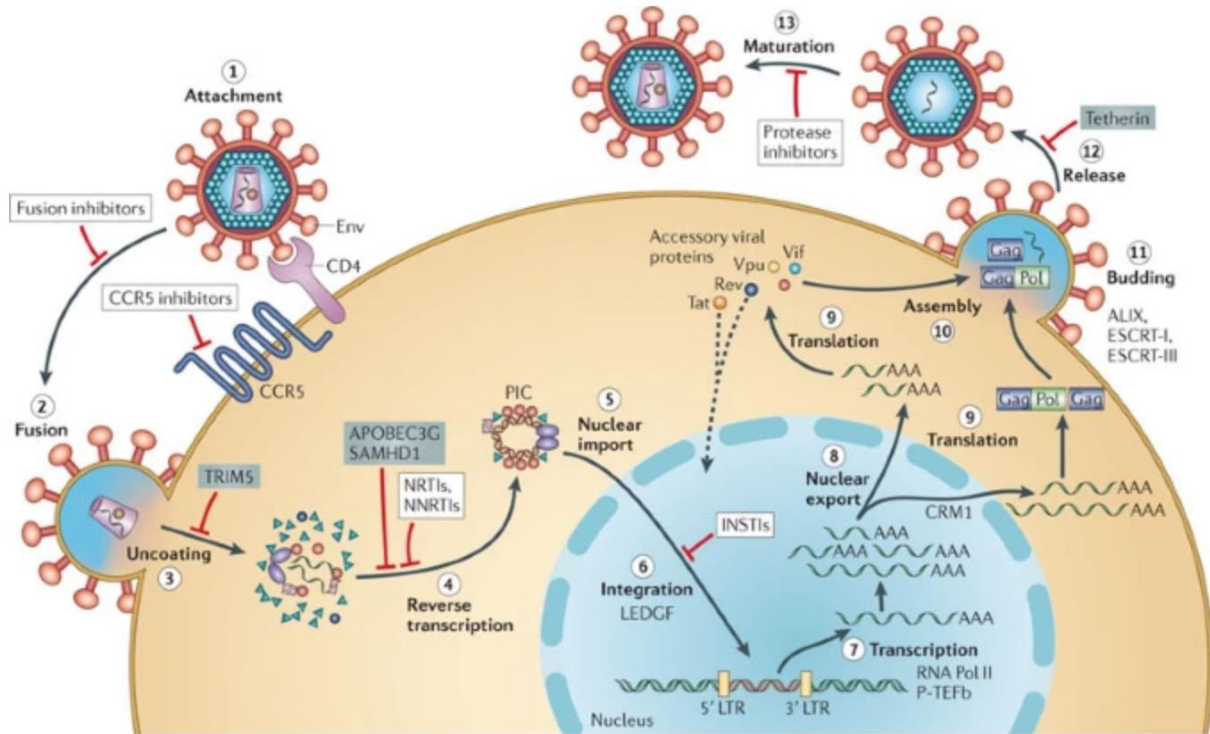


**Figure 5. Overview of the HIV-1 replication cycle (from Engelman et al).** The infection cycle of HIV-1 begins when the envelope glycoprotein (Env) binds the CD4 receptor and the co-receptors CCR5 or CXCR4, leading to viral-to-cellular membranes fusion and to the entry of the viral content into the cell (CCR5 in figure, steps 1-3). The viral genome contained within a protein complex, the viral core, then migrates to the nuclear pore and into the nucleus, while the viral RNA genome is reverse transcribed in double-stranded DNA (steps 4-5). The exact timing of these events has been recently revisited so that, according to some reports, reverse transcription and uncoating occur directly at the nuclear pore or even inside the nucleus. The viral DNA is then integrated into the host genome, where it is transcribed as a cellular gene giving raise to multiple viral proteins. Some of these proteins assemble into virions at the plasma membrane and are released outside the cell (steps 7-13). Several of these steps are targeted by either drugs already in use in clinical practice or by antiviral restriction factors. INSTI, integrase strand transfer inhibitor; LTR, long terminal repeat; NNRTI, non-nucleoside reverse transcriptase inhibitor; NRTI, nucleoside reverse transcriptase inhibitor.

The final consequence is the incorporation of less mature envelope proteins into the new viral particles and the underlying decrease in their infectivity. They subsequently showed that the ability to interact with the HIV-1 envelope protein was a property retained by the IFITM3 protein from a non-human primate (Wilkins et al., 2016). However, they did not show whether IFITM3 from non-

human primates also induces the decline in mature envelope incorporation in virions. Recently, there are two teams together showed that the sensitivity to the defect of infectivity induced by IFITMs varied according to the strain of HIV used (Wang et al., 2017). They showed, in the case of IFITM3, that the level of inhibition of infectivity of the different strains was correlated with the level of defective maturation of the envelope protein. In addition, transmission of the "V3 loop" region of the envelope of a strain resistant to IFITM3 confers resistance to a strain previously susceptible to the defect in infectivity induced by IFITM3. The results of these three studies (Wang et al., 2017; Wilkins et al., 2016; Yu et al., 2015) show that the IFITM2 and IFITM3 proteins decrease the amount of mature envelope incorporated into virions. These three studies have in common that they used the HEK 293T cell line (renal embryonic cells) as virus-producing cells. However, two other teams did not observe any defect in the incorporation of mature envelope induced by IFITMs when they are produced in SupT1 (T cell line) or U87 (neuroblastic cell line) (Compton et al., 2014; Compton et al., 2016; Foster et al., 2016). These two teams used the NL4-3 strain of HIV-1, which is however sensitive to the failure of mature envelope incorporation induced by IFITM3 in the study. Viruses produced in SupT1 do indeed have an infectivity defect when produced in the presence of IFITM3 (Compton et al., 2014). In the study using the U87 line, the authors looked at the effect of the expression of IFITMs on replication, so we have the inhibitory effect of IFITMs in target cells and producer cells and we cannot know if viruses produced in the presence of IFITMs nonetheless exhibit a defect in infectivity in the absence of a decrease in the incorporation of the envelope protein (Foster et al., 2016). Viruses produced in HEK293T have a defective mature envelope incorporation when produced in the presence of a high amount of IFITM3 (Compton et al., 2016). These different studies show that the effect of IFITM2 and 3 on the maturation and incorporation of the envelope protein depends on the cell type. While this partly explains the defect in infectivity of the viruses produced in HEK293T, it does not explain

why IFITM1 also induces a defect in infectivity when it does not interact with the envelope and why we have a defect of infectivity of viruses produced in other cell types without reducing their amount of incorporated envelope. There are one or more unknown mechanisms.

It is not known whether incorporation of IFITMs into viruses is necessary or sufficient to induce the defect in infectivity. Results indicate that the amount of IFITMs incorporated does not correlate with antiviral activities (Foster et al., 2016; Tartour et al., 2014; Yu et al., 2015). Another study, however, demonstrated the importance of the localization of IFITM3 to induce the defect in infectivity (Compton et al., 2016). An IFITM3 mutant lacking the endocytosis motif is localized predominantly to the plasma membrane, is incorporated in greater quantities into viruses and induces a defect in increased infectivity. The importance of incorporation to induce infectivity defect is unclear. Several hypotheses are conceivable. It is possible that the physical presence of IFITMs in the viral membrane disrupts membrane fluidity passively or actively. It is also possible that their incorporation is only a side effect of their presence at the site of viral budding. The defect in infectivity is then only a reflection of their effects in the producer cells which disrupt the production of fully infectious viral particles. Their presence in producer cells is likely to modify the properties of the cell's lipid membranes in the same way as in target cells (lipid or protein composition). As the viral membrane derives from the cell membrane, it will be impacted.

Most studies focus on the defect in infectivity induced by IFITMs. We have already seen that IFITMs decrease viral production (Chutiwitoonchai et al., 2013; Lu et al., 2011). This is regularly observed in the various studies without new explanations being found. In general, it has been observed that the decrease in viral production is observed at high amounts of expression of IFITMs and that the effect is stronger for IFITM1 than IFITM2 and 3 (Compton et al., 2016; Wang et al., 2017; Wilkins et al., 2016).

## **2.5 Mechanism of membrane fusion inhibition by IFITMs**

IFITMs have been soon recognized as inhibitors of viral-to-cellular membrane fusion (Figure 6). However, the underlying mechanism through which IFITMs achieve this goal remains debated. IFITM3 has been shown to interact with the vesicle-membrane-protein-associated protein A (VAPA) and to disrupt the binding of this protein with the oxysterol-binding protein (OSBP), a key player in cellular cholesterol homeostasis (Amini-Bavil-Olyaei et al., 2013). As a result of this interaction, the authors indicated a surge in endosome-associated cholesterol that could have explained their increased rigidity and lower propensity to undergo fusion with viral membranes. This model however has not been confirmed by following studies, including from our laboratory that failed to observe an increased in the intracellular levels of cholesterol in the presence of IFITM3 (Desai et al., 2014; Lin et al., 2013; Wrensch et al., 2014). Therefore, although modulation of the lipid composition of membranes remains an attractive hypothesis to explain the membrane fusion impairment, whether this is at play in the case of IFITM3 and of IFITMs in general, remains a matter of speculation.

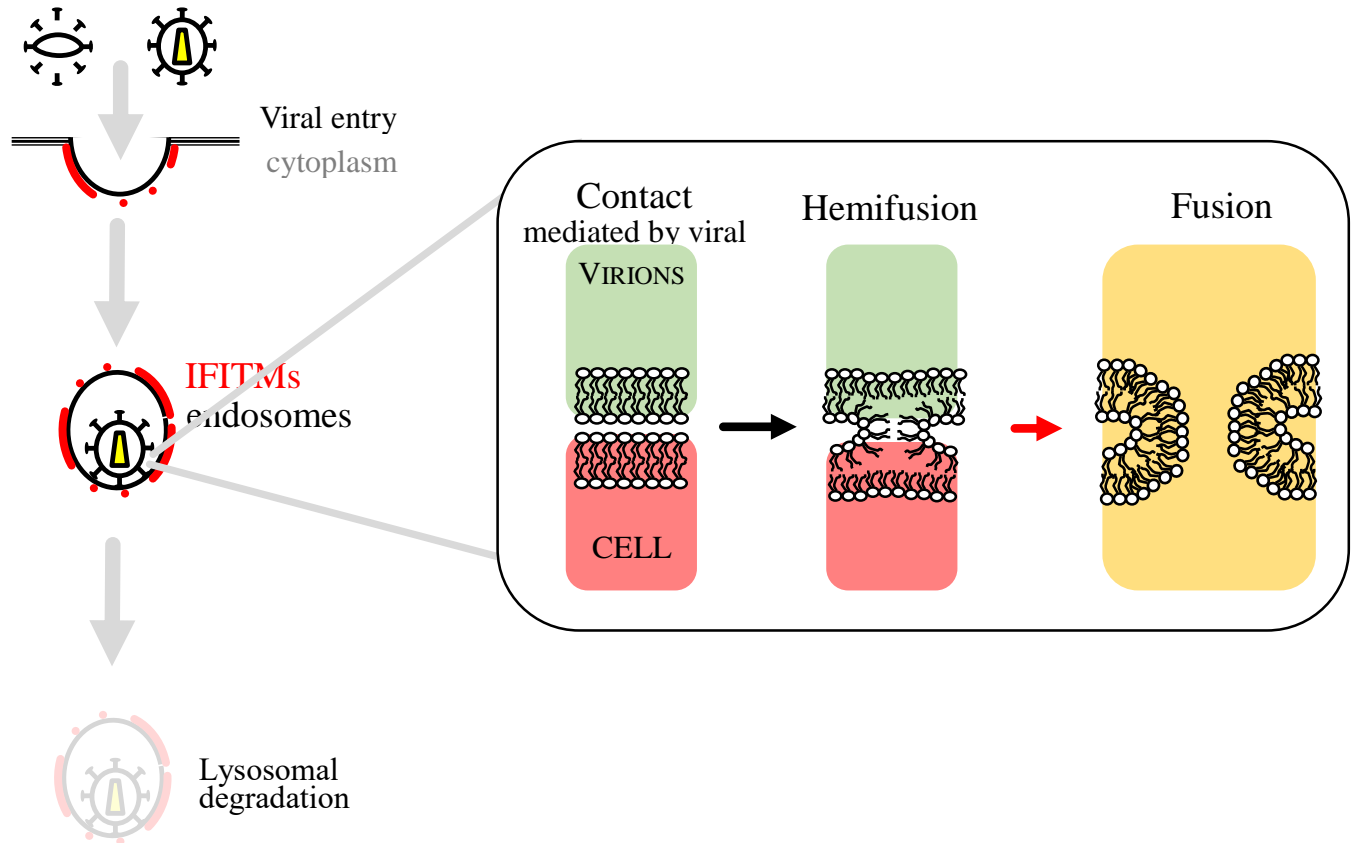


**Figure 6. Mechanism of membrane fusion.** After viral glycoprotein-cellular receptor binding, the first leaflet of viral and cellular membranes fuse (a process called hemifusion), followed by the fusion of the second leaflet and the formation of a functional pore through which viral material can access the cytoplasm. Most of the studies have been carried out on IFITM3 that inhibits the transition between hemifusion to full fusion.

However, it remains of interest that amphotericin B, which forms complexes with sterols and is known to fluidify membranes (Kamiński, 2014), is able to oppose the negative effects of IFITMs in viral infection, suggesting that lipids may play a role in the antiviral effects described for these antiviral factors.

A second hypothesis is the modification of the properties of membranes (fluidity, curvature and composition). Two studies have shown that the presence of IFITMs reduces membrane fluidity and induces negative membrane curvatures that are detrimental to fusion (Li et al., 2013; Lin et al., 2013). We do not know how the IFITMs induce these phenomena. It is known that IFITM3 can

form multimers thanks to two phenylalanines located in its first hydrophobic domain (John et al., 2013). It is thus assumed that the IFITMs by interacting together form an intramembrane network which decreases membrane fluidity. It is also possible that they modify the membrane fluidity by modifying the protein or lipid composition of the membranes. Recently, a study identified the membrane metalloprotease ZMPSTE24 as a cell partner.

### **3. Other physiological roles of IFITM proteins**

#### **3.1. Involvement in placental dysfunctions**

The fusion of trophoblast cells into a multinucleated syncytiotrophoblast (ST) layer is a critical step of placental development and this step relies on membrane-to-membrane fusion events. A recent study clearly showed that IFITM overexpression, as it could be observed upon IFN signaling and viral infection, was responsible for IFITM-driven inhibition of trophoblast fusion and fetus abortion (Zani et al., 2019). If mechanistically this study is in perfect line with the reported function of IFITMs as membrane fusion inhibitors, they indicate that IFITMs may play deleterious effects on the cell physiology. In a more physiological perspective, they also raise the possibility that viral infections, which are normally associated to IFN production, may also exert negative effects on specific processes and lead for instance to fetus abortion.

#### **3.2. Regulation of immune responses**

In addition to their direct antiviral action to fight against viral replication, several studies have shown that IFITMs proteins may play a more general regulatory role in immune responses. Indeed, a study has shown that IFITMs may participate in the transmission of the antiviral state between cells by being incorporated into exosomes. Exosomes are extracellular vesicles that contain a number of cytoplasmic elements (RNA, proteins) and that deliver them to neighboring cells. In this context, exosomes incorporating IFITM3 have been shown to protect target cells from subsequent Dengue virus infection (Zhu et al., 2015), suggesting that through mechanisms that remains to be determined, IFITMs may contribute to the overall establishment of an antiviral state. However, in

light of their action as membrane fusion inhibitors, the results of this study are nevertheless paradoxical insofar as we know, the presence of IFITM3 should reduce the ability of exosomes to fuse with target cells and to diminish the ability of such vesicles to deliver their content. It is surprising that exosomes containing IFITM3 are able to fuse with the membrane of target cells.

A recent study also suggested a role for IFITM3 as a negative feedback regulator of IFN responses (Jiang et al., 2018). The authors used the Sendai virus which is not blocked by IFITM3 and which induces a potent secretion of interferon from infected cells. They observed that the overexpression of IFITM3 prevented the secretion of interferon from infected cells in a mechanism that involved the autophagic degradation of IRF3, a factor transcription essential for the synthesis of interferons (Feeley et al., 2011; Yount et al., 2012). If this result is confirmed, it would suggest that IFITM3 could also act as a negative regulator of type I interferon responses and thus contribute both to viral inhibition at early time points and to IFN-I responses silencing at late times after induction. This would be the first example of protein capable of acting both as a direct antiviral effector, as well as a direct feedback regulator of IFN responses.

Finally, a single study showed that IFITM3 could play a role in the migration of antigen-presenting cells in mice undergoing viral infection (Infusini et al., 2015). Indeed, the authors showed that during infection with Influenza virus, the overexpression of IFITM3 in respiratory dendritic cells was necessary for two things: to fight the viral infection and to allow the migration of the dendritic cells to the lymph nodes to start adaptive immune responses. In the absence of upregulation of IFITM3, dendritic cells were more susceptible to infection and did not migrate to lymph nodes. While it is difficult to dissect the roles of IFITM3 between these two functions because infected and uninfected DCs could exhibit distinct migratory properties linked only to their infected/uninfected status, this study raises the possibility that IFITMs may exert a role during cell

migration, property that was first associated to these proteins in mice more than a decade ago (see below).

### **3.3. Involvement in carcinogenesis, migration of primordial germ cells and osteogenesis**

Prior to 2009 and the discovery of their antiviral functions, IFITMs were first studied for their roles in functions other than viral infection.

Perhaps not surprisingly for IFN-regulated proteins, IFITMs are overexpressed in several types of tumors: colon, stomach, head and neck, breast, and glial tumors (Hatano et al., 2008; Hu et al., 2014; Li et al., 2011; Yang et al., 2013; Yu et al., 2011; Zhao et al., 2013) and the increased expression of IFITMs can even be used as a marker of cancer progression, in particular for colon tumors (Andreu et al., 2006; Fan et al., 2008). While this may suggest a pro-tumoral role, other studies have shown that the artificial upregulation of IFITM proteins inhibits cell proliferation and cancer cell invasion (Hatano et al., 2008; Yang et al., 2013; Yu et al., 2011). For example, IFITM1 is involved in the antiproliferative action of interferon  $\delta$  and acts by stabilizing the p53 protein (Yang et al., 2007) and IFITM1 has also been shown to be part of a membrane complex composed of CD81, CD19 and CD21 resulting in cell cycle arrest in B lymphocytes (Bradbury et al., 1992). A more indirect role has been hypothesized more recently following the observation that the presence of IFITM2 in macrophages present near pancreatic tumors leads to the secretion of cytokines promoting tumor cells (Rosati et al., 2015) and in this case a receptor like function has been postulated. As such, the links between cancer and IFITMs appear unclear and highly dependent on the cellular context.

IFITMs were also shown to be important in the establishment of primordial germ cells during development in knockout *ifitm* mouse models. However, following studies failed to confirm such role, as these mice show no developmental problems (Desai et al., 2014; Lange et al., 2008; Tanaka et al., 2004; Tanaka et al., 2005).

Finally, the IFITM5 protein has so far no antiviral role, but it has been clearly linked to osteogenesis imperfecta, a genetic disease characterized by smaller bones with deformities. IFITM5 is indeed also called BRIL ("Bone Restricted IFITM-like protein") and is involved in bone mineralization (Moffatt et al., 2008). Several mutations have been identified in patients affected by this disease most of which result in proteins that are severely truncated or highly unstable (Farber et al., 2014; Hanagata, 2016). In agreement with their role in this disease, knockout mice for *ifitm5* exhibit smaller bones although without deformities (Hanagata et al., 2011).

#### **4. IFITM3 Polymorphisms in humans**

A few polymorphisms have been identified in the *ifitm3* gene in humans (John et al., 2013). In particular, the rs12252 T / C polymorphism has been associated with a high hospitalization rates for severe forms of influenza in Great Britain (Everitt et al., 2013). The frequency of the rs12252 C allele is low in European and African populations, but its frequency is high in Asian populations (Zhang et al., 2013). The CC genotype is overrepresented in patients hospitalized with severe influenza compared to the normal TT genotype. This polymorphism (C instead of T) is predicted to alter a splice site of the *ifitm3* gene and result in the formation of a protein truncated by the first 21 amino acids. We have previously seen the importance of the N-terminal part of the IFITM3 protein for its localization and therefore its antiviral activity. In vitro studies have shown that this

truncated protein (called  $\Delta 21$ ) has a different cellular localization from the wild protein (Jia et al., 2012; Williams et al., 2014). Unlike wild-type IFITM3, IFITM3  $\Delta 21$  is localized at the plasma membrane. Therefore, its antiviral activity against the entry of influenza virus (which enters through the endosomal route) is reduced. However, the IFITM3  $\Delta 21$  used in these studies was created by cloning and the existence of such truncated protein has never been demonstrated in people carrying the rs12252C allele and RNAseq data failed to identify mRNA forms corresponding to the expected IFITM3 splice variant in individuals that are homozygous for the rs12252C allele (Randolph et al., 2017). As such, the relevance of this association at the protein level, remains debated, despite the fact that several studies have confirmed the association of this polymorphism with cases of severe influenza (Lee et al., 2017; Wang et al., 2014; Xuan et al., 2015; Yang et al., 2015; Zhang et al., 2013), albeit not all (Gaio et al., 2016; Mills et al., 2014; Randolph et al., 2017).

Interestingly, this polymorphism has also been associated with a faster progression to the AIDS stage in a Chinese cohort of patients infected with HIV-1 (Zhang et al., 2015) and has also been associated with the severity of Hantaan virus infection (Yang et al., 2015). In the case of HIV-1, this association is paradoxical, because the resulting hypothetical IFITM3  $\Delta 21$  protein displays increased antiviral effects against HIV, whether it is present in target cells or in virus-producing cells (Compton et al., 2016). Given that the resistance to IFITMs in the case of HIV-1 appears dynamic and that chronic strains are less inhibited by IFITM1 and plasma membrane concentrated IFITMs (as should be the IFITM3  $\Delta 21$  isoform) (Foster et al., 2016), this may provide a potential explanation as to why people infected with HIV-1 and carrying the rs12252 C allele progress more rapidly to AIDS.

Overall, despite the existence and the association of a main polymorphism of IFITM3 to increased disease severities, doubts still exist on the significance and existence of the hypothesized splice variant in individuals carrying this polymorphism. As to the existence of additional polymorphisms in IFITM3 as well as in other IFITM members, little to no studies have been carried out so far (Naderi et al., 2016; Shen et al., 2013), so that it is difficult to conclude as to their true significance in disease severity against several viruses.

## 5.The ER-Golgi secretory pathway

### 5.1. ER and Golgi organelles

The endoplasmic reticulum (ER) is a membrane contiguous with the nuclear membrane and represents the entry organelle for the secretory pathway. Proteins synthesized from ribosomes and bearing an ER-docking signal sequence bind to the rough ER and are progressively pushed inside the ER lumen. Some proteins, like ER enzymes remain resident in the ER. However, the majority progresses through the *cis*, *median* and *trans* Golgi where they are modified, glycosylated and trafficked to their final destination. It is estimated that about 25% of the human proteome may transit through the ER-Golgi (Gomez-Navarro and Miller, 2016).

The Golgi apparatus is adjacent to the nucleus and the ER in mammalian cells and is deemed as a central intracellular membrane-bound organelle. Its structure as it can be observed by electron microscopy (EM) is in most cells composed of stacks or cisternae overlaying one another, with multiple stacks often lined up and interconnected by tubular structures to form a ribbon. The Golgi stacks are polarized and mainly divided into three functional parts: the *cis*, the *median* and the *trans*-Golgi. Between the ER and the Golgi is the ERGIC (ER-to-Golgi intermediate compartment), a compartment located adjacent to ER exit sites.

Protein movement between ER and Golgi stacks involves vesicles which range in size from 60-90 nm that can move forward (coatamer protein complex II, COPII-mediated) or backward (coatamer protein complex I, COPI-mediated), movements that are important for the flow and the

maintenance of both lipid and protein homeostasis within the cell (this part will be detailed below and a schematic and simplified representation is provided in Figure 7).

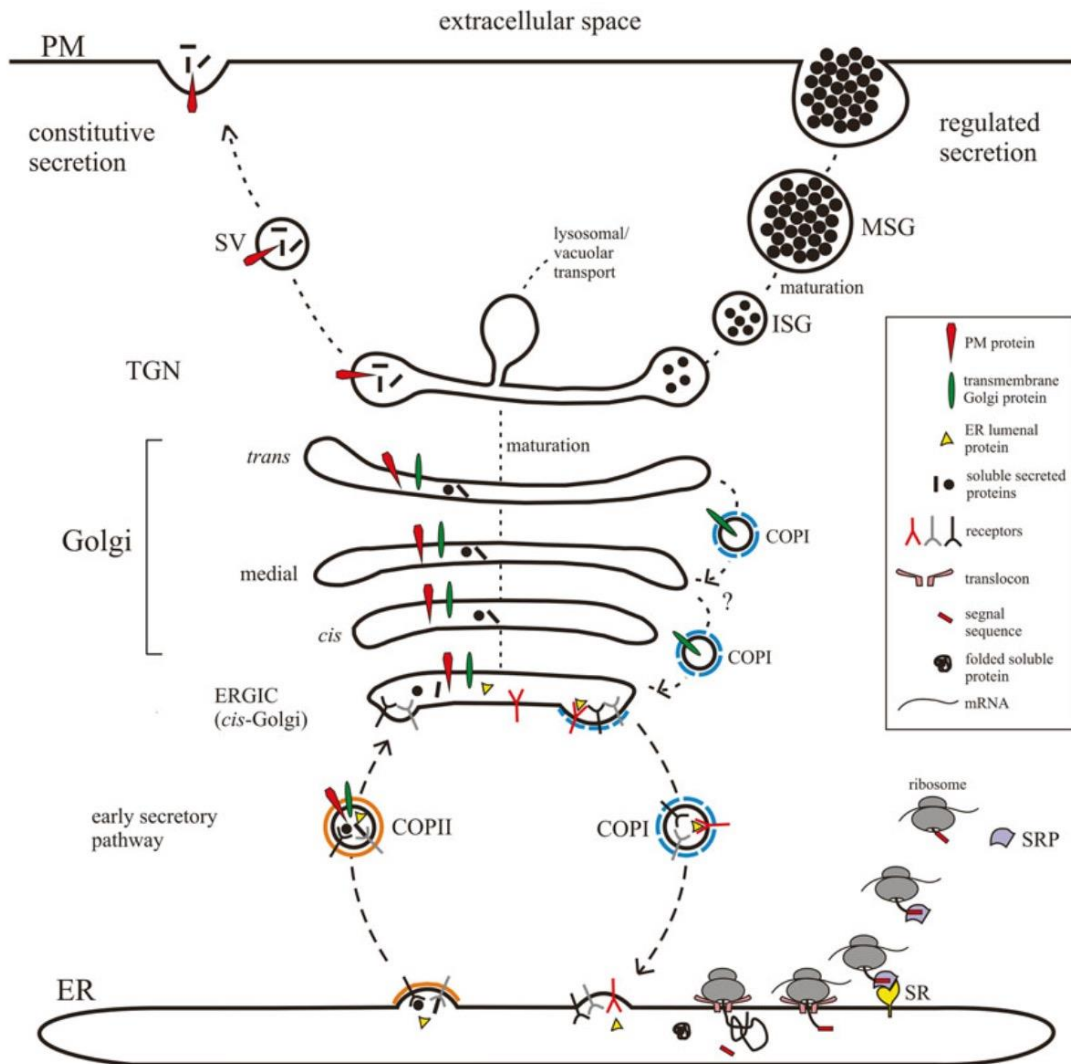


**Figure 7. Schematic representation of the ER-Golgi secretory pathway.** Proteins are recognized through signal sequence recognition by the signal recognition particle (SRP) and are translocated into the ER lumen. In the ER, the signal sequence is removed and proteins are then passed through the ERGIC (in animals) or the cis- Golgi (in yeasts and plants) via COPII vesicles. PM proteins and secreted proteins are transported via cisternal maturation to the Trans-Golgi network (TGN), whereas integral Golgi proteins remain on site. At the TGN, proteins destined to be secreted are sorted in secretory vesicles (SVs) or immature secretory granules (ISGs).

Starting from the 1960s, morphological studies have shown connections in the space between cisternae that are involved in the adhesion of cisternae into stacks (Cluett and Brown, 1992; Franke and Scheer, 1972; Mollenhauer, 1965), which were later on identified as Golgi matrix proteins (Slusarewicz et al., 1994). Since then, several Golgi matrix proteins have been identified to be responsible for maintaining the architecture and functions of the Golgi apparatus.

Golgins are a family of Golgi-associated coiled-coil proteins that are necessary for vesicle tethering at the Golgi and maintenance of Golgi integrity (Gillingham and Munro, 2016; Muschalik and Munro, 2018; Witkos and Lowe, 2015) and also involved in the dynamic regulation of the structure of the organelle itself. Golgins lack significant sequence homology between themselves and localize to different regions of the Golgi, which is indicative of specific functions. Most golgins are peripheral membrane proteins attached to Golgi membranes via their C-ter and all associate to small GTPases of the Rab, Arf and Arl families (Munro, 2011; Sinka et al., 2008). These interactions mediate both membrane attachment and selective localization of specific golgins to a specific sub-compartment of the Golgi (Witkos and Lowe, 2015). The coiled-coil regions provide the golgins with an extended structure required for the tethering function, while the interactions with Rab GTPases control these molecules in their open (extended) or closed (folded) confirmation (Cheung et al., 2015). In addition, golgins often contain specific sequence and structural features at the N- and C-terminal termini that allow them to recognize vesicles and Golgi cisternal membranes based on the curvature and lipid composition of the membranes (Drin et al., 2007; Drin et al., 2008; Magdeleine et al., 2016).

Among golgins, GM130 (also known as GOLGA2) was the first identified Golgi matrix protein and is currently one of the best-studied, as it contributes to Golgi ribbon morphology and is involved in vesicular transport. GM130 is predominantly concentrated in the *cis*-Golgi (Nakamura

et al., 1995), where it forms a stable complex with GRASP65. Depletion of GM130 leads to the disruption of the Golgi ribbon and protein glycosylation defects (Puthenveedu and von Zastrow, 2006). However, GM130 knockout (KO) mice are viable although they exhibit Golgi fragmentation and impaired secretory trafficking especially in the central nervous system and in Purkinje neurons in particular, resulting in cell death and ataxia (Liu et al., 2017).

Besides the Golgi matrix proteins and their cofactors described above, other proteins including SNAREs, kinases, methyltransferases, and GTPases have also been reported to be involved in the structural maintenance of the Golgi.

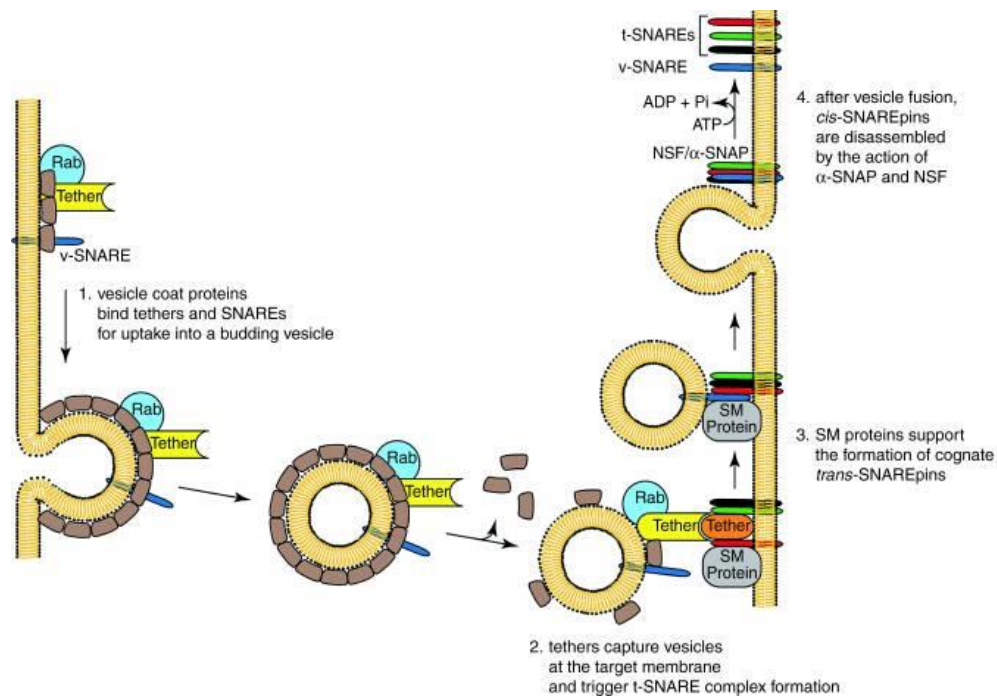


**Figure 8. Fusion between Golgi SNAREs vesicles (from CSH perspectives).** SNARE-mediated membrane fusion and SNARE recycling. SNAREs are recruited by vesicle coat components for uptake into a budding vesicle. The initial interaction of a vesicle with its target membrane is mediated by tethering proteins and a small Rab GTPase. Components of the tethering machinery trigger the formation of t-SNARE complexes, which assemble with their cognate v-SNAREs, driving membrane fusion between the vesicle and the receiving Golgi compartment. In the presence of SNAPs, ATP-hydrolysis by NSF segregates v- and t-SNAREs for another round of fusion.

SNARE proteins mediate vesicle fusion and will be detailed later on. Instead Rab proteins are a group of key regulators of mammalian Golgi organization. Many Rab proteins, including Rab1, Rab2 and Rab8 (Aizawa and Fukuda, 2015), Rab18 and Rab43 (Dejgaard et al., 2008), Rab6/41 (Goud et al., 1990; Martinez et al., 1997), and Rab30 (Kelly et al., 2012), play a role in Golgi structure organization (reviewed previously in detail, (Goud et al., 2018)). Rab proteins can switch between an inactive GDP-bound form and an active GTP-bound form. It has been proposed that Rab proteins involved in Golgi functions can be divided into two categories: class 1 Rabs, for which the Golgi ribbon is disrupted by Rab inactivation but appears normal with overexpression; and class 2 Rabs, in which Rab inactivation has little effect on Golgi ribbon organization, while overexpression leads to the redistribution of Golgi enzymes to the ER (Liu and Storrie, 2015). Overall, the entire morphology and functions of the Golgi apparatus are the object of intense regulation, which is not surprising in light of the central place of this organelle in the cellular physiology.

## **5.2. Anterograde and Retrograde transport**

With the exception of ER and Golgi resident proteins, proteins that enter the secretory pathway must first transit from the ER to the Golgi and then leave the Golgi to reach their final destination at the plasma membrane, lysosomes etc. The transport of this cargo is mediated by multiple-vesicular carriers that bud from one compartment on the pathway and fuse with the next (forward transport). Instead, components that must be recycled back use a similar method to mediate retrograde or backward transport. These movements are of course highly important to maintain the protein and lipid homeostasis in the entire cell.

Vesicular transport in this setting relies in a simplified manner on two components: COPI and COPII multiprotein complexes that form the vesicle itself and a docking system that is responsible for the binding and fusion of the vesicle with the Golgi stack. This last system is specified by interactions between pairs of vesicle and target soluble N-ethylmaleimidesensitive fusion protein (NSF) attachment protein receptors (v- and t-SNAREs, respectively). Once in apposed membranes, the binding of specific SNAREs pair, induces the fusion between the membrane of the vesicle and the membrane of the stack, leading to the release of the Cargo in the stack, which constitutes an effective movement of the proteins that have entered into the secretory pathway through the compartment.

This mechanism resembles loosely the fusion between viral and cellular membranes that occur when a viral envelope binds its cellular receptor.

Even in this case, SNAREs play a key role in the maintenance of the Golgi and indeed depletion of the Vesicle-associated membrane protein 4 (VAMP4) a v-SNARE located at the TGN and shown to play a role in retrograde trafficking from early endosomes to the TGN (Steggmaier et al., 1999) leads to Golgi fragmentation. Similarly, depletion of the cognate SNAREs of VAMP4, syntaxin 6, syntaxin 16, and Vti1a also lead to similar phenotypes.

Most SNAREs are C-terminally-anchored transmembrane proteins and their main body is exposed in the cytoplasm. In the simplest model of SNARE function (Figure 8), transport vesicles carry specific vesicle-membrane SNAREs (v-SNAREs) that leave one stack and dock into the next through target-membrane SNAREs (t-SNAREs) the binding to which induces membranes fusion. After the dissociation of the v-SNARE–t-SNARE complex, the v-SNAREs are recycled through retrograde transport to refurbish the compartment for novel cycles of transport. A series of v and t-SNAREs interacting couples have been characterized over the years.

For example, GS15 was identified as homologous to other SNAREs (Xu et al., 1997) and was later found to be concentrated mostly, although not completely, in the medial-cisternae of the Golgi apparatus. Biochemical studies suggest that it forms a complex with three other SNAREs (Syntaxin5, GS28, and Ykt6) to form a distinct GS15/Syn5/GS28/Ykt6 SNARE complex. From what was observed in the localization data, each cisterna of Golgi contains a mixture of all seven of the subunits comprising the two Golgi-localized SNAREpins, v-rBet1: t-syntaxin 5/membrin, ERS24 and v-GS15: t-syntaxin 5/mYkt6, GOS28, although their ratios in the mixture vary largely across the stack (Volchuk et al., 2004; Xu et al., 2002). Particularly every Golgi cisterna contains varying ratios of two alternative sets of t-SNARE light chains (membrinERS24 vs. mYkt6GOS28) that will compete for binding to a common heavy chain (syntaxin 5), to form one or the other t-SNARE.

Overall, several complexes have been described some of which have a stronger impact in cis, median or trans-Golgi fusion events. What governs the specific enrichment of given v or t-SNAREs at a particular location remains unclear.

## **Objectives**

This thesis was carried out under the supervision of Dr Andrea Cimorelli within "host-pathogen interaction during lentiviral infection" team and was more specifically focused on the study of the biology of IFITM3, an important antiviral factor with a broad spectrum of viral inhibition. Starting from an initial observation carried out in the laboratory on a particular IFITM3 mutant, we have decided to study the role of the CIL in the passage and egress of the protein through the Golgi. The results gathered during my thesis work have allowed me to identify a particular region within the CIL of IFITM3 that regulates the normal egress of this protein through the Golgi. This step is very important as the abnormal retention of IFITM3 in this compartment leads to drastic changes and to a generalized defect in glycoprotein trafficking. These defects appear linked to the ability of Golgi-retained IFITM3 to inhibit fusion between v- and t-SNAREs bearing vesicles, in line with the more general inhibitory functions of IFITMs in membrane fusion.

Importantly, we also determine that the domain that regulates IFITM3 trafficking is conserved across other members of the dispanin A subfamily and functionally conserved in PRRT2, member of the dispanin B subfamily and involved in paroxysmal kinesigenic dyskinesia (PKD), the most common type of paroxysmal movement disorder.

Overall, these results identify a novel region important for the trafficking of IFITM3 through the Golgi and highlight the importance that tight regulation of this process may bear for the cell physiology.

## **Results**

**Identification of a mutation in the CIL loop of IFITM3 that modifies glycoprotein trafficking through Golgi.**

A previous mutagenesis study of IFITM3 (Appourchaux et al. 2019) focused in the identification of domains that regulated the antiviral properties against HIV-1 identified an interesting mutant that was able to consistently decrease the extent of WT HIV-1 envelope incorporation into virion particles (Figure 9a). Given that this phenotype was not observed for WT IFITM3 (or only mildly so), this mutant was not further investigated in this previous work. However, given that IFITM3 has been associated in other studies in possible effects on protein accumulation and that envelope incorporation defects can be due to an ER-Golgi defect, we decided to further characterize this mutant here. Furthermore, the CIL domain is conserved among IFITM proteins, but its functions remain poorly understood.

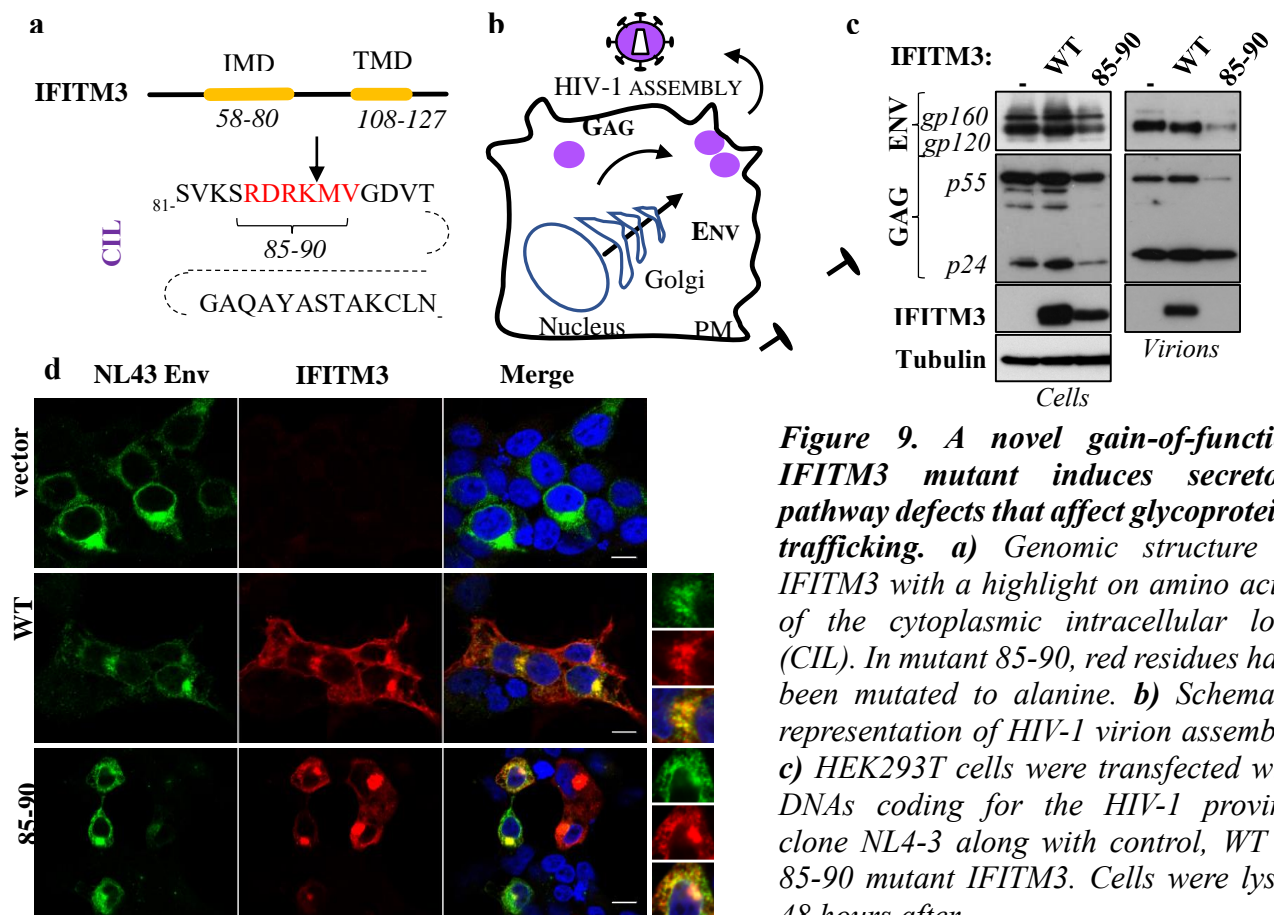
Formation of infectious HIV-1 requires the assembling of two classes of structural proteins: Gag and Env (Figure 9b). While Gag is translated from cytoplasmic mRNAs from free ribosomes, the Envelope glycoprotein undergoes co-translational ER translocation and reaches the plasma membrane following the ER-Golgi secretory pathway. As such, loss of Envelope incorporation in virion particles may reflect potential effects of IFITM3 along this axis that we decided to investigate further.

When transfected into cells infected with HIV-1, the IFITM3 mutant 85-90 induced a moderate decrease in the levels of cell-associated Gag and Env when compared with cells in control group or over expressing WT IFITM3. On the other hand, when the extent of Env proteins incorporated in HIV-1 virions particles was examined, the 85-90 IFITM3 mutant induced a large decrease compared to WT IFITM3 or control (Figure 9c). When examined by confocal microscopy, HIV-1 Env was found to display an important perinuclear localization in the presence of this mutant (Figure 9d). Overall, these observations suggest that the expression of the 85-90 mutant may lead

to a defect along the secretory pathway followed by the HIV glycoprotein with a likely implication of the Golgi apparatus.

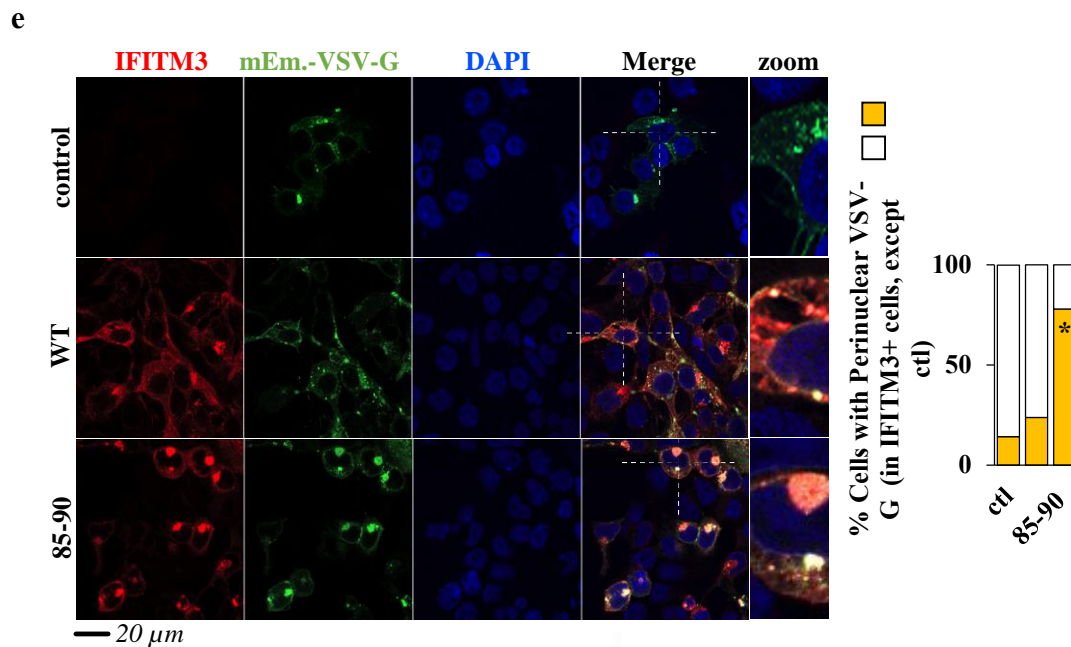
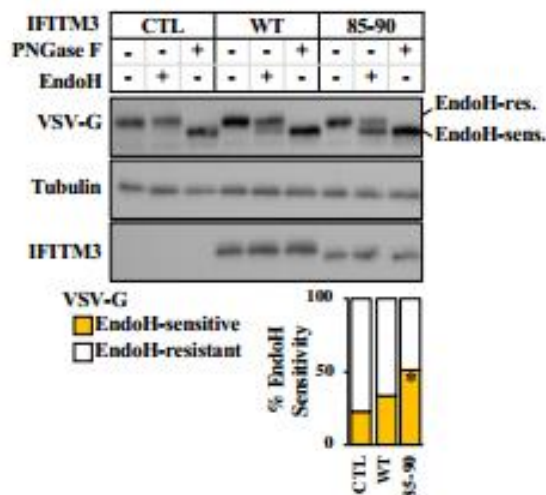
After these initial confirmatory results, we decided to determine whether this defect could be more generally reflective of an interference with Golgi-mediated trafficking, in other viral glycoproteins.

To this end, I co-expressed distinctly the 85-90 IFITM3 mutant and WT IFITM3 along with a fluorescent G protein from the Vesicular Stomatitis Virus fused to a fluorescent reporter (mEm.-VSV-G, Figure 9e). A strong perinuclear accumulation of mEm.-VSV-G was observed in cells expressing the mutant IFITM3 compared to WT group (Figure 9e).



**Figure 9. A novel gain-of-function IFITM3 mutant induces secretory pathway defects that affect glycoproteins trafficking.** **a)** Genomic structure of IFITM3 with a highlight on amino acids of the cytoplasmic intracellular loop (CIL). In mutant 85-90, red residues have been mutated to alanine. **b)** Schematic representation of HIV-1 virion assembly. **c)** HEK293T cells were transfected with DNAs coding for the HIV-1 proviral clone NL4-3 along with control, WT or 85-90 mutant IFITM3. Cells were lysed 48 hours after

transfection, while virion particles released in the supernatant were first purified by ultracentrifugation through a 25% sucrose cushion. Both cellular and viral lysates were analyzed by WB. **d)** HEK293T cells were ectopically transfected with WT NL4-3 DNAs, or the NL43Env plasmid along with the indicated IFITMs. Representative confocal microscopy images presenting the of double-positive cells displaying perinuclear accumulation of Env protein.

**f**

**Figure 9. continued. e)** HEK293T cells were ectopically transfected with DNAs coding for the indicated IFITM3s along with the G protein of the Vesicular Stomatitis virus fused to the mEmerald fluorescent reporter (mEm.-VSV-G), prior to confocal microscopy analysis twenty-four hours later. Representative confocal microscopy images and graph presenting the proportion of double-positive cells displaying perinuclear accumulation of mEm.-VSV-G (binary scoring; three independent experiments; between 50 and 100 cells scored per sample). \*,  $p$  value <0.0001 following a one-way Anova, Tukey's multiple comparison test; non-statistically significant

differences, not shown. **f)** Lysates obtained from cells expressing VSV-G along with control, WT and mutant IFITM3 were either untreated or treated with EndoH or PNGaseF prior to WB and densitometry quantification of the EndoH-sensitive and -resistant VSV-G forms. Panels present representative results, while the graph presents the proportions of EndoH-sensitive and -resistant VSV-G obtained in 5 independent experiments. \*,  $p$  value of 0.0021 following a one-way Anova, Tukey's multiple comparison test over control.

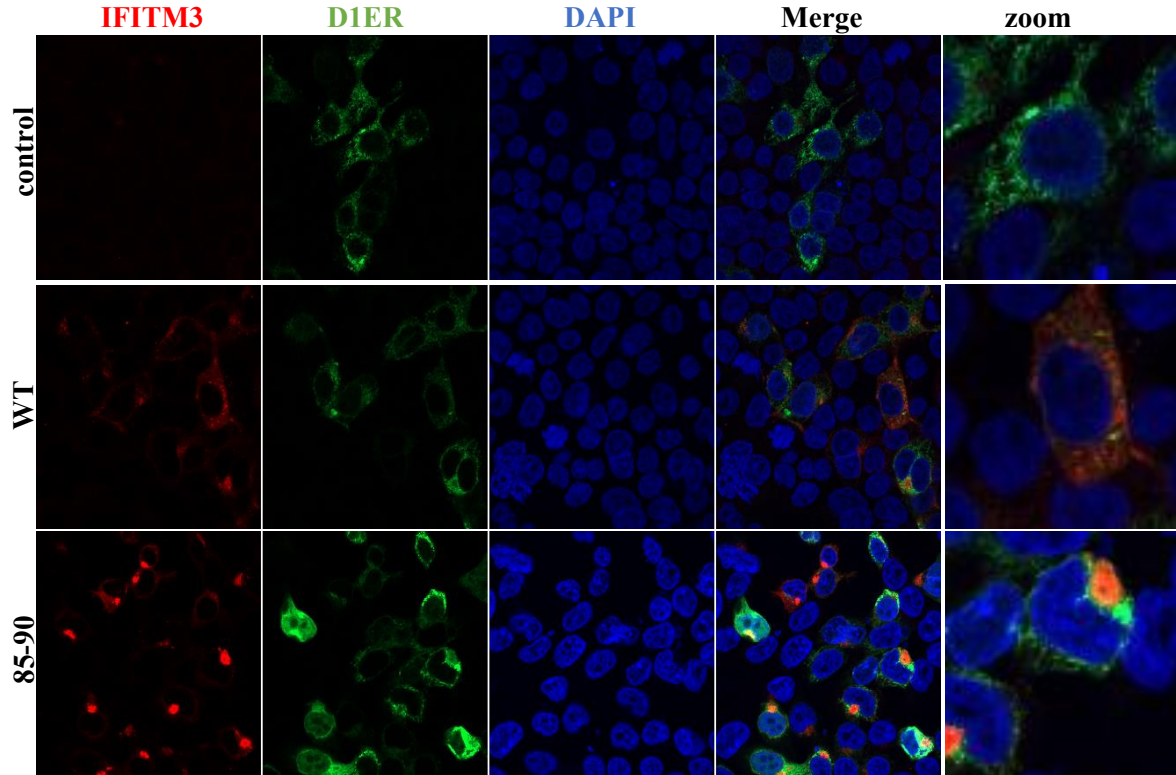
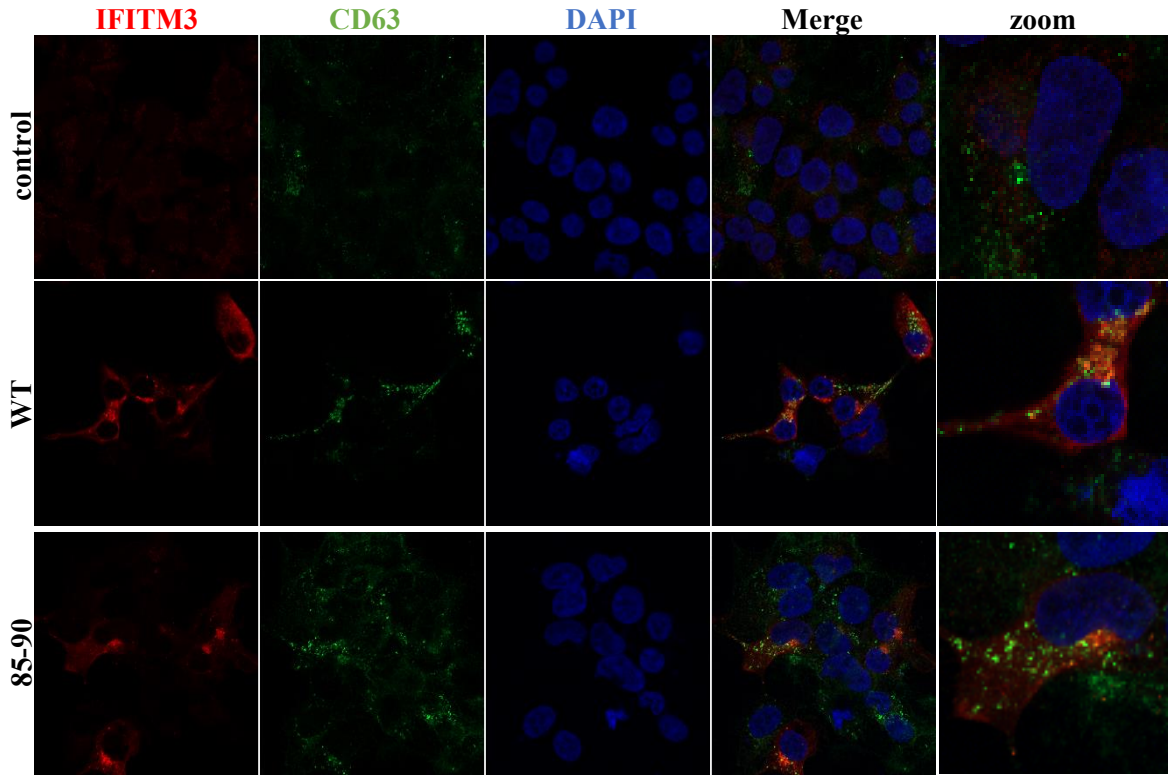
To further confirm a Golgi-related defect, we employed susceptibility to EndoH, a commonly used technique to appreciate progression of glycosylated proteins through Golgi vesicles. Under these conditions, in WT transfected group, the portion of digested VSV-G is less than the non-digested

one; It was converse situation in the mutated 85-90 group, higher portion of proteins be digested by EndoH. We conclude that VSV-G proteins glycosylation and progression through the Golgi were blocked by the presence the mutant 85-90 mutant and to a lower extension from the WT IFITM3 (Figure 9f).

Overall, these results clearly indicate that the 85-90 IFITM3 mutant leads to a disruption of normal Golgi functions, indicating it as a novel gain-of-function IFITM3 mutant. Interestingly, WT IFITM3 seemed to induce some defect in Golgi trafficking although to a very light and non-significant level at these protein levels. The expression of higher levels of IFITM3 and the analysis of the phenotypic changes imparted by them is ongoing.

**The 85-90 IFITM3 mutant accumulates in the cis-Golgi and leads to structural changes in the Golgi apparatus.** To determine better how IFITM3 blocked glycoprotein envelope proteins trafficking, we checked several cellular markers specific for ER, endosomes and Golgi by co-transfection with specific markers or by detection of endogenous proteins. Confocal analysis indicated that the 85-90 IFITM3 mutant did not strongly colocalize with ER or endosomes (Figure 10). Instead, this mutant colocalized with the cis-Golgi marker GM130 (Figure 11a). Furthermore, the mutant induced gross morphological changes in the appearance of the Golgi itself: punctiform in control and WT-IFITM3 expressing cells and inflated in cells expressing the 85-90 IFITM3 mutant. 3D-reconstruction of positive cells (Figure 11b) states better the structural changes.

Through electron microscopy observation, the shape of the Golgi apparatus changed from its classical punctiform distribution to a more shrunk shape also gives a convincing expansion of large



vesicles (Figure 11c, although the Golgi appearance in HEK293T cells even in control cells is not textbook).

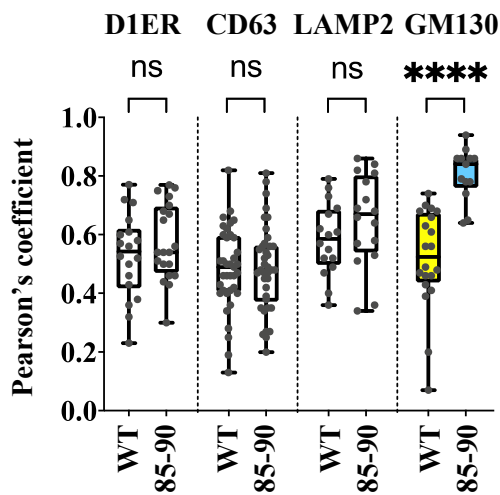
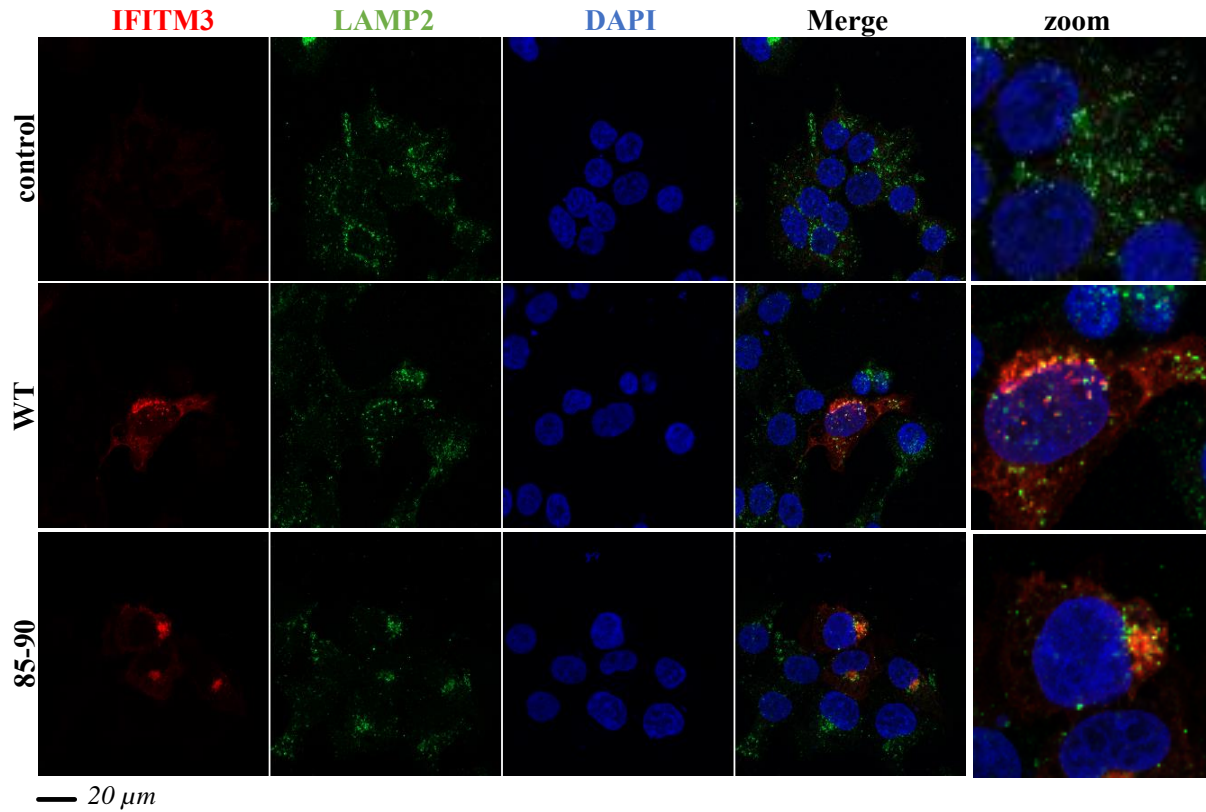


**Figure 10.** The 85-90 IFITM3 mutant does not colocalize with CD63, LAMP2 nor with the ER. HEK293T cells ectopically expressing the indicated IFITM3s, or co-transfected with the ER reporter D1ER were analyzed by confocal microscopy with the indicated markers. Whiskers and boxes plot of the Pearson's colocalization coefficients (25-75 percentiles with individual cells represented as dots;  $n=16$  to 38 per condition in three independent experiments). A one-way Anova with Tukey's multiple comparison test was applied for each marker to evaluate differences in localization between WT and 85-90 IFITM3 mutant (non statistical significant differences are represented by white boxes;  $p < 0.0001$  by colored ones).

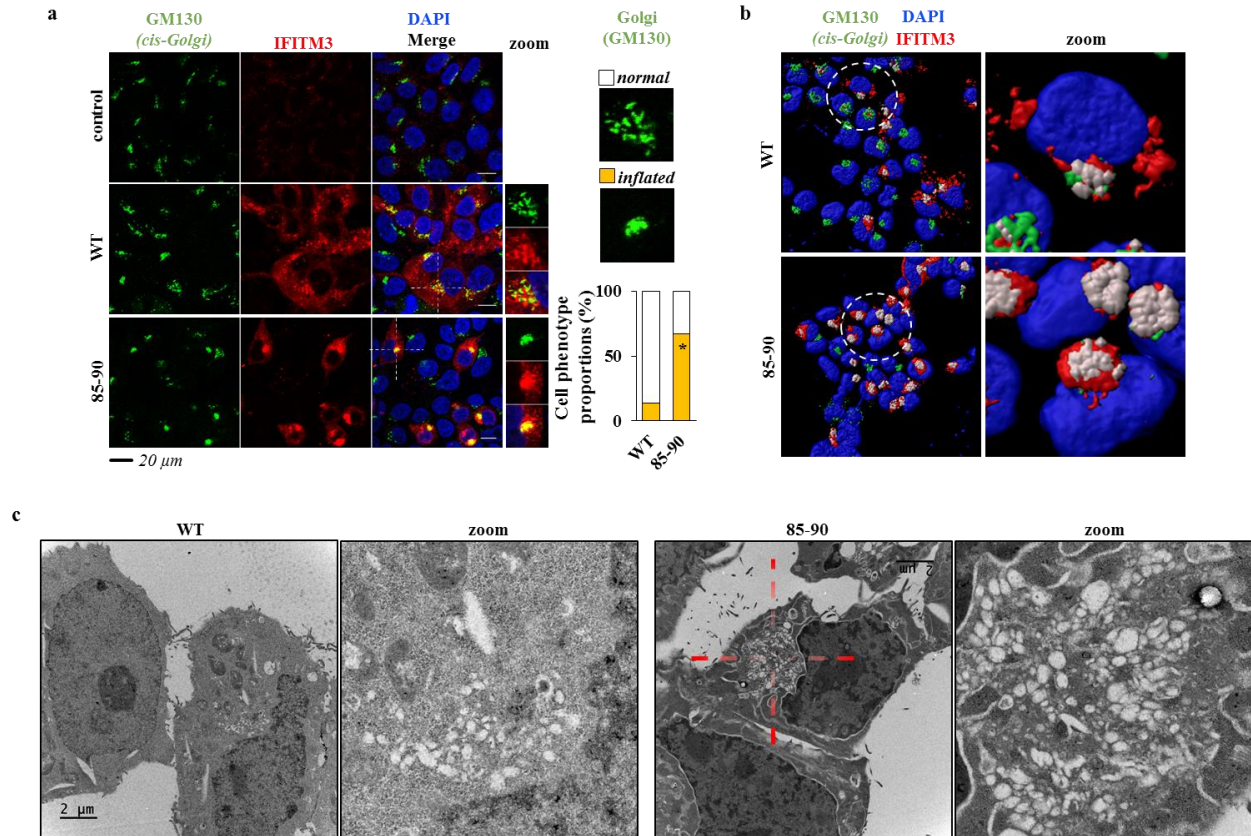


**Figure 11. The 85-90 IFITM3 mutant colocalizes with and induces gross morphological changes in the Golgi. a and b)** Confocal microscopy analysis and 3D-reconstruction of cells expressing the indicated IFITM3 proteins. Representative images and graph presenting phenotype proportions in at least 100 cells scored per condition (binary scoring: inflated or normal Golgi, three independent experiments). \*,  $p=8.3 \times 10^{-9}$  following an unpaired, two-tailed Student *t* test. **c)** Representative electron microscopy analyses of HEK293T cells expressing WT or 85-90 IFITM3 proteins. The region enlarged at the right of each panel corresponds to the red inset.

One of the most broadly studied mechanism of antiviral function of IFITM3 is their ability to interfere with viral-to cellular membranes fusion. We thus hypothesized that dynamic morphological of Golgi could be affected by IFITM3 and its membrane-fusion inhibition property. The routine fusion of v-SNARE vesicles with t-SNAREs compartments is indeed key to maintain protein and membrane fluxes through the Golgi apparatus.

To test this hypothesis, we analyzed the ability of the 85-90 IFITM3 mutant to inhibit the fluorescent resonance energy transfer (FRET) between v and t SNAREs fused to CFP and YFP.

The determination of this kind of fusion inhibition in living cells and in the entire Golgi is complex and most studies have instead used reconstituted and minimal lipid vesicles and components, while we opted for a whole cell approach. In GS15-CFP and ERS24-YFP double positive cells, FRET occurs upon fusion between GS15-CFP and ERS24-YFP bearing vesicles (*v*- and *t*-SNAREs, respectively), as a signal of membrane fusion in this compartment (Figure 12a) while no FRET is expected if membrane fusion does not happen.

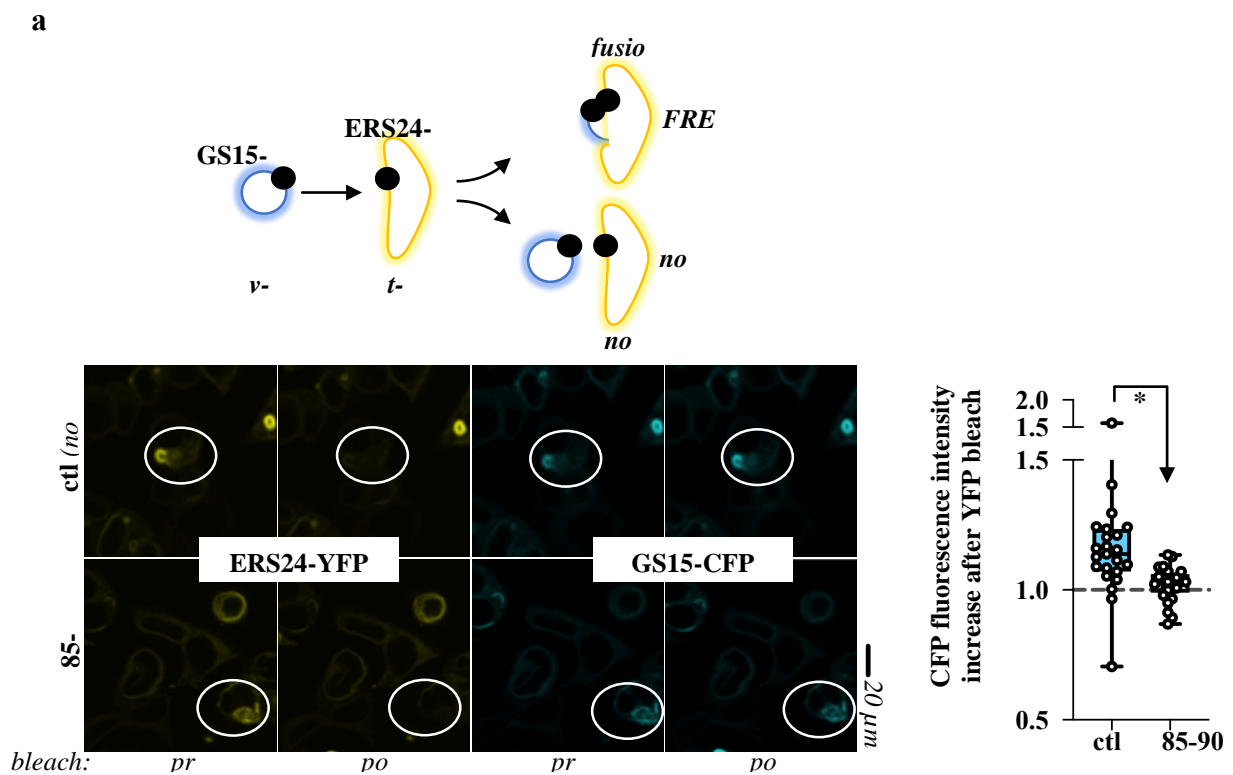


**Figure 12. The 85-90 IFITM3 mutant impairs fusion between *v*- and *t*-SNAREs.** a) Schematic representation of the FRET experiment and representative images pre and post ERS24-YFP bleach. FRET experiments were performed on live HEK293T cells in which an excess of DNA coding for the 85-90 IFITM3 mutant was used over GS15-CFP and ERS24-YFP (five-fold excess) to ensure that the majority of cells analyzed were also IFITM3-positive. The boxes and whiskers plot presents the normalized decrease and values distribution in FRET observed in control and 85-90 IFITM3 expressing cells from three independent experiments and >20 cells examined. \*, *p* value of 0.0008, following an unpaired two-tailed Student *t* test.

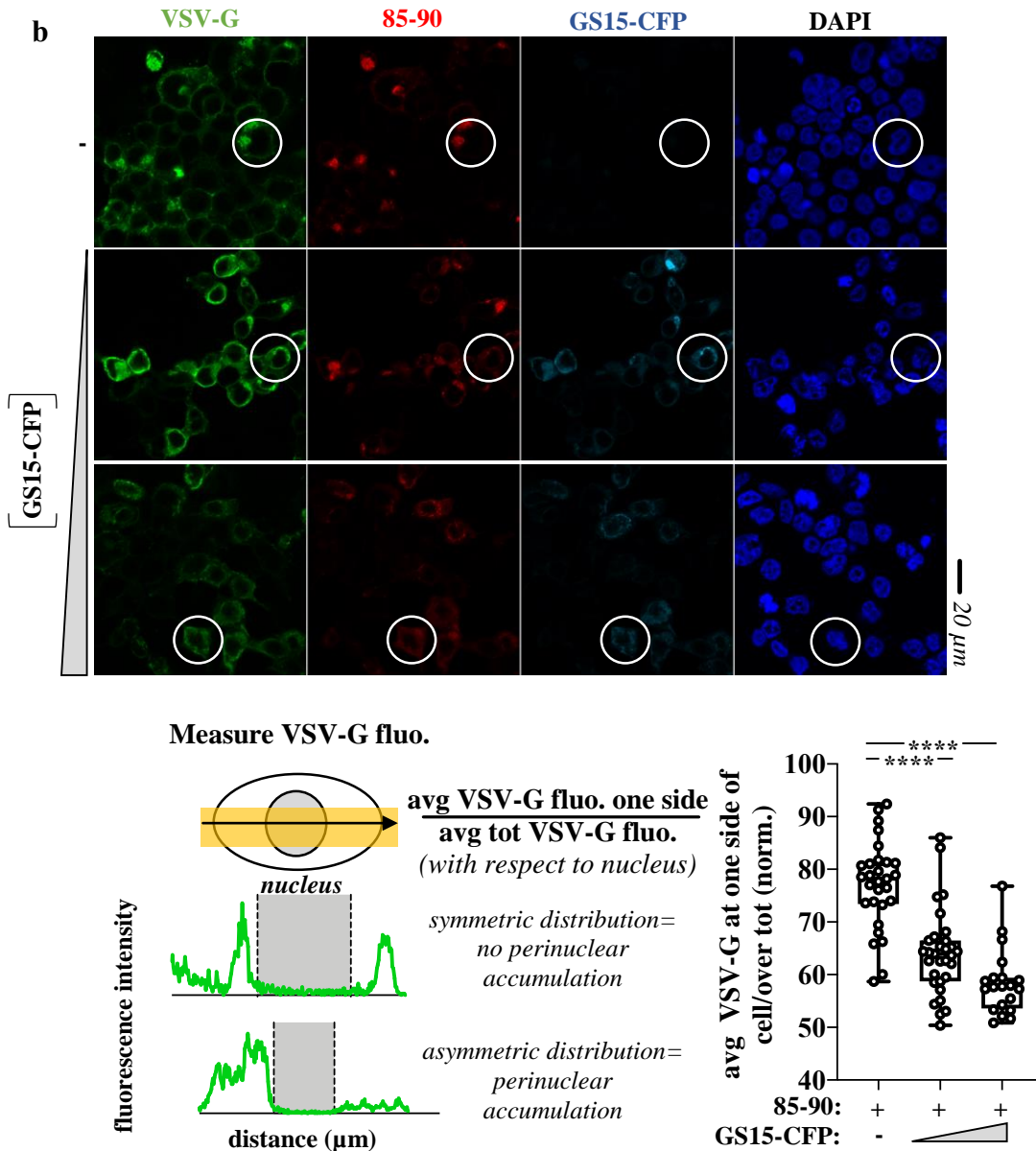


**Figure 12, continued. b)** HEK293T cells expressing constant amounts of 85-90 IFITM3 and VSV-G were co-transfected with increasing amounts of GS15-CFP coding DNA, prior to confocal microscopy analysis (GS15/85-90 ratios of 0.2 and 0.5). Given that VSV-G accumulation in the Golgi leads to its asymmetrical perinuclear distribution in the cell, VSV-G fluorescence was determined for each cell according to the presented scheme. The fluorescence measured over distance in the cell was used to calculate the proportion of VSV-G protein present at one side (the left side was set as the side with higher protein accumulation). Representative pictures and graph presenting the distribution of VSV-G at one side of the cell in triple-positive cells ( $n=2$  with 20 to 31 cells analyzed per condition). White circles highlight example cells of increased FRET (a) and of phenotypic differences in the perinuclear accumulation of VSV-G (b), respectively. \*\*\*\*,  $p$  value of  $<0.0001$  following a one-way Anova, Tukey's multiple comparison test over 85-90 IFITM3 condition with no GS15-CFP.

Experiments were carried out in living cells and under these conditions, the over-expression of the 85-90 IFITM3 mutant in GS15-CFP and ERS24-YFP double positive cells leads to a detectable and statistically significant decrease in FRET compared to the no IFITM3 group (Figure 12a). This indicating that this mutant does indeed interfere with v- to t-SNAREs fusion, in agreement with the major function ascribed to IFITM3 as a membrane fusion inhibitor.

To further support this conclusion, I overexpressed the v-SNARE GS15 and checked whether it could rescue the effect of 85-90 IFITM3 mutant, as v-SNAREs overexpression was reported to bypass membrane fusion defects occurring between Golgi membranes, and we thus hypothesized it could relieve the defect imposed by the IFITM3 mutant. To this end, I co-transfected constant amount of both 85-90 IFITM3 mutant and VSV-G with increasing dose of GS15, and then analyzed the distribution of VSV-G in triple-positive cells (Figure 12b). In this case, we considered the redistribution of VSV-G from an asymmetric to a symmetric distribution by determining the levels of fluorescence at each end of the nucleus. The results obtained indicated that GS15 was able to relieve the perinuclear accumulation of the VSV-G glycoprotein induced by the IFITM3 mutant, supporting our hypothesis that the accumulation of the 85-90 IFITM3 mutant in the Golgi is due to the inhibition of v- to t-SNAREs fusion. During the revision process, reviewers asked for further controls in the FRET experiments and in particular to determine effects of WT IFITM3 in FRET and to determine the specificity of FRET for SNARE-mediated fusion by including a well-known SNARE-inhibition, NEM. These experiments are at present ongoing and are aimed at clearly validating the FRET-based assay in terms of IFITM3 action.

**The 85-90 mutation defines a domain in CIL that regulates the exit of wild-type IFITM3 from the Golgi.** The IFITM3 mutant can be due to the fact that the protein does not leave the Golgi during its transit there or else that it exits the apparatus and is then redirected there. To assess whether the 85-90 mutation induced retention or relocalization of IFITM3 at the Golgi, we performed a time-course analysis of both WT and mutant IFITM3 from early to late time points after ectopic DNA transfection (Figure 13).

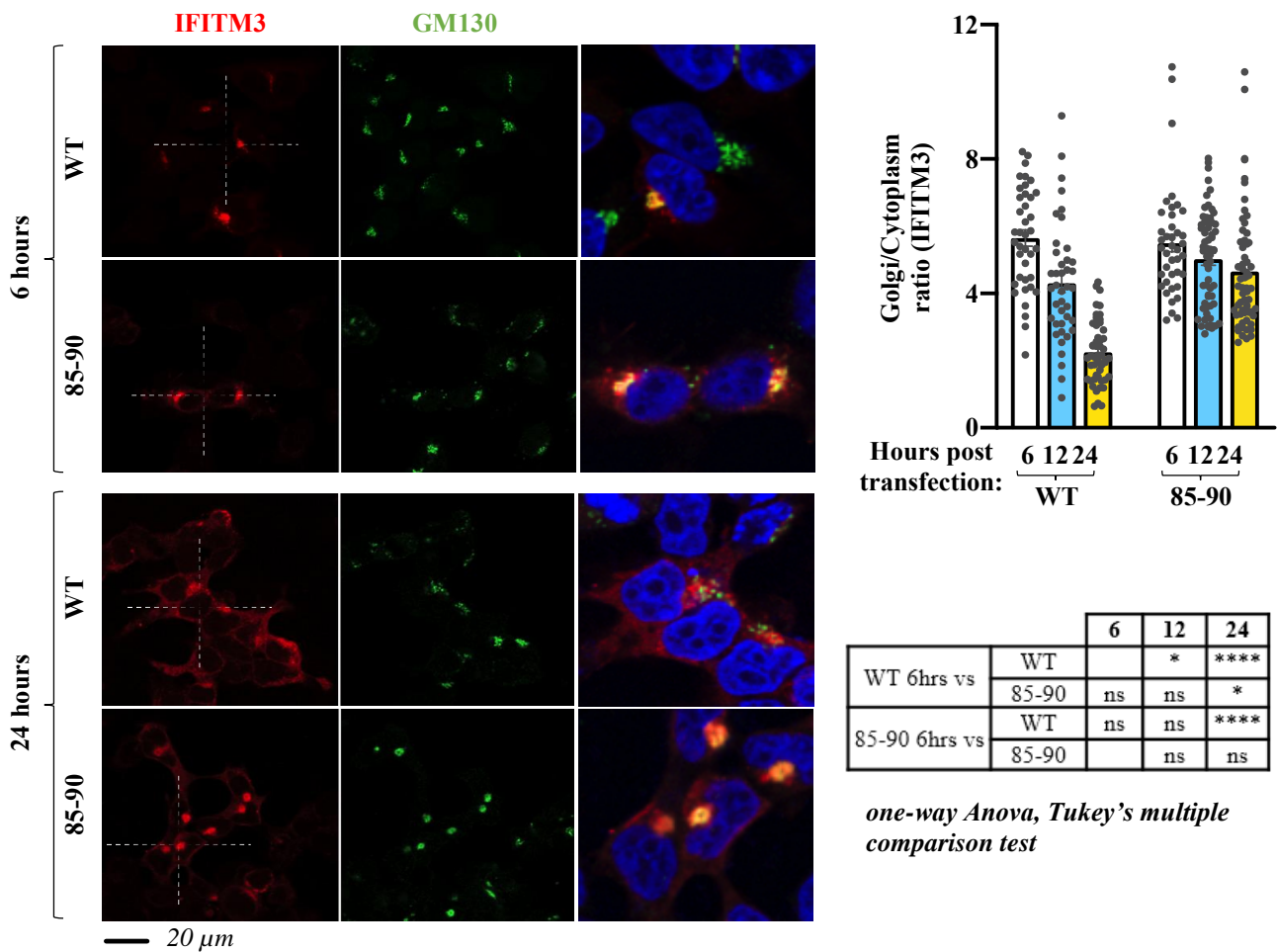


**Figure 13. Time course confocal microscopy analysis indicates that the 85-90 IFITM3 mutation affects the normal egress of IFITM3 from the Golgi.** HEK293T cells were examined by confocal microscopy at different times post ectopic DNA transfection to determine the localization of IFITM3 proteins over time. Representative pictures and graph presenting the distribution of IFITM3 in the Golgi (calculated as a Golgi/cytoplasm ratio on 39 to 62 cells per time point and per condition in two independent experiments, AVG, SEM and individual values). The table presents *p* values obtained after a one-way Anova, Tukey's multiple comparison test between the indicated conditions: ns: non significant; \*, *p* value <0.05; \*\*\*\*, *p* value <0.0001.

While both proteins exhibited a predominant Golgi distribution at 6 hours post transfection, such concentration gradually diminished in the case of WT IFITM3, in agreement with its functional exit from the Golgi.

On the contrary, little changes were observed over time in the presence of the 85-90 IFITM3 mutant. IFITM3 remained in this compartment, supporting the notion that the 85-90 mutation induces the retention, rather than the redistribution, of IFITM3 in the Golgi. In agreement with this observation,

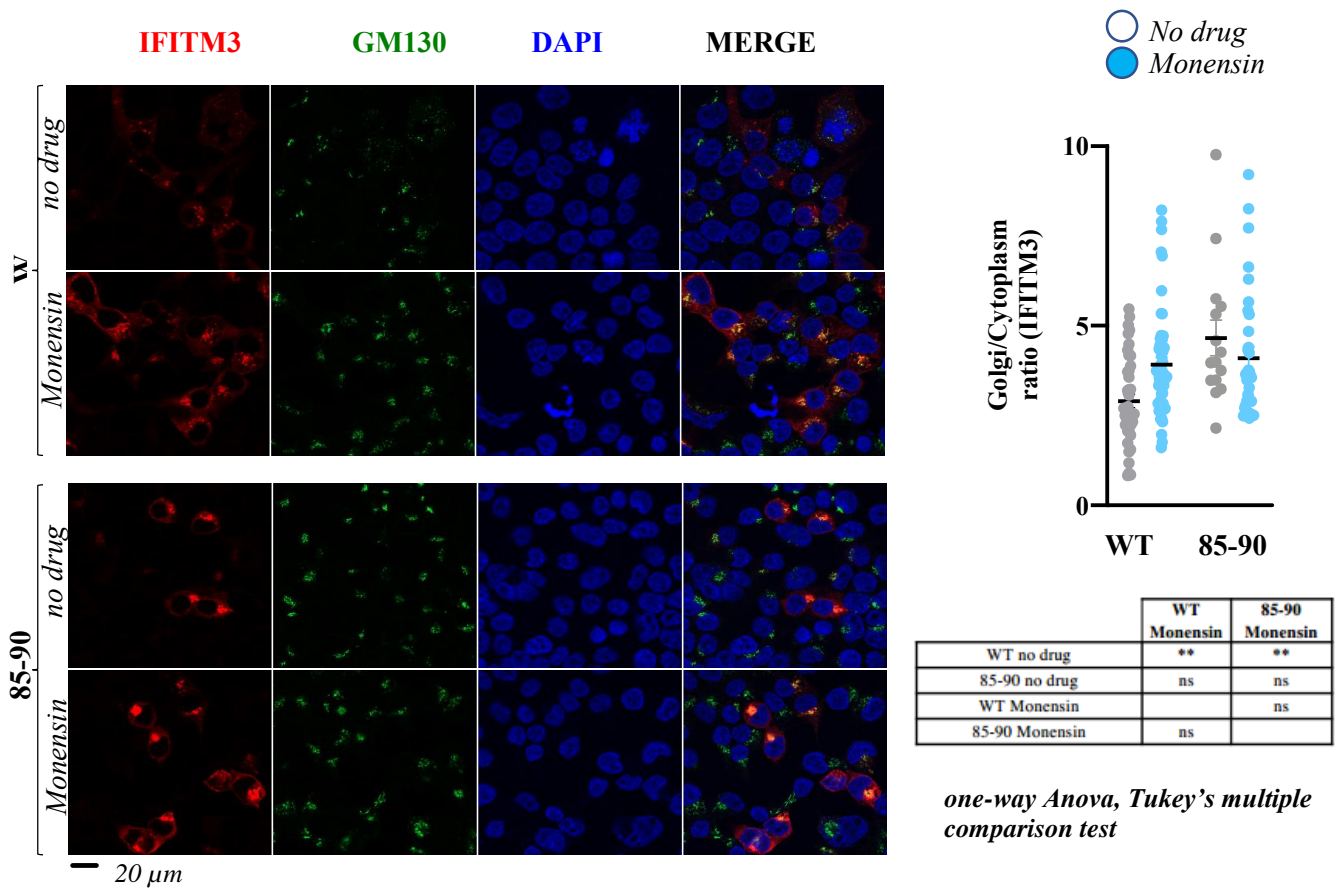


**Figure 14. The broad trafficking inhibitor Monensin affects the egress from the Golgi of WT IFITM3, but not of the 85-90 mutant.** Cells expressing the indicated IFITM3 protein were either treated or untreated with Monensin for 3 hours at 0.2 mM, prior to confocal microscopy analysis. Panels present typical staining, while the graph presents the proportion of IFITM3 in the Golgi as an IFITM3 Golgi/cytoplasmic ratio (AVG= lines and individual values displayed as dots). The lower table presents the result of the indicated statistical analyses: ns, non significant; \*\*  $p$  values < 0.006.

incubation of cells with the broad trafficking inhibitor Monensin induced accrued Golgi accumulation of WT IFITM3, but as expected did not modify the distribution pattern of the 85-90 mutant (Figure 14).

Overall, these results indicated that the 85-90 mutation defines a protein domain within the CIL that regulates the normal egress of IFITM3 from the cis-Golgi.

### **Identification of the amino acids in the CIL that mediate the retention of IFITM3 in the Golgi.**

To more precisely map the residues that regulated the egress of IFITM3 from the Golgi, individual amino acids of the CIL were mutated to alanine and analyzed by confocal microscopy (Figure 15a-b and Figure 16). Residues that were Alanines in the CIL were instead mutated to glycines.

Mutants were expressed to detectable levels upon WB analysis, with two exceptions (D92A and G95A that were barely detectable by WB). I noticed that the D92A mutant acquired also a nuclear localization unusual for IFITM proteins, however this was not characterized further. Mutagenesis study identified a number of residues whose mutation led to accumulation of IFITM3 into the Golgi (S81, V82, K83, S84, R85, D86, A96, Q97, Q98, S101, T102, A103, K104, L106 and N107), indicating that several residues within the CIL participate to this phenotype. Interestingly however, the mutations that resulted in levels of IFITM3 localization in the Golgi equivalent to those of the 85-90 mutant were essentially clustered in a patch (from residues S81 to D86) that was posited at the boundary between the end of the intra-membrane domain of IFITM3 (IMD) and the start of the CIL and that overlapped with the 85-90 stretch.

Thus, the complete mutagenesis of the CIL allowed us to more precisely refine the domain responsible for the exit of IFITM3 from the Golgi (<sub>81</sub>SVKSRD<sub>86</sub>, numbers refer to position on human IFITM3).

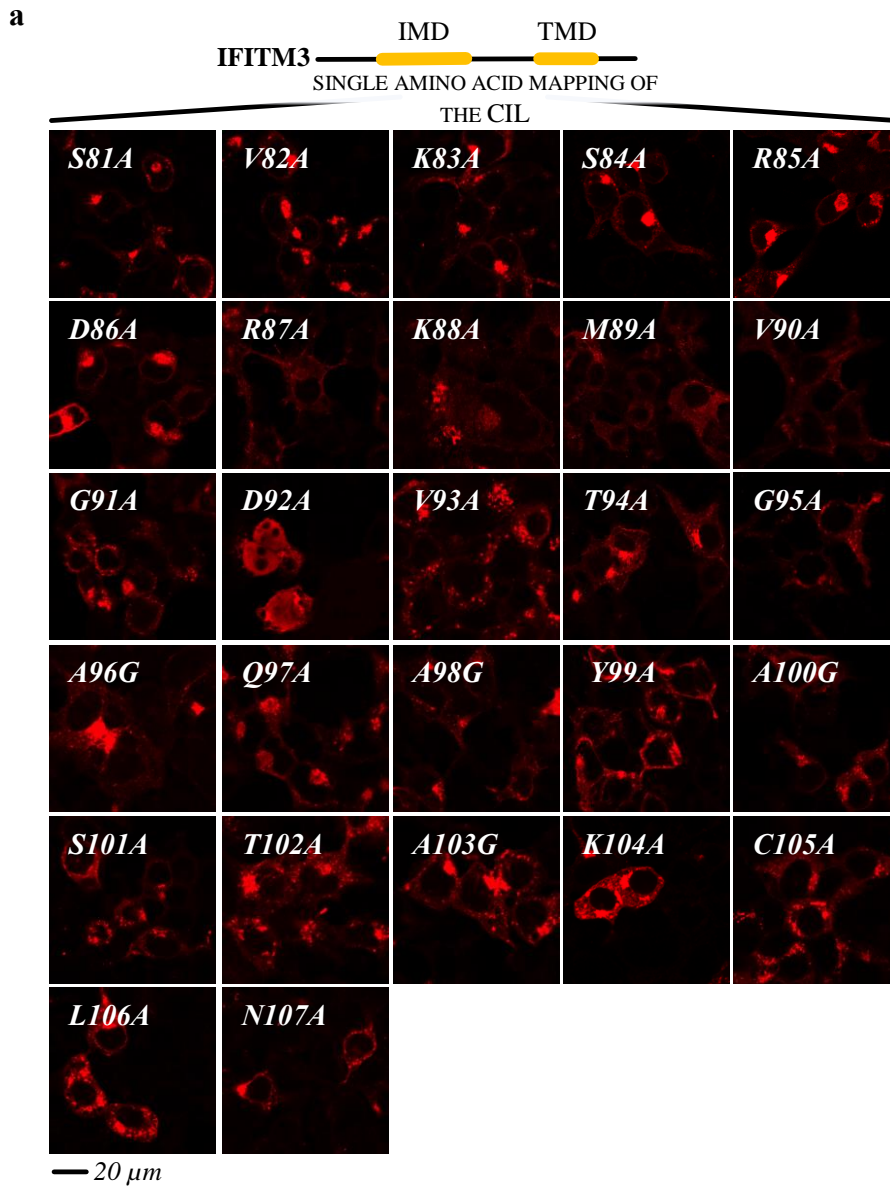


**Figure 15. Mutagenesis of the entire CIL of IFITM3 finely maps the domain involved in the egress of IFITM3 from the Golgi.** a) Individual amino acid of the CIL were changed to alanine or to glycine when alanine residues were present, prior to confocal microscopy analysis. Representative pictures are shown here (IFITM3 only).

The Golgi egress domain identified in IFITM3 seems conserved in other members of the **dispanin subfamily**. IFITMs belong to the larger dispanin family (CD225 family) which is itself divided into four subfamilies (A to D, Figure 17a)

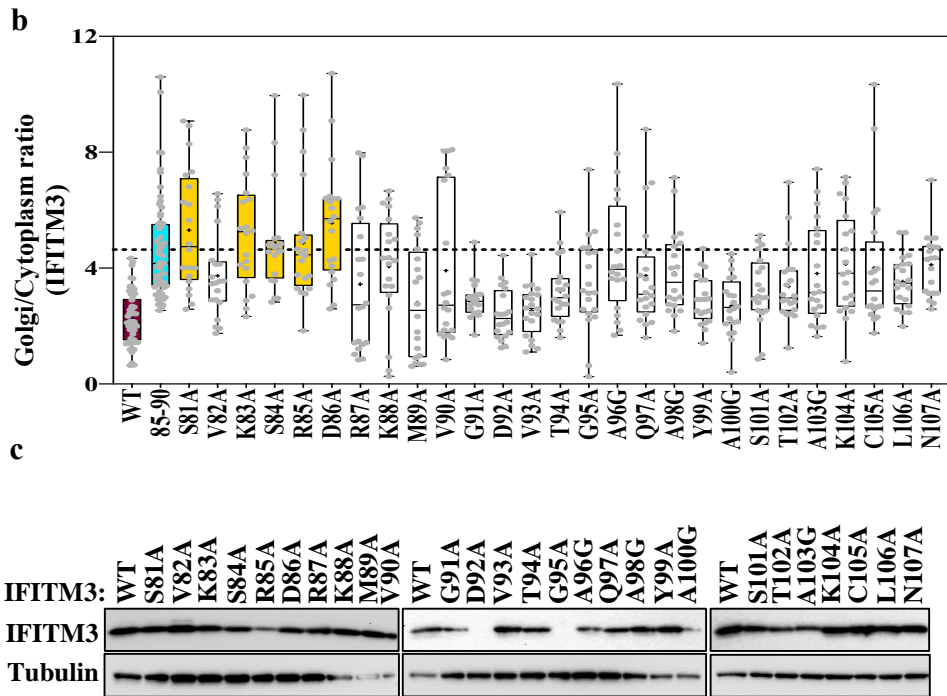


**Figure 15, continued. b)** Quantification of the IFITM3 proportion in Golgi is provided as a Golgi/cytoplasm ratio in the box and whisker plot (20 cells per mutant in two to three independent experiments analyzed). Asterisks and lines within the box indicate averages and median values, respectively. Yellow boxes indicate mutants with Golgi/cytoplasm IFITM3 ratios equivalent to the 85-90 IFITM3 mutant and non-statistically significant when compared to 85-90 following an ordinary one-way Anova, Dunnett's multiple comparison test. **c)** Representative WB analysis of mutant proteins.

The A subfamily is mainly composed of IFITM1, 2 and 3, as well as IFITM5 and IFITM10, among which IFITM1, 2 and 3 was IFN induced protein while IFITM5 and IFITM10 are not IFN regulated and exert unclear functions. The alignment of residues spanning the IFITM3 SVKSRD domain in human IFITMs, as well as their comparison in vertebrates (Figure 17a, aligned sequences on the left for human IFITMs and Logo on the right for vertebrate IFITMs, respectively) indicated the presence of a consensus sequence conserved across vertebrate members of the dispanin A subfamily: S-x-K-x-R-D. Among IFITM1, 2 and 3 instead, the SVKSRD domain was strictly conserved even among vertebrate members, indicating its strong conservation. This patch was not strongly conserved at the amino acidic level in the other remaining subfamilies.

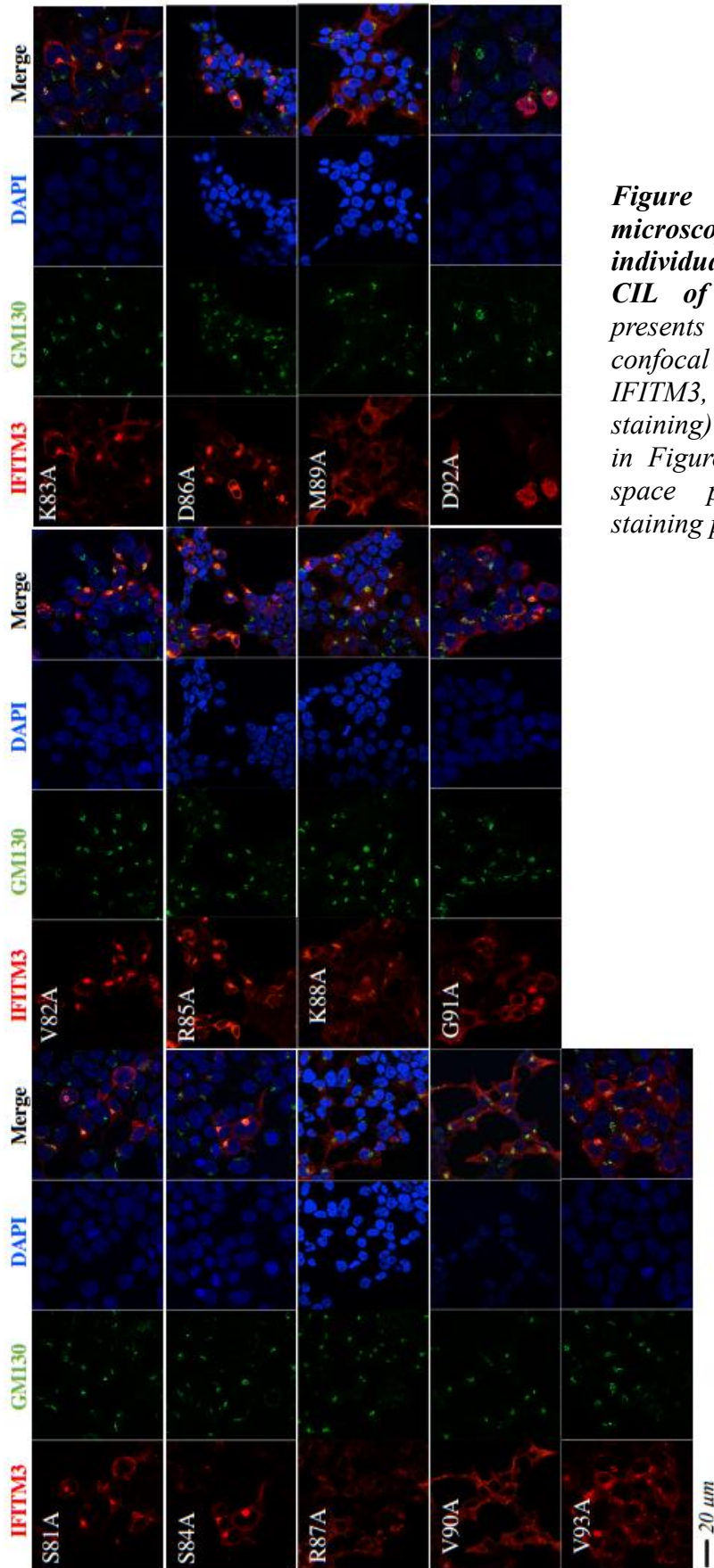


*Figure 16. Complete confocal microscopy analyses of the individual point mutants of the CIL of IFITM3. This figure presents the entire panel of confocal microscopy analyses (i.e. IFITM3, GM130 and DAPI staining) of the mutants presented in Figure 15, which for lack of space presents only IFITM3 staining panels.*

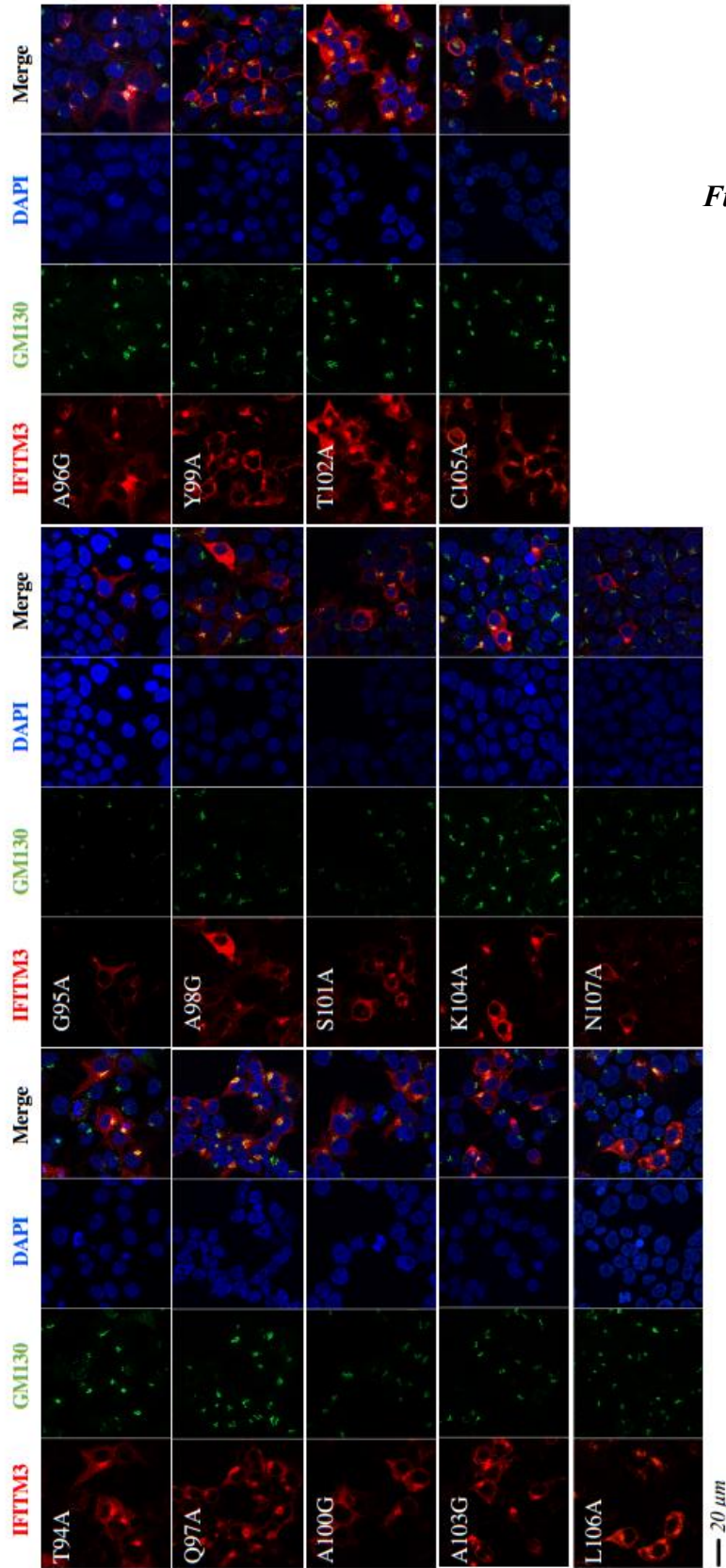
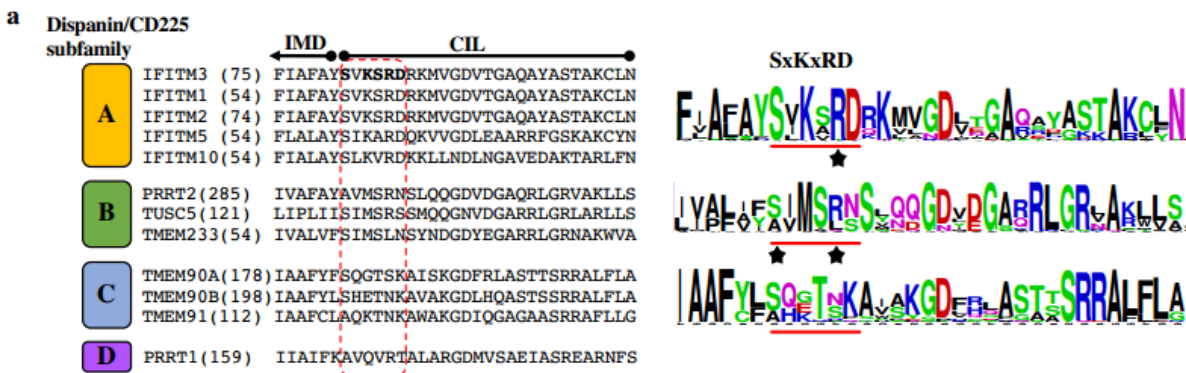


Figure 16, continued. As before

To determine whether this consensus domain exerted similar functions in other IFITM proteins belonging to the A subfamily, a single point mutation was introduced in the corresponding domain of IFITM1 (R64A). Different from the phenotype of IFITM3, IFITM1 is mostly localized at the plasma membrane due to the lack of specific trafficking domains at its N-terminus when compared to IFITM3.

While when the single point mutant is introduction in the IFITM Golgi egress domain, IFITM1 changed the location from the plasma membrane to the Golgi, as observed by confocal microscopy analysis suggesting mutant in the functional domain was sufficient to drive the redistribution of the mutant and indicating a functional conservation of this domain in antiviral IFITMs (Figure 17b).



**Figure 17. The Golgi egress domain of IFITM3 is conserved across vertebrate members of the dispanin/CD225 subfamily A and is functionally conserved in PRRT2, a member of the B subfamily as shown by genetic mutations associated to PKD. a)** Alignment of the indicated portions of human members of the different dispanin/CD225 subfamilies. The relevant domain is circled in red. The position of the first amino acid of each sequence is shown within parentheses. Left, logo files obtained after alignment of vertebrate orthologues of the indicated genes for each subfamily, except D.

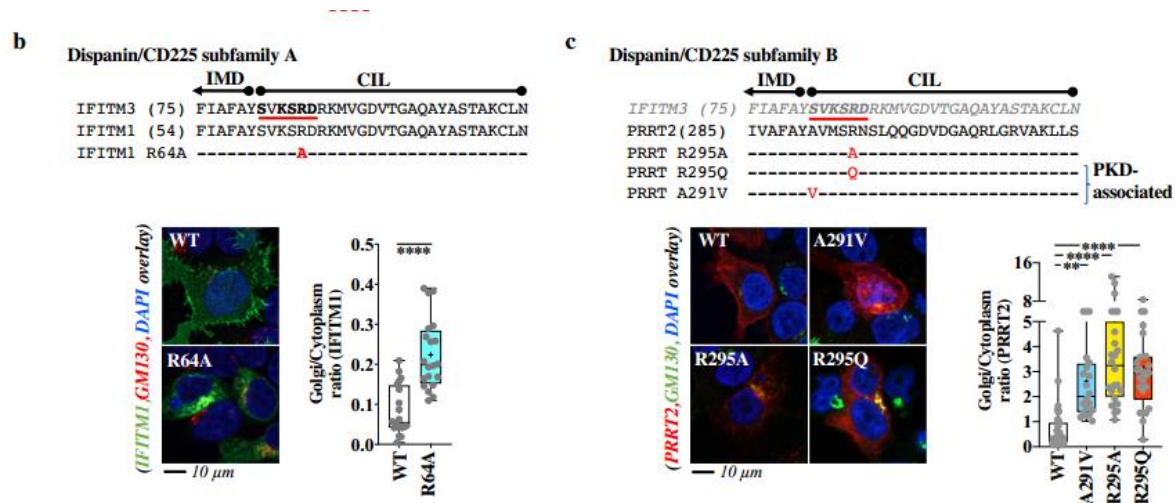


**Figure 17, continued. b)** Single point mutation and confocal microscopy analysis of the Golgi egress domain of IFITM1. **c)** Point mutations and confocal microscopy analysis of PRRT2 mutants in the region corresponding to the Golgi egress domain of IFITM3. R295Q and A291V are genetic mutations associated to PKD. Representative pictures are shown for each protein. Whiskers and boxes plots of the quantification of the proportion of each protein in the Golgi as a Golgi/cytoplasm ratio (25-75 percentiles with individual cells represented as dots; group average indicated by an asterisk, n=20 in three independent experiments). Colored boxes represent statistical significant differences after a two-tailed Student *t* test or a One-way Anova Dunnett's multiple comparison test (b and c, respectively) of the examined mutant over WT. \*\*, *p* value of 0.0019; \*\*\*\*, *p* value < 0.0001.

Although the functions of certain proteins belonging to the dispanin family remain unknown (as is the case for TMEME90A, TMEM91, TMEM233 and TMEM265), the information existing on other members (TUSC5, TMEM90B and PRRT2) indicate functions revolving around vesicular trafficking and vesicular behaviour. Among these proteins, PRRT2 acts as a regulator of neurotransmitter vesicles in neuron cells and is genetically linked to paroxysmal kinesigenic dyskinesia (PKD, the most common type of paroxysmal movement disorder), as well as benign familial infantile seizures (BFIS). Although the Golgi egress domain identified in IFITM proteins did not appear to be conserved at the amino acid level in other subfamilies, we decided to investigate whether it could be functionally conserved in PRRT2 as a prototype member of the B

subfamily. Indeed, we noticed that two mutations in PRRT2 have been identified in patients affected by PKD in the same CIL region at the boundary between the IMD and the CIL (A291V and R295Q, corresponding to the underlined positions 1 and 5 of the S-V-K-S-R-D domain).

To test this hypothesis, the R295Q and 1291V mutations along with a R295A alanine mutation were separately introduced in PRRT2 and analyzed by confocal microscopy (Figure 17c). While WT PRRT2 exhibited a predominant plasma membrane distribution, introduction of the above-mentioned mutations led to accrued redistribution of PRRT2 in the Golgi, similarly to what described above for IFITM3.

Above all, these results indicate that the boundary between the IMD and the CIL of members of the dispanin family is important for the regulation of their trafficking from the Golgi. This domain can be clearly defined in members of the dispanin A subfamily as a consensus sequence conserved in vertebrates, and despite sequence dissimilarity, it seems to maintain similar functions in other subfamilies, or at least in PRRT2 using de novo generated as well as PKD-associated genetic mutations.

## **Discussion**

During my thesis, I tried to highlight a novel aspect of the biology of IFITM3 and specifically its exit from the Golgi, thus focusing more on the cell biology aspect of IFITMs rather than directly on their antiviral functions. IFITMs are transmembrane proteins and in this respect it is not surprising that they transit from this organelle. Through the characterization of mutants in the CIL, I have been able to however highlight that exit from the Golgi requires a specific sequence within IFITM3 that is conserved among IFIM2 and IFITM1.

Mutations in this domain lead to a drastic accumulation of IFITM3 in the Golgi and this organelle inflates and becomes dysfunctional with respect to glycoprotein passage.

To explain this, I tried to determine whether the 85-90 IFITM3 mutant could inhibit what resembles most to a viral particle fusing with a cellular membrane: the fusion between vesicles bearing v-SNAREs and those bearing a t-SNARE. V- to t-SNARE fusion is difficult to study in living cells and is essentially studied in minimal reconstituted systems. By using a FRET-based reading, I was however able to determine that FRET decreased in the presence of the 85-90 IFITM3 mutant, as expected in case of membrane fusion inhibition between v- and t-SNAREs vesicles.

This assay was extremely difficult and to completely validate it, similar experiments should have been carried out also with WT IFITM3 and also with known inhibitors of SNAREs fusion (NEM).

However, to support the fact of a SNARE-mediated inhibition mechanism the overexpression of GS15 described to relieve SNAREs-bearing membrane fusion defects relieved also the defects of the IFITM3 mutant and effectively induced the exit of this protein and of the VSV-G glycoprotein from the Golgi, making it likely that the accumulation of the 85-90 IFITM3 mutant impaired the fusion between membranes bearing different SNAREs.

More importantly, these results suggested that WT IFITM3 could also exert these effects on the Golgi. At concentrations that were similar to mutant, such changes were very low, but preliminary

experiments I'm trying to finish, indicate that the Golgi defects can be observed also in the case of WT IFITM3 and that depend in this case from the overall levels of the protein that is expressed.

In this respect, these results may suggest that whatever controls IFITM3 exit from the Golgi may also influence the overall trafficking of glycoproteins through the Golgi. Although more studies need to be done to prove this, we hypothesize that this can be a reason for the multiple effects of IFITM3 that have been described on glycoprotein levels and perhaps in B cell signaling, which is itself influenced by the extent of B cellular receptor (BCR) present at the plasma membrane and thus trafficked through the Golgi.

An important point to determine is whether endogenous IFITM3 will be able to carry out similar functions as ectopically expressed one. I already know that long stimulation of primary macrophages with interferon, which induces high expression of IFITMs, leads to an accumulation of IFITM3 in the Golgi. Whether this leads to changes in the extent of glycoprotein trafficking through this apparatus remains to be determined.

Finally, it is unclear whether the CIL domain identified here acts to directly bind a Rab protein (in which case it could be potentially attached to a Golgi-resident protein and drive its exit from there, or whether the domain acts by influencing the status of palmitoylation at close cysteine residues.

The Rothman's lab hypothesized that exit from the Golgi could follow, for certain proteins, a gradient of palmitoylation (more modified proteins would induce curvatures in Golgi membranes that would favour their transport and exit from there). Unfortunately, I have not had the time to fully explore these issues, although I had time to examine the role of several Rabs in the process of exit of IFITM3 from the Golgi (Rab 6, 9 and 27 seem to play a role in the exit of IFITM3 from the Golgi). However, the approach used was to express dominant-negative forms of different Rabs and to focus on those that induced a similar Golgi accumulation of the WT IFITM3 than the 85-90 mutant itself. Although several Rabs were found to contribute to this, the final proof would have

been a co-immunoprecipitation between IFITM3 and these Rabs, which for technical difficulties could not be consistently performed. Similarly, the extent of protein palmitoylation proved challenging to establish in the lab in a short time, so that this hypothesis could not be tested.

Therefore, the key results of my thesis work are that the CIL regulates a novel step of the biology of IFITM3 which is the exit from the Golgi (an overall model is presented in Figure 18). This process (ie the accumulation of IFITM3) is very controlled both transcriptionally and post-translationally, to avoid negative effects of IFITM3 on the Golgi functions. It remains however to be determined whether, even under normal expression conditions, such as interferon-stimulation, IFITMs can modulate the extent of glycoprotein trafficking from the Golgi, which would have important consequences for the cell itself.

Lastly, I have been able to demonstrate that the domain that drives the exit of IFITM3 also plays a similar role in PRRT2, which is a distant member to IFITM3 than other IFITMs. In this case, only a few amino acids are conserved among human proteins (IFITMs vs PRRT2), although this conservation becomes even less important when considering animal IFITMs and PRRT2 proteins. However, it is of interest that certain mutations that inactivate the functions of PRRT2 in PKD patients fall within the CIL domain that governs exit of IFITM3 from the Golgi and also lead to the relocalization of PRRT2 (which is normally at the plasma membrane) in this apparatus. It is possible that these mutations lead to the functional inactivation of PRRT2 given that this protein is no longer present where it should be.

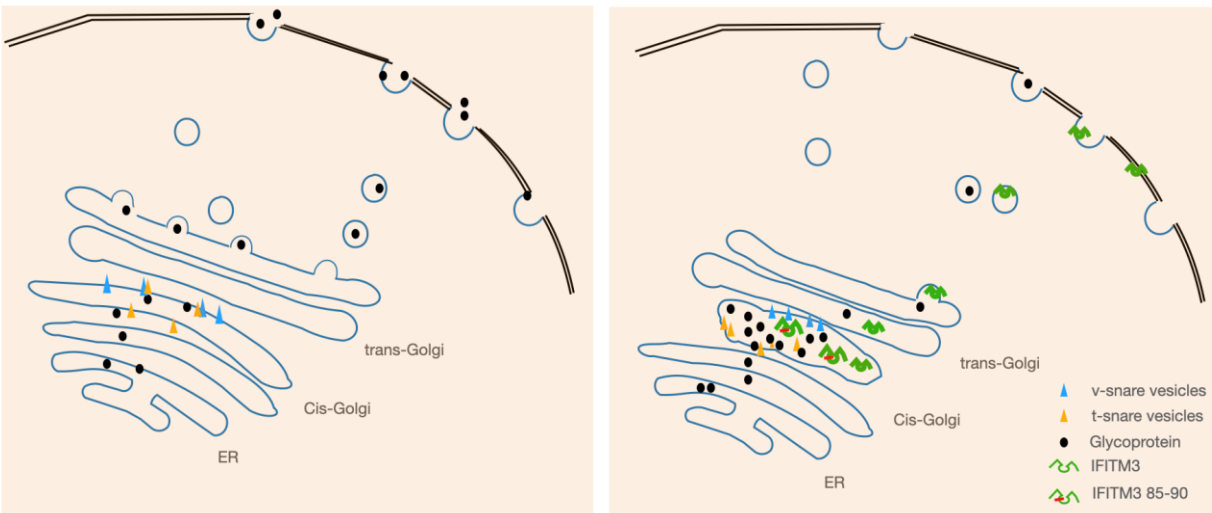


**Figure 18. A model for the IFITM3-mediated disruption of Golgi trafficking.** In our model the retention of IFITM3 in the Golgi leads to an abnormal accumulation of this protein at this location that, as usual for IFITM molecules, leads to the inhibition of membrane fusion events. In this case, the key events inhibited by IFITM3 are fusion events between vesicles bearing v- and t-SNAREs. As these events are key to maintain protein fluxes within the Golgi, this leads to heavy Golgi dysfunction and problems in glycoprotein trafficking. While the 85-90 IFITM3 mutant is completely within the cis-Golgi, even the WT IFITM3 can accumulate in part there in conditions of prolonged exposure to IFN for example. In this case, IFITM3 may exert modulatory effects in Golgi trafficking that remain to be characterized. By extension, all events that interfere with the exit of IFITM3 from the Golgi may in turn affect the organelle functionality and have consequences on the cell physiology.

## **Material and Methods**

### **Cells, plasmids and antibodies**

Human embryonic kidney cells (HEK293T, ATCC cat. CRL-3216) were maintained in complete DMEM media with 10% Fetal Calf Serum (Sigma cat. F7524). Untagged WT IFITM3 (gene ID: 10410) and IFITM1 (gene ID: 8519) and corresponding mutants were either previously described (85-90; <sup>13,41</sup>), or cloned (all others) by standard mutagenesis techniques in the plasmid pQCXIP (Clontech). WT human PRRT2 (gene ID: 112476) was synthesized as N-terminal HA tag fusion protein (Genewiz) in pcDNA3 vector (Thermofisher) and single point mutants were generated on this matrix by standard molecular biology techniques.

The HIV-1 proviral clone NL4-3 and the VSV-G expression constructs have been described elsewhere<sup>42</sup>. The mEmerald-VSV-G (mEm.-VSV-G) coding construct was a gift from Michael Davidson (Addgene, 54307); pcDNA-D1ER coding for an ER targeted enhanced CFP was a gift from Amy Palmer & Roger Tsien (Addgene cat. 36325 <sup>43</sup>). GS15-CFP and ERS24-YFP (cyanin and yellow fluorescent proteins, respectively) were obtained by Oleg Varlamov from the Oregon National Primate Research Center, USA <sup>20</sup>. The following primary antibodies were used for WB or confocal microscopy, as indicated. Mouse monoclonals: anti- $\alpha$ -Tubulin, anti-HA and anti-VSV-G (Sigma cat. T5168, cat. H3663 and cat. V5507, respectively), anti-LAMP2 (Santa Cruz Biotechnology, cat. sc-18822), anti-CD63 and anti-GM130 (BD biosciences cat. 556019 and cat. 610823); anti-HIV-1 p24 (obtained through the NIH HIV Reagent Program, Division of AIDS, NIAID, NIH, contributed by Dr. Bruce Chesebro and Kathy Wehrly, cat. ARP-3537). Rabbit polyclonal antibodies: anti-IFITM3 (Proteintech cat. 11714-1-AP), anti-IFITM1 (Proteintech, cat. 60074) and anti-GM130 (abcam cat. Ab52649). The sheep polyclonal antibody anti-HIV-1 Env was obtained through the NIH HIV Reagent Program, Division of AIDS, NIAID, NIH (contributed by Dr. Michael Phelan, cat. ARP-288).

The following secondary antibodies were used for WB: anti-mouse, anti-rabbit and anti-sheep IgG-Peroxidase conjugated (Sigma, cat. A9044 and cat. AP188P and Dako cat. P0163); while the following ones were used for confocal microscopy: donkey anti-rabbit IgG–Alexa Fluor 594 conjugate and donkey anti-mouse IgG–Alexa Fluor 488 conjugate (cat. A-21207 and cat. A-21202; Life Technologies).

### **Ectopic DNA transfections, viral production and confocal microscopy analyses**

HEK293T cells were directly seeded on 0.01% poly-L-lysine-coated coverslips (Sigma, cat. P4832) and analyzed 24 hours after ectopic DNA transfection (unless otherwise specified, Lipofectamine 3000 cat. L3000008, ThermoFisher, according to the manufacturer's instructions). Cells were washed three times with PBS 1x, fixed with 4% paraformaldehyde (Euromedex, cat. 15713) for 10 min, quenched with 50 mM NH<sub>4</sub>Cl (Sigma cat. A4514) for 10 min, and permeabilized with PBS–0.5% Triton X-100 (Sigma, cat. X100) for 5 min. After a blocking step in PBS–5% milk, cells were incubated with primary antibodies for 1 hour at room temperature (dilution 1:100), washed and then incubated with fluorescent secondary antibodies (dilution 1:100). A 4',6-diamidino-2-phenylindole (DAPI)-containing mounting medium was used (ThermoFisher, cat. 62248). Images were acquired using a spectral Zeiss LSM800 confocal microscope and analyzed with Fiji software (version 2.0.0). For 3D-reconstruction, z-stack collections were analyzed with the Imaris 9.2.0 software (Oxford Instruments Group). Colocalisations were quantified using the Pearson overlap coefficient (Fiji software).

IFITMs and PRRT2 coding DNAs were routinely transfected at a concentration of 1 µg per well of a 24 well plate along with 0.2 µg of VSV-G or of mEm.-VSV-G. When specified, increasing doses of GS15 coding DNA were also added (0, 0.2, 0.5 and 1 µg).

Monensin was used at a final concentration of 0.2 mM for 3 hours, prior to analysis (Sigma, cat. M5273).

Production of HIV-1 virions particles was instead carried out by calcium phosphate DNA transfection of the HIV-1 proviral clone NL4-3 (ratio 3 to 1, NL4-3 over IFITM). Virion particles released in the supernatant of transfected cells were harvested forty-eight hours post transfection, syringe-filtered (0.45µm filters, Minisart, cat. 146622) to remove cellular debris and purified by ultracentrifugation over a 25% sucrose cushion (28.000 rpm for 2 hours; Beckman Coulter ultracentrifuge).

In confocal microscopy experiments using the GM130 Golgi marker, IFITM or VSV-G relocalization was quantified for each cell as the ratio between the signal present at the Golgi over the signal present in the cytoplasm (Golgi/cytoplasm ratio). When the GM130 marker was not used, perinuclear accumulation was either scored visually (as in Fig 1, in light of the extremely clear phenotype; binary scoring: perinuclear or non-perinuclear), or quantified by determining the average percentage of accumulation of VSV-G at the left or right part of the nucleus (asymmetric distribution= perinuclear accumulation; symmetric distribution= non-perinuclear accumulation).

To bypass artificial measurements due to differences in size between left and right portions of the cell, the avg of the signals measured at each side of the cell were used. This measurement diminishes the absolute values of the protein present at one side, but offers the advantage of making measures independent from cell size differences. Visual scoring in Fig 1 was also confirmed through this analysis.

### **Electron microscopy**

Samples were fixed in mixture of 4% paraformaldehyde (TAAB Laboratories Equipment Ltd, United Kingdom, cat. F/P001) and 1% glutaraldehyde (Electron Microscopy Science, USA, cat. 16310) in 0.1 M phosphate buffer (pH 7.4) for 24 hours, washed three  $\times$  30 min in 0.1 M of phosphate buffer, and post-fixed for one hour with 2% osmium tetroxide (Electron Microscopy Science, USA, cat. 19190) in 0.15 M of phosphate buffer. After washing in 0.1 M of phosphate buffer for 20 min and two  $\times$  20 min in distilled H<sub>2</sub>O, samples were dehydrated in a graded series of ethanol solutions (50% ethanol two  $\times$  10 min; 70% ethanol three  $\times$  15 min and last portion for 14 hours; 90% ethanol three  $\times$  20 min; and 100% ethanol three  $\times$  20 min). Final dehydration was performed by 100% propylene oxide (PrOx, ThermoFisher (Kandel) GmbH, Germany, Lot X19E013) three  $\times$  20 min. Then, samples were incubated in PrOx/EPON epoxy resin (Fluka, Switzerland) mixture in a 3:1 ratio for two hours with closed caps, 16 hours with open caps, and in 100% EPON for 24 hours at room temperature. Samples were replaced in new 100% EPON and incubated at 37 °C for 48 hours and at 60 °C for 48 hours for polymerization. Serial ultra-thin sections (thickness 70 nm) were cut with a “Leica Ultracut UCT” ultramicrotome (Leica Microsysteme GmbH, Wien, Austria), placed on TEM nickel one-slot grids (Agar Scientific, Ltd. United Kingdom, cat. G2500N) coated with Formvar film and stained 20 min with 5% uranyl acetate (Merck, Darmstadt, Germany, cat. 8473) and 5 min Reynolds lead citrate. The sections were then observed at 100 kV with a Jeol 1011 TEM (JEOL, Tokyo, Japan) connected to a Gatan digital camera driven by Digital Micrograph software (GMS 3, Gatan, Pleasanton, CA, USA).

### **Fluorescence Resonance Energy Transfer (FRET) microscopy**

Analyses were performed on live cells plated on a 35 mm glass-bottom dish and transfected with 2  $\mu$ g of DNA coding the 85-90 IFITM3 mutant and 0.5  $\mu$ g each of GS15-CFP and ERS24-YFP to ensure that the majority of cells examined were IFITM3-positive. After replacing media with

phenol-red MEM supplemented with 10%FCS, cells were analyzed by confocal microscopy and images were acquired at a temperature of 37°C with a spectral Zeiss LSM710 confocal microscope, equipped with an argon laser and a 63X oil immersion objective. CFP and YFP were excited with a 458 and a 514 nm lasers (emission windows set at 465-505 nm and 525-600 nm, respectively) and images were acquired with a 512x512 resolution, 8 bit line average. Photobleaching of the donor YFP was performed with 4 sequential illuminations of the selected cell (4 frames, line average 2, iterations at 400, scan speed at 8, 514 nm laser AOTF setting at 100%). Four scans were acquired after each bleaching (two before and two after). FRET efficiency was calculated from the ratio of the CFP fluorescence measured post- and pre-YFP bleaching. Analyses were performed on 15–20 individual cells per sample group. The FRET control plasmid pECFP18aaEYFP from addgene.) was used for setup (Addgene cat. 109330, gift from Gabriele Kaminski Schierle)<sup>44</sup>. Images were analyzed using the ROI manager in Fiji software.

### **Glycosidase treatment assays and WB quantification**

Cell lysates expressing IFITM3 and VSV-G proteins were collected and split in three aliquots that were either untreated, or treated with Endoglycosidase H (EndoH, NEB, P0702S) or N-glycosylase F (PNGaseF, NEB P0704S), according to the manufacturer's instructions. Treated lysates were then analyzed by WB, images acquired using Image Lab Touch Software (version 2.0.0.27, Chemidoc Imaging System from Bio-Rad) and bands were quantified by densitometry using the volume tool in the same software.

### **Softwares**

Electron microscopy: Digital Micrograph software (GMS 3, Gatan, Pleasanton, CA, USA). Confocal microscopy: Fiji software (version 2.0.0), Zen (version 2.3, Zeiss) and Imaris 9.2.0 software (Oxford Instruments Group). WB: Image Lab Touch Software (version 2.0.0.27, Chemidoc Imaging System from Bio-Rad).

Statistics and graphs: Graphpad Prism8 (8.4.3, Graphpad software, LLC).

### **Statistical analyses**

The statistical analyses used in this study were calculated with the Graphpad Prism8 software: Student t tests (unpaired, two-tailed), one-way Anova tests with either Tukey's or Dunnett's multiple comparisons, as indicated in the figure legends.

## **References**

- Aizawa, M., Fukuda, M., 2015. Small GTPase Rab2B and Its Specific Binding Protein Golgi-associated Rab2B Interactor-like 4 (GARI-L4) Regulate Golgi Morphology. *The Journal of biological chemistry* 290, 22250-22261.
- Amini-Bavil-Olyaei, S., Choi, Y.J., Lee, J.H., Shi, M., Huang, I.C., Farzan, M., Jung, J.U., 2013. The antiviral effector IFITM3 disrupts intracellular cholesterol homeostasis to block viral entry. *Cell host & microbe* 13, 452-464.
- Anafu, A.A., Bowen, C.H., Chin, C.R., Brass, A.L., Holm, G.H., 2013. Interferon-inducible transmembrane protein 3 (IFITM3) restricts reovirus cell entry. *The Journal of biological chemistry* 288, 17261-17271.
- Andreu, P., Colnot, S., Godard, C., Laurent-Puig, P., Lamarque, D., Kahn, A., Perret, C., Romagnolo, B., 2006. Identification of the IFITM family as a new molecular marker in human colorectal tumors. *Cancer research* 66, 1949-1955.
- Bailey, C.C., Huang, I.C., Kam, C., Farzan, M., 2012. Ifitm3 limits the severity of acute influenza in mice. *PLoS pathogens* 8, e1002909.
- Bailey, C.C., Kondur, H.R., Huang, I.C., Farzan, M., 2013. Interferon-induced transmembrane protein 3 is a type II transmembrane protein. *The Journal of biological chemistry* 288, 32184-32193.
- Blyth, G.A., Chan, W.F., Webster, R.G., Magor, K.E., 2016. Duck Interferon-Inducible Transmembrane Protein 3 Mediates Restriction of Influenza Viruses. *Journal of virology* 90, 103-116.
- Bradbury, L.E., Kansas, G.S., Levy, S., Evans, R.L., Tedder, T.F., 1992. The CD19/CD21 signal transducing complex of human B lymphocytes includes the target of antiproliferative antibody-1 and Leu-13 molecules. *Journal of immunology (Baltimore, Md. : 1950)* 149, 2841-2850.
- Brass, A.L., Huang, I.C., Benita, Y., John, S.P., Krishnan, M.N., Feeley, E.M., Ryan, B.J., Weyer, J.L., van der Weyden, L., Fikrig, E., Adams, D.J., Xavier, R.J., Farzan, M., Elledge, S.J., 2009. The IFITM proteins mediate cellular resistance to influenza A H1N1 virus, West Nile virus, and dengue virus. *Cell* 139, 1243-1254.
- Chauhan, A., Khandkar, M., 2015. Endocytosis of human immunodeficiency virus 1 (HIV-1) in astrocytes: a fiery path to its destination. *Microbial pathogenesis* 78, 1-6.
- Chen, Y.X., Welte, K., Gebhard, D.H., Evans, R.L., 1984. Induction of T cell aggregation by antibody to a 16kd human leukocyte surface antigen. *Journal of immunology (Baltimore, Md. : 1950)* 133, 2496-2501.
- Chesarino, N.M., McMichael, T.M., Hach, J.C., Yount, J.S., 2014a. Phosphorylation of the antiviral protein interferon-inducible transmembrane protein 3 (IFITM3) dually regulates its endocytosis and ubiquitination. *The Journal of biological chemistry* 289, 11986-11992.
- Chesarino, N.M., McMichael, T.M., Yount, J.S., 2014b. Regulation of the trafficking and antiviral activity of IFITM3 by post-translational modifications. *Future microbiology* 9, 1151-1163.
- Cheung, P.Y., Limouse, C., Mabuchi, H., Pfeffer, S.R., 2015. Protein flexibility is required for vesicle tethering at the Golgi. *eLife* 4.
- Chutiwitoonchai, N., Hiyoshi, M., Hiyoshi-Yoshidomi, Y., Hashimoto, M., Tokunaga, K., Suzu, S., 2013. Characteristics of IFITM, the newly identified IFN-inducible anti-HIV-1 family proteins. *Microbes and infection* 15, 280-290.

- Cluett, E.B., Brown, W.J., 1992. Adhesion of Golgi cisternae by proteinaceous interactions: intercisternal bridges as putative adhesive structures. *Journal of cell science* 103 ( Pt 3), 773-784.
- Compton, A.A., Bruel, T., Porrot, F., Mallet, A., Sachse, M., Euvrard, M., Liang, C., Casartelli, N., Schwartz, O., 2014. IFITM proteins incorporated into HIV-1 virions impair viral fusion and spread. *Cell host & microbe* 16, 736-747.
- Compton, A.A., Roy, N., Porrot, F., Billet, A., Casartelli, N., Yount, J.S., Liang, C., Schwartz, O., 2016. Natural mutations in IFITM3 modulate post-translational regulation and toggle antiviral specificity. *EMBO reports* 17, 1657-1671.
- Dejgaard, S.Y., Murshid, A., Erman, A., Kizilay, O., Verbich, D., Lodge, R., Dejgaard, K., Ly-Hartig, T.B., Pepperkok, R., Simpson, J.C., Presley, J.F., 2008. Rab18 and Rab43 have key roles in ER-Golgi trafficking. *Journal of cell science* 121, 2768-2781.
- Desai, T.M., Marin, M., Chin, C.R., Savidis, G., Brass, A.L., Melikyan, G.B., 2014. IFITM3 restricts influenza A virus entry by blocking the formation of fusion pores following virus-endosome hemifusion. *PLoS pathogens* 10, e1004048.
- Drin, G., Casella, J.F., Gautier, R., Boehmer, T., Schwartz, T.U., Antonny, B., 2007. A general amphipathic alpha-helical motif for sensing membrane curvature. *Nature structural & molecular biology* 14, 138-146.
- Drin, G., Morello, V., Casella, J.F., Gounon, P., Antonny, B., 2008. Asymmetric tethering of flat and curved lipid membranes by a golgin. *Science (New York, N.Y.)* 320, 670-673.
- Everitt, A.R., Clare, S., McDonald, J.U., Kane, L., Harcourt, K., Ahras, M., Lall, A., Hale, C., Rodgers, A., Young, D.B., Haque, A., Billker, O., Tregoning, J.S., Dougan, G., Kellam, P., 2013. Defining the range of pathogens susceptible to Ifitm3 restriction using a knockout mouse model. *PLoS one* 8, e80723.
- Fackler, O.T., Peterlin, B.M., 2000. Endocytic entry of HIV-1. *Current biology : CB* 10, 1005-1008.
- Fan, J., Peng, Z., Zhou, C., Qiu, G., Tang, H., Sun, Y., Wang, X., Li, Q., Le, X., Xie, K., 2008. Gene-expression profiling in Chinese patients with colon cancer by coupling experimental and bioinformatic genomewide gene-expression analyses: identification and validation of IFITM3 as a biomarker of early colon carcinogenesis. *Cancer* 113, 266-275.
- Farber, C.R., Reich, A., Barnes, A.M., Becerra, P., Rauch, F., Cabral, W.A., Bae, A., Quinlan, A., Glorieux, F.H., Clemens, T.L., Marini, J.C., 2014. A novel IFITM5 mutation in severe atypical osteogenesis imperfecta type VI impairs osteoblast production of pigment epithelium-derived factor. *Journal of bone and mineral research : the official journal of the American Society for Bone and Mineral Research* 29, 1402-1411.
- Feeley, E.M., Sims, J.S., John, S.P., Chin, C.R., Pertel, T., Chen, L.M., Gaiha, G.D., Ryan, B.J., Donis, R.O., Elledge, S.J., Brass, A.L., 2011. IFITM3 inhibits influenza A virus infection by preventing cytosolic entry. *PLoS pathogens* 7, e1002337.
- Foster, T.L., Wilson, H., Iyer, S.S., Coss, K., Doores, K., Smith, S., Kellam, P., Finzi, A., Borrow, P., Hahn, B.H., Neil, S.J.D., 2016. Resistance of Transmitted Founder HIV-1 to IFITM-Mediated Restriction. *Cell host & microbe* 20, 429-442.
- Franke, W.W., Scheer, U., 1972. Structural details of dictyosomal pores. *Journal of ultrastructure research* 40, 132-144.

- Friedman, R.L., Manly, S.P., McMahon, M., Kerr, I.M., Stark, G.R., 1984. Transcriptional and posttranscriptional regulation of interferon-induced gene expression in human cells. *Cell* 38, 745-755.
- Gaio, V., Nunes, B., Pechirra, P., Conde, P., Guimar, R., Dias, C.M., Barreto, M., 2016. Hospitalization Risk Due to Respiratory Illness Associated with Genetic Variation at IFITM3 in Patients with Influenza A(H1N1)pdm09 Infection: A Case-Control Study. *PloS one* 11, e0158181.
- Gillingham, A.K., Munro, S., 2016. Finding the Golgi: Golgin Coiled-Coil Proteins Show the Way. *Trends in cell biology* 26, 399-408.
- Gomez-Navarro, N., Miller, E., 2016. Protein sorting at the ER-Golgi interface. *The Journal of cell biology* 215, 769-778.
- Goud, B., Liu, S., Storrie, B., 2018. Rab proteins as major determinants of the Golgi complex structure. *Small GTPases* 9, 66-75.
- Goud, B., Zahraoui, A., Tavitian, A., Saraste, J., 1990. Small GTP-binding protein associated with Golgi cisternae. *Nature* 345, 553-556.
- Hanagata, N., 2016. IFITM5 mutations and osteogenesis imperfecta. *Journal of bone and mineral metabolism* 34, 123-131.
- Hanagata, N., Li, X., Morita, H., Takemura, T., Li, J., Minowa, T., 2011. Characterization of the osteoblast-specific transmembrane protein IFITM5 and analysis of IFITM5-deficient mice. *Journal of bone and mineral metabolism* 29, 279-290.
- Hatano, H., Kudo, Y., Ogawa, I., Tsunematsu, T., Kikuchi, A., Abiko, Y., Takata, T., 2008. IFN-induced transmembrane protein 1 promotes invasion at early stage of head and neck cancer progression. *Clinical cancer research : an official journal of the American Association for Cancer Research* 14, 6097-6105.
- Hickford, D., Frankenberg, S., Shaw, G., Renfree, M.B., 2012. Evolution of vertebrate interferon inducible transmembrane proteins. *BMC genomics* 13, 155.
- Hu, J., Wang, S., Zhao, Y., Guo, Q., Zhang, D., Chen, J., Li, J., Fei, Q., Sun, Y., 2014. Mechanism and biological significance of the overexpression of IFITM3 in gastric cancer. *Oncology reports* 32, 2648-2656.
- Huang, I.C., Bailey, C.C., Weyer, J.L., Radoshitzky, S.R., Becker, M.M., Chiang, J.J., Brass, A.L., Ahmed, A.A., Chi, X., Dong, L., Longobardi, L.E., Boltz, D., Kuhn, J.H., Elledge, S.J., Bavari, S., Denison, M.R., Choe, H., Farzan, M., 2011. Distinct patterns of IFITM-mediated restriction of filoviruses, SARS coronavirus, and influenza A virus. *PLoS pathogens* 7, e1001258.
- Infusini, G., Smith, J.M., Yuan, H., Pizzolla, A., Ng, W.C., Londrigan, S.L., Haque, A., Reading, P.C., Villadangos, J.A., Wakim, L.M., 2015. Respiratory DC Use IFITM3 to Avoid Direct Viral Infection and Safeguard Virus-Specific CD8+ T Cell Priming. *PloS one* 10, e0143539.
- Jia, R., Pan, Q., Ding, S., Rong, L., Liu, S.L., Geng, Y., Qiao, W., Liang, C., 2012. The N-terminal region of IFITM3 modulates its antiviral activity by regulating IFITM3 cellular localization. *Journal of virology* 86, 13697-13707.
- Jia, R., Xu, F., Qian, J., Yao, Y., Miao, C., Zheng, Y.M., Liu, S.L., Guo, F., Geng, Y., Qiao, W., Liang, C., 2014. Identification of an endocytic signal essential for the antiviral action of IFITM3. *Cellular microbiology* 16, 1080-1093.
- Jiang, D., Weidner, J.M., Qing, M., Pan, X.B., Guo, H., Xu, C., Zhang, X., Birk, A., Chang, J., Shi, P.Y., Block, T.M., Guo, J.T., 2010. Identification of five interferon-induced cellular proteins that inhibit west nile virus and dengue virus infections. *Journal of virology* 84, 8332-8341.

- Jiang, L.Q., Xia, T., Hu, Y.H., Sun, M.S., Yan, S., Lei, C.Q., Shu, H.B., Guo, J.H., Liu, Y., 2018. IFITM3 inhibits virus-triggered induction of type I interferon by mediating autophagosome-dependent degradation of IRF3. *Cellular & molecular immunology* 15, 858-867.
- John, S.P., Chin, C.R., Perreira, J.M., Feeley, E.M., Aker, A.M., Savidis, G., Smith, S.E., Elia, A.E., Everitt, A.R., Vora, M., Pertel, T., Elledge, S.J., Kellam, P., Brass, A.L., 2013. The CD225 domain of IFITM3 is required for both IFITM protein association and inhibition of influenza A virus and dengue virus replication. *Journal of virology* 87, 7837-7852.
- Kamiński, D.M., 2014. Recent progress in the study of the interactions of amphotericin B with cholesterol and ergosterol in lipid environments. *European biophysics journal : EBJ* 43, 453-467.
- Kane, M., Zang, T.M., Rihn, S.J., Zhang, F., Kueck, T., Alim, M., Schoggins, J., Rice, C.M., Wilson, S.J., Bieniasz, P.D., 2016. Identification of Interferon-Stimulated Genes with Antiretroviral Activity. *Cell host & microbe* 20, 392-405.
- Kelly, E.E., Giordano, F., Horgan, C.P., Jollivet, F., Raposo, G., McCaffrey, M.W., 2012. Rab30 is required for the morphological integrity of the Golgi apparatus. *Biology of the cell* 104, 84-101.
- Lange, U.C., Adams, D.J., Lee, C., Barton, S., Schneider, R., Bradley, A., Surani, M.A., 2008. Normal germ line establishment in mice carrying a deletion of the Ifitm/Fragilis gene family cluster. *Molecular and cellular biology* 28, 4688-4696.
- Lee, N., Cao, B., Ke, C., Lu, H., Hu, Y., Tam, C.H.T., Ma, R.C.W., Guan, D., Zhu, Z., Li, H., Lin, M., Wong, R.Y.K., Yung, I.M.H., Hung, T.N., Kwok, K., Horby, P., Hui, D.S.C., Chan, M.C.W., Chan, P.K.S., 2017. IFITM3, TLR3, and CD55 Gene SNPs and Cumulative Genetic Risks for Severe Outcomes in Chinese Patients With H7N9/H1N1pdm09 Influenza. *The Journal of infectious diseases* 216, 97-104.
- Li, D., Peng, Z., Tang, H., Wei, P., Kong, X., Yan, D., Huang, F., Li, Q., Le, X., Li, Q., Xie, K., 2011. KLF4-mediated negative regulation of IFITM3 expression plays a critical role in colon cancer pathogenesis. *Clinical cancer research : an official journal of the American Association for Cancer Research* 17, 3558-3568.
- Li, K., Markosyan, R.M., Zheng, Y.M., Golfetto, O., Bungart, B., Li, M., Ding, S., He, Y., Liang, C., Lee, J.C., Gratton, E., Cohen, F.S., Liu, S.L., 2013. IFITM proteins restrict viral membrane hemifusion. *PLoS pathogens* 9, e1003124.
- Lin, T.Y., Chin, C.R., Everitt, A.R., Clare, S., Perreira, J.M., Savidis, G., Aker, A.M., John, S.P., Sarlah, D., Carreira, E.M., Elledge, S.J., Kellam, P., Brass, A.L., 2013. Amphotericin B increases influenza A virus infection by preventing IFITM3-mediated restriction. *Cell reports* 5, 895-908.
- Liu, C., Mei, M., Li, Q., Roboti, P., Pang, Q., Ying, Z., Gao, F., Lowe, M., Bao, S., 2017. Loss of the golgin GM130 causes Golgi disruption, Purkinje neuron loss, and ataxia in mice. *Proceedings of the National Academy of Sciences of the United States of America* 114, 346-351.
- Liu, S., Storrie, B., 2015. How Rab proteins determine Golgi structure. *International review of cell and molecular biology* 315, 1-22.
- Lu, J., Pan, Q., Rong, L., He, W., Liu, S.L., Liang, C., 2011. The IFITM proteins inhibit HIV-1 infection. *Journal of virology* 85, 2126-2137.
- Magdeleine, M., Gautier, R., Gounon, P., Barelli, H., Vanni, S., Antony, B., 2016. A filter at the entrance of the Golgi that selects vesicles according to size and bulk lipid composition. *eLife* 5.
- Martinez, O., Antony, C., Pehau-Arnaudet, G., Berger, E.G., Salamero, J., Goud, B., 1997. GTP-bound forms of rab6 induce the redistribution of Golgi proteins into the endoplasmic reticulum.

- Proceedings of the National Academy of Sciences of the United States of America 94, 1828-1833.
- Melvin, W.J., McMichael, T.M., Chesarino, N.M., Hach, J.C., Yount, J.S., 2015. IFITMs from Mycobacteria Confer Resistance to Influenza Virus When Expressed in Human Cells. *Viruses* 7, 3035-3052.
- Mills, T.C., Rautanen, A., Elliott, K.S., Parks, T., Naranbhai, V., Ieven, M.M., Butler, C.C., Little, P., Verheij, T., Garrard, C.S., Hinds, C., Goossens, H., Chapman, S., Hill, A.V., 2014. IFITM3 and susceptibility to respiratory viral infections in the community. *The Journal of infectious diseases* 209, 1028-1031.
- Miyauchi, K., Kim, Y., Latinovic, O., Morozov, V., Melikyan, G.B., 2009. HIV enters cells via endocytosis and dynamin-dependent fusion with endosomes. *Cell* 137, 433-444.
- Moffatt, P., Gaumont, M.H., Salois, P., Sellin, K., Bessette, M.C., Godin, E., de Oliveira, P.T., Atkins, G.J., Nanci, A., Thomas, G., 2008. Bril: a novel bone-specific modulator of mineralization. *Journal of bone and mineral research : the official journal of the American Society for Bone and Mineral Research* 23, 1497-1508.
- Mollenhauer, H.H., 1965. TRANSITION FORMS OF GOLGI APPARATUS SECRETION VESICLES. *Journal of ultrastructure research* 12, 439-446.
- Mudhasani, R., Tran, J.P., Retterer, C., Radoshitzky, S.R., Kota, K.P., Altamura, L.A., Smith, J.M., Packard, B.Z., Kuhn, J.H., Costantino, J., Garrison, A.R., Schmaljohn, C.S., Huang, I.C., Farzan, M., Bavari, S., 2013. IFITM-2 and IFITM-3 but not IFITM-1 restrict Rift Valley fever virus. *Journal of virology* 87, 8451-8464.
- Muñoz-Moreno, R., Cuesta-Geijo, M., Martínez-Romero, C., Barrado-Gil, L., Galindo, I., García-Sastre, A., Alonso, C., 2016. Antiviral Role of IFITM Proteins in African Swine Fever Virus Infection. *PloS one* 11, e0154366.
- Munro, S., 2011. Sean Munro: revealing the Golgi's true identity. Interview by Ben Short. *The Journal of cell biology* 192, 4-5.
- Muschalik, N., Munro, S., 2018. Golgins. *Current biology : CB* 28, R374-r376.
- Naderi, M., Hashemi, M., Abedipour, F., Bahari, G., Rezaei, M., Taheri, M., 2016. Evaluation of interferon-induced transmembrane protein-3 (IFITM3) rs7478728 and rs3888188 polymorphisms and the risk of pulmonary tuberculosis. *Biomedical reports* 5, 634-638.
- Nakamura, N., Rabouille, C., Watson, R., Nilsson, T., Hui, N., Slusarewicz, P., Kreis, T.E., Warren, G., 1995. Characterization of a cis-Golgi matrix protein, GM130. *The Journal of cell biology* 131, 1715-1726.
- Narayana, S.K., Helbig, K.J., McCartney, E.M., Eyre, N.S., Bull, R.A., Eltahla, A., Lloyd, A.R., Beard, M.R., 2015. The Interferon-induced Transmembrane Proteins, IFITM1, IFITM2, and IFITM3 Inhibit Hepatitis C Virus Entry. *The Journal of biological chemistry* 290, 25946-25959.
- Puthenveedu, M.A., von Zastrow, M., 2006. Cargo regulates clathrin-coated pit dynamics. *Cell* 127, 113-124.
- Qian, J., Le Duff, Y., Wang, Y., Pan, Q., Ding, S., Zheng, Y.M., Liu, S.L., Liang, C., 2015. Primate lentiviruses are differentially inhibited by interferon-induced transmembrane proteins. *Virology* 474, 10-18.
- Randolph, A.G., Yip, W.K., Allen, E.K., Rosenberger, C.M., Agan, A.A., Ash, S.A., Zhang, Y., Bhangale, T.R., Finkelstein, D., Cvijanovich, N.Z., Mourani, P.M., Hall, M.W., Su, H.C., Thomas,

- P.G., 2017. Evaluation of IFITM3 rs12252 Association With Severe Pediatric Influenza Infection. *The Journal of infectious diseases* 216, 14-21.
- Rosati, A., Basile, A., D'Auria, R., d'Avenia, M., De Marco, M., Falco, A., Festa, M., Guerriero, L., Iorio, V., Parente, R., Pascale, M., Marzullo, L., Franco, R., Arra, C., Barbieri, A., Rea, D., Menichini, G., Hahne, M., Bijlsma, M., Barcaroli, D., Sala, G., di Mola, F.F., di Sebastiano, P., Todoric, J., Antonucci, L., Corvest, V., Jawhari, A., Firpo, M.A., Tuveson, D.A., Capunzo, M., Karin, M., De Laurenzi, V., Turco, M.C., 2015. BAG3 promotes pancreatic ductal adenocarcinoma growth by activating stromal macrophages. *Nature communications* 6, 8695.
- Sällman Almén, M., Bringeland, N., Fredriksson, R., Schiöth, H.B., 2012. The dispanins: a novel gene family of ancient origin that contains 14 human members. *PloS one* 7, e31961.
- Savidis, G., Perreira, J.M., Portmann, J.M., Meraner, P., Guo, Z., Green, S., Brass, A.L., 2016. The IFITMs Inhibit Zika Virus Replication. *Cell reports* 15, 2323-2330.
- Schoggins, J.W., 2014. Interferon-stimulated genes: roles in viral pathogenesis. *Current opinion in virology* 6, 40-46.
- Schoggins, J.W., Wilson, S.J., Panis, M., Murphy, M.Y., Jones, C.T., Bieniasz, P., Rice, C.M., 2011. A diverse range of gene products are effectors of the type I interferon antiviral response. *Nature* 472, 481-485.
- Shan, J., Zhao, B., Shan, Z., Nie, J., Deng, R., Xiong, R., Tsun, A., Pan, W., Zhao, H., Chen, L., Jin, Y., Qian, Z., Lui, K., Liang, R., Li, D., Sun, B., Lavillette, D., Xu, K., Li, B., 2017. Histone demethylase LSD1 restricts influenza A virus infection by erasing IFITM3-K88 monomethylation. *PLoS pathogens* 13, e1006773.
- Shan, Z., Han, Q., Nie, J., Cao, X., Chen, Z., Yin, S., Gao, Y., Lin, F., Zhou, X., Xu, K., Fan, H., Qian, Z., Sun, B., Zhong, J., Li, B., Tsun, A., 2013. Negative regulation of interferon-induced transmembrane protein 3 by SET7-mediated lysine monomethylation. *The Journal of biological chemistry* 288, 35093-35103.
- Shen, C., Wu, X.R., Jiao, W.W., Sun, L., Feng, W.X., Xiao, J., Miao, Q., Liu, F., Yin, Q.Q., Zhang, C.G., Guo, Y.J., Shen, A.D., 2013. A functional promoter polymorphism of IFITM3 is associated with susceptibility to pediatric tuberculosis in Han Chinese population. *PloS one* 8, e67816.
- Sinka, R., Gillingham, A.K., Kondylis, V., Munro, S., 2008. Golgi coiled-coil proteins contain multiple binding sites for Rab family G proteins. *The Journal of cell biology* 183, 607-615.
- Sloan, R.D., Kuhl, B.D., Mesplède, T., Münch, J., Donahue, D.A., Wainberg, M.A., 2013. Productive entry of HIV-1 during cell-to-cell transmission via dynamin-dependent endocytosis. *Journal of virology* 87, 8110-8123.
- Slusarewicz, P., Nilsson, T., Hui, N., Watson, R., Warren, G., 1994. Isolation of a matrix that binds medial Golgi enzymes. *The Journal of cell biology* 124, 405-413.
- Smith, S.E., Gibson, M.S., Wash, R.S., Ferrara, F., Wright, E., Temperton, N., Kellam, P., Fife, M., 2013. Chicken interferon-inducible transmembrane protein 3 restricts influenza viruses and lyssaviruses in vitro. *Journal of virology* 87, 12957-12966.
- Steegmaier, M., Klumperman, J., Foletti, D.L., Yoo, J.S., Scheller, R.H., 1999. Vesicle-associated membrane protein 4 is implicated in trans-Golgi network vesicle trafficking. *Molecular biology of the cell* 10, 1957-1972.
- Tanaka, S.S., Nagamatsu, G., Tokitake, Y., Kasa, M., Tam, P.P., Matsui, Y., 2004. Regulation of expression of mouse interferon-induced transmembrane protein like gene-3, Ifitm3 (mil-1,

- fragilis), in germ cells. *Developmental dynamics : an official publication of the American Association of Anatomists* 230, 651-659.
- Tanaka, S.S., Yamaguchi, Y.L., Tsoi, B., Lickert, H., Tam, P.P., 2005. IFITM/Mil/fragilis family proteins IFITM1 and IFITM3 play distinct roles in mouse primordial germ cell homing and repulsion. *Developmental cell* 9, 745-756.
- Tartour, K., Appourchaux, R., Gaillard, J., Nguyen, X.N., Durand, S., Turpin, J., Beaumont, E., Roch, E., Berger, G., Mahieux, R., Brand, D., Roingeard, P., Cimarelli, A., 2014. IFITM proteins are incorporated onto HIV-1 virion particles and negatively imprint their infectivity. *Retrovirology* 11, 103.
- Tartour, K., Cimarelli, A., 2015. [IFITM, a common barrier to many viruses]. *Medecine sciences : M/S* 31, 377-382.
- Volchuk, A., Ravazzola, M., Perrelet, A., Eng, W.S., Di Liberto, M., Varlamov, O., Fukasawa, M., Engel, T., Söllner, T.H., Rothman, J.E., Orci, L., 2004. Countercurrent distribution of two distinct SNARE complexes mediating transport within the Golgi stack. *Molecular biology of the cell* 15, 1506-1518.
- Wang, Y., Pan, Q., Ding, S., Wang, Z., Yu, J., Finzi, A., Liu, S.L., Liang, C., 2017. The V3 Loop of HIV-1 Env Determines Viral Susceptibility to IFITM3 Impairment of Viral Infectivity. *Journal of virology* 91.
- Wang, Z., Zhang, A., Wan, Y., Liu, X., Qiu, C., Xi, X., Ren, Y., Wang, J., Dong, Y., Bao, M., Li, L., Zhou, M., Yuan, S., Sun, J., Zhu, Z., Chen, L., Li, Q., Zhang, Z., Zhang, X., Lu, S., Doherty, P.C., Kedzierska, K., Xu, J., 2014. Early hypercytokinemia is associated with interferon-induced transmembrane protein-3 dysfunction and predictive of fatal H7N9 infection. *Proceedings of the National Academy of Sciences of the United States of America* 111, 769-774.
- Warren, C.J., Griffin, L.M., Little, A.S., Huang, I.C., Farzan, M., Pyeon, D., 2014. The antiviral restriction factors IFITM1, 2 and 3 do not inhibit infection of human papillomavirus, cytomegalovirus and adenovirus. *PloS one* 9, e96579.
- Wee, Y.S., Roundy, K.M., Weis, J.J., Weis, J.H., 2012. Interferon-inducible transmembrane proteins of the innate immune response act as membrane organizers by influencing clathrin and v-ATPase localization and function. *Innate immunity* 18, 834-845.
- Weidner, J.M., Jiang, D., Pan, X.B., Chang, J., Block, T.M., Guo, J.T., 2010. Interferon-induced cell membrane proteins, IFITM3 and tetherin, inhibit vesicular stomatitis virus infection via distinct mechanisms. *Journal of virology* 84, 12646-12657.
- Weston, S., Czesio, S., White, I.J., Smith, S.E., Kellam, P., Marsh, M., 2014. A membrane topology model for human interferon inducible transmembrane protein 1. *PloS one* 9, e104341.
- Wilkins, J., Zheng, Y.M., Yu, J., Liang, C., Liu, S.L., 2016. Nonhuman Primate IFITM Proteins Are Potent Inhibitors of HIV and SIV. *PloS one* 11, e0156739.
- Williams, D.E., Wu, W.L., Grotefend, C.R., Radic, V., Chung, C., Chung, Y.H., Farzan, M., Huang, I.C., 2014. IFITM3 polymorphism rs12252-C restricts influenza A viruses. *PloS one* 9, e110096.
- Winkler, M., Gärtner, S., Wrensch, F., Krawczak, M., Sauermann, U., Pöhlmann, S., 2017. Rhesus macaque IFITM3 gene polymorphisms and SIV infection. *PloS one* 12, e0172847.
- Witkos, T.M., Lowe, M., 2015. The Golgin Family of Coiled-Coil Tethering Proteins. *Frontiers in cell and developmental biology* 3, 86.
- Wrensch, F., Hoffmann, M., Gärtner, S., Nehlmeier, I., Winkler, M., Pöhlmann, S., 2017. Virion Background and Efficiency of Virion Incorporation Determine Susceptibility of Simian

Immunodeficiency Virus Env-Driven Viral Entry to Inhibition by IFITM Proteins. *Journal of virology* 91.

Wrensch, F., Winkler, M., Pöhlmann, S., 2014. IFITM proteins inhibit entry driven by the MERS-coronavirus spike protein: evidence for cholesterol-independent mechanisms. *Viruses* 6, 3683-3698.

Xu-Yang, Z., Pei-Yu, B., Chuan-Tao, Y., Wei, Y., Hong-Wei, M., Kang, T., Chun-Mei, Z., Ying-Feng, L., Xin, W., Ping-Zhong, W., Chang-Xing, H., Xue-Fan, B., Ying, Z., Zhan-Sheng, J., 2016. Interferon-Induced Transmembrane Protein 3 Inhibits Hantaan Virus Infection, and Its Single Nucleotide Polymorphism rs12252 Influences the Severity of Hemorrhagic Fever with Renal Syndrome. *Frontiers in immunology* 7, 535.

Xu, Y., Martin, S., James, D.E., Hong, W., 2002. GS15 forms a SNARE complex with syntaxin 5, GS28, and Ykt6 and is implicated in traffic in the early cisternae of the Golgi apparatus. *Molecular biology of the cell* 13, 3493-3507.

Xu, Y., Wong, S.H., Zhang, T., Subramaniam, V.N., Hong, W., 1997. GS15, a 15-kilodalton Golgi soluble N-ethylmaleimide-sensitive factor attachment protein receptor (SNARE) homologous to rbet1. *The Journal of biological chemistry* 272, 20162-20166.

Xuan, Y., Wang, L.N., Li, W., Zi, H.R., Guo, Y., Yan, W.J., Chen, X.B., Wei, P.M., 2015. IFITM3 rs12252 T>C polymorphism is associated with the risk of severe influenza: a meta-analysis. *Epidemiology and infection* 143, 2975-2984.

Yang, G., Xu, Y., Chen, X., Hu, G., 2007. IFITM1 plays an essential role in the antiproliferative action of interferon-gamma. *Oncogene* 26, 594-603.

Yang, M., Gao, H., Chen, P., Jia, J., Wu, S., 2013. Knockdown of interferon-induced transmembrane protein 3 expression suppresses breast cancer cell growth and colony formation and affects the cell cycle. *Oncology reports* 30, 171-178.

Yang, X., Tan, B., Zhou, X., Xue, J., Zhang, X., Wang, P., Shao, C., Li, Y., Li, C., Xia, H., Qiu, J., 2015. Interferon-Inducible Transmembrane Protein 3 Genetic Variant rs12252 and Influenza Susceptibility and Severity: A Meta-Analysis. *PloS one* 10, e0124985.

Yount, J.S., Karssemeijer, R.A., Hang, H.C., 2012. S-palmitoylation and ubiquitination differentially regulate interferon-induced transmembrane protein 3 (IFITM3)-mediated resistance to influenza virus. *The Journal of biological chemistry* 287, 19631-19641.

Yount, J.S., Moltedo, B., Yang, Y.Y., Charron, G., Moran, T.M., López, C.B., Hang, H.C., 2010. Palmitoylome profiling reveals S-palmitoylation-dependent antiviral activity of IFITM3. *Nature chemical biology* 6, 610-614.

Yu, F., Ng, S.S., Chow, B.K., Sze, J., Lu, G., Poon, W.S., Kung, H.F., Lin, M.C., 2011. Knockdown of interferon-induced transmembrane protein 1 (IFITM1) inhibits proliferation, migration, and invasion of glioma cells. *Journal of neuro-oncology* 103, 187-195.

Yu, J., Li, M., Wilkins, J., Ding, S., Swartz, T.H., Esposito, A.M., Zheng, Y.M., Freed, E.O., Liang, C., Chen, B.K., Liu, S.L., 2015. IFITM Proteins Restrict HIV-1 Infection by Antagonizing the Envelope Glycoprotein. *Cell reports* 13, 145-156.

Zani, A., Zhang, L., McMichael, T.M., Kenney, A.D., Chemudupati, M., Kwiek, J.J., Liu, S.L., Yount, J.S., 2019. Interferon-induced transmembrane proteins inhibit cell fusion mediated by trophoblast syncytins. *The Journal of biological chemistry* 294, 19844-19851.

- Zhang, W., Zhang, L., Zan, Y., Du, N., Yang, Y., Tien, P., 2015. Human respiratory syncytial virus infection is inhibited by IFN-induced transmembrane proteins. *The Journal of general virology* 96, 170-182.
- Zhang, Y.H., Zhao, Y., Li, N., Peng, Y.C., Giannoulatou, E., Jin, R.H., Yan, H.P., Wu, H., Liu, J.H., Liu, N., Wang, D.Y., Shu, Y.L., Ho, L.P., Kellam, P., McMichael, A., Dong, T., 2013. Interferon-induced transmembrane protein-3 genetic variant rs12252-C is associated with severe influenza in Chinese individuals. *Nature communications* 4, 1418.
- Zhao, B., Wang, H., Zong, G., Li, P., 2013. The role of IFITM3 in the growth and migration of human glioma cells. *BMC neurology* 13, 210.
- Zhao, X., Guo, F., Liu, F., Cuconati, A., Chang, J., Block, T.M., Guo, J.T., 2014. Interferon induction of IFITM proteins promotes infection by human coronavirus OC43. *Proceedings of the National Academy of Sciences of the United States of America* 111, 6756-6761.
- Zhu, R., Wang, J., Lei, X.Y., Gui, J.F., Zhang, Q.Y., 2013. Evidence for *Paralichthys olivaceus* IFITM1 antiviral effect by impeding viral entry into target cells. *Fish & shellfish immunology* 35, 918-926.
- Zhu, X., He, Z., Yuan, J., Wen, W., Huang, X., Hu, Y., Lin, C., Pan, J., Li, R., Deng, H., Liao, S., Zhou, R., Wu, J., Li, J., Li, M., 2015. IFITM3-containing exosome as a novel mediator for anti-viral response in dengue virus infection. *Cellular microbiology* 17, 105-118.

## Annexes

**Main thesis work article. bioRxiv preprint doi: <https://doi.org/10.1101/2021.03.29.437470>; this version was posted on March 29, 2021.**

**This work constitutes essentially the entire body of the thesis work presented above**

A novel domain within the CIL regulates egress of IFITM3 from the Golgi and prevents its deleterious accumulation in this apparatus

Li Zhong<sup>1</sup>, Rustem Uzbekov<sup>2,3</sup>, Chloé Journo<sup>1</sup>, Philippe Roingeard<sup>2,4</sup> and Andrea Cimorelli<sup>1</sup>

<sup>1</sup> Centre International de Recherche en Infectiologie (CIRI), Univ Lyon, Inserm, U1111, Université Claude Bernard Lyon 1, CNRS, UMR5308, ENS de Lyon, Lyon-France

<sup>2</sup> Plateforme IBiSA de Microscopie Electronique, Université de Tours et CHU de Tours, 37032 Tours, France

<sup>3</sup> Faculty of Bioengineering and Bioinformatics, Moscow State University, Leninskye gory 73, 119992 Moscow, Russia

<sup>4</sup> INSERM U1259, Université de Tours et CHU de Tours, 37032 Tours, France

§ Correspondent footnote: correspondence should be addressed to Andrea Cimorelli, CIRI, 46 Allée d'Italie, 69364 Lyon, France. E-mail: [acimarel@ens-lyon.fr](mailto:acimarel@ens-lyon.fr)  
Orcid: 0000-0003-0892-0488

Keywords: IFITM, Interferon, HIV, virus, innate immunity, Golgi, Trafficking, PRRT2

## Abstract

The InterFeron-Induced TransMembrane proteins (IFITMs) are broad viral inhibitors that protect cells by preventing viral-to-cellular membrane fusion and they belong to the dispanin/CD225 family that includes vesicle trafficking regulators and proteins of unknown functions into four subfamilies (A-D). In this study, we uncover a novel domain that regulates the egress of IFITM3 from the Golgi and that is required to prevent IFITM3-driven v- to t-SNAREs membrane fusion inhibition and Golgi dysfunctions.

The S-x-K-x-R-D domain is conserved among vertebrate members of the dispanin/CD225 A subfamily that regroups all IFITMs and through the study of mutations identified in patients affected by paroxysmal kinesigenic dyskinesia (PKD), we determine that it is functionally conserved also in PRRT2, member of the B subfamily.

Overall, our study defines a novel domain that regulates the egress of dispanin/CD225 members from the Golgi and stresses the importance that regulation of this process bears to preserve the functions of this apparatus.

## Introduction

The InterFeron-Induced TransMembrane proteins (IFITMs) are broad viral inhibitors that prevent membrane fusion between viral and cellular membranes, thus protecting the cell from infection 1. IFITMs belong to the dispanin/CD225 family of proteins that originated from metazoan lineages and diversified into four distinct subfamilies (A through D) that include proteins of known and yet unknown functions 2. The A subfamily regroups all IFITMs which in humans are: IFITM1, 2 and 3, that we will refer to hereafter as IFITMs, that are interferon (IFN)-induced proteins essentially studied in the context of viral infection 3; IFITM5 that plays undefined roles in Osteogenesis imperfecta type V, a bone-specific disease<sup>4</sup> and IFITM10 whose functions are unknown. An additional known member of the dispanin/CD225 family is the neuron specific PRoline-Rich Transmembrane protein 2 (PRRT2, B subfamily) that is involved in neurotransmitter vesicles regulation and has been genetically linked to benign familial infantile seizures (BFIS) and to paroxysmal kinesigenic dyskinesia (PKD), the most common type of paroxysmal movement disorder 5. Members of the dispanin/CD225 family are characterized by a similar structure consisting of an intramembrane domain (IMD, previously defined as transmembrane domain 1, TM1), a cytoplasmic intracellular loop (CIL) and a transmembrane domain TMD (previously defined as transmembrane domain 2, TM2, as schematically shown in Fig. 1a for IFITM3). By virtue of this structure, IFITMs decorate cellular membranes in which they act as membrane fusion

inhibitors. The distribution and activities of IFITMs on cellular membranes are highly regulated and are driven not only by distinct N and C termini responsible for the more prominent distribution of individual IFITMs at the plasma or at inner membranes as is the case for IFITM1 with respect to IFITM2 and 3, respectively, but also by several post-translational modifications and in particular palmitoylation on cysteine residues, ubiquitination and methylation on lysines, as well as phosphorylation on a specific tyrosine residue 6–10.

More recently, IFITMs have been linked to cellular functions independent from their protective role against viral infection in the regulation of glucose metabolism in mice, of phosphatidylinositol 3-kinase (PI3K) mediated signaling in B cells 11 and of trophoblast fusion during placental formation in vivo 12, overall supporting the notion that IFITM proteins likely act well beyond a viral context.

In this study, through an in-depth characterization of a novel gain-of-function IFITM3 mutant, we have been able to identify a novel protein domain with the CIL of IFITM3 that regulates its egress from the Golgi apparatus. Mutations within this domain lead to the retention of IFITM3 in this organelle, where IFITM3 interferes with the fusion mediated between vesicle and target Soluble N-éthylmaleimide-sensitive-factor Attachment protein REceptor ( $\nu$ - and t-SNAREs), impairing the functionalities of the Golgi secretory pathway.

Functional as well as in silico analyses allowed us to precisely define the Golgi egress 81S-x-K-x-R-D86 domain which is positioned after the IMD, at the beginning of the CIL and it is conserved across vertebrate members of the dispanin/CD225 A subfamily. Through the analysis of mutations identified in patients affected by PKD, we do show here that, despite no conservation at the amino acid level, this domain is functionally conserved also in PRRT2, a member of the B subfamily, thus raising the possibility of a general functional role in Golgi trafficking common to dispanin/CD225 subfamilies.

Overall, these results identify a domain that regulates egress of IFITM and IFITM-like proteins from the Golgi and given the deleterious effects that dysregulation of this process bears on the overall functionalities of this apparatus, they highlight the importance that correct regulation of IFITM trafficking has for the cell.

## Results

**A gain of function IFITM3 mutant affects glycoprotein trafficking.** During a previous mutagenesis study of the broad viral inhibitor IFITM3, we identified a mutant in the cytoplasmic intracellular loop region of IFITM3 (CIL, mutant 85-90 in which six consecutive residues were mutated to alanine, Fig. 1a) that exerted a strong inhibitory effect on the incorporation of HIV-1 Envelope glycoproteins at the surface of released virion particles<sup>13</sup>. At its simplest, the formation of infectious HIV-1 virion particles requires the gathering on the plasma membrane of two classes of structural viral proteins: Gag (and Gag-Pro-Pol, not marked here for clarity's sake) and Env (Fig. 1b). While Gag is translated from cytoplasmic mRNAs from free ribosomes, the Envelope glycoprotein undergoes co-translational ER translocation and reaches the plasma membrane following the ER-Golgi secretory pathway<sup>14</sup>. As such, loss of Envelope incorporation in virion particles may reflect potential effects of IFITM3 along this axis that we decided to investigate further.

Indeed, when expressed in HEK293T cells undergoing HIV-1 virion assembly (Fig. 1b-c), the 85-90 IFITM3 mutant induced only a moderate, yet detectable, decrease in the levels of cell-associated Gag and Env proteins when compared to control or WT IFITM3-expressing cells, but as expected it induced a drastic decrease in the amount of Env glycoprotein incorporated in purified virion particles (Fig. 1c). From this starting observation, we decided to determine whether this defect could be more generally reflective of an interference with Golgi-mediated trafficking, independently from HIV-1. To this end, the 85-90 IFITM3 mutant was co-expressed along with a fluorescent G protein of the Vesicular Stomatitis Virus (mEm.-VSV-G, Fig. 1d), prior to confocal microscopy analysis. Under these conditions, a strong perinuclear accumulation of mEm.-VSV-G was observed in cells expressing the mutant IFITM3, overall suggesting a defect in Golgi-mediated trafficking (Fig. 1d).

To further support this result, we analyzed the EndoH susceptibility of a non-tagged VSV-G followed by WB analysis, as an independent and commonly used technique to appreciate the progression of glycosylated proteins from the ER through the Golgi (Fig. 1e). Under these conditions, expression of WT IFITM3 led to a small but detectable accumulation of EndoH-sensitive VSV-G when compared to control cells which however did not reach statistical significance under the conditions used here. However, the proportion of EndoH-sensitive VSV-G protein was significantly increased upon expression of the 85-90 IFITM3 mutant, indicating a strong defect in the ER-Golgi secretory pathway in the presence of this mutant protein.

Overall, these results indicate that the expression of the 85-90 IFITM3 mutant affects the normal functionalities of the cellular ER-Golgi secretory pathway, highlighting it as a novel gain-of-function IFITM3 mutant.

**The 85-90 IFITM3 mutant accumulates in and leads to structural changes of the Golgi apparatus.** The 85-90 IFITM3 mutant did not significantly colocalize with the ER, nor with endosomal vesicles (Extended data Fig. 1). Instead, this mutant was strongly localized at the cis-Golgi (GM130 marker, Fig. 2a and 2b for a 3D-reconstruction of positive cells) and induced gross morphological changes in the appearance of the Golgi: punctiform in control and WT-IFITM3 expressing cells and inflated in cells expressing the 85-90 IFITM3 mutant. These structural changes were not only apparent after 3D-reconstruction of positive cells following confocal microscopy analysis (Fig. 2b), but also after electron microscopy analysis which more precisely indicated that the shape of the Golgi apparatus had lost its classical punctiform distribution in favor of an expansion of large vesicles (Fig. 2c).

**The 85-90 IFITM3 mutant affects fusion between t and v-SNAREs.** One of the key features of IFITM family members is their ability to interfere with viral-to cellular membranes fusion<sup>15–17</sup>. We thus hypothesized that Golgi dysfunctions could be caused by the interference of IFITM3 with the ability of v-SNARE vesicles to fuse to t-SNAREs compartments, a process that is key to maintain protein and membrane fluxes, that is key for the integrity of the Golgi and that is reminiscent of the fusion between membranes that is observed after the engagement of a viral envelope glycoprotein with its cellular receptor 1819. To test this hypothesis, we analyzed the ability of the 85-90 IFITM3 mutant to inhibit the fluorescent resonance energy transfer (FRET) that occurs upon fusion between GS15-CFP and ERS24-YFP bearing vesicles (v- and t-SNAREs, respectively), as a measure of membrane fusion inhibition in this compartment, as described<sup>20</sup> (Fig. 3a). Given that this analysis was carried out in living cells, an excess of the 85-90 IFITM3 mutant was used to ensure that the majority of GS15-CFP and ERS24-YFP double positive cells were also IFITM3-positive. Under these conditions, a statistically significant decrease in FRET was observed upon expression of the 85-90 IFITM3 mutant with respect to control cells, indicating that this mutant does indeed interfere with v- to t-SNAREs fusion, in agreement with the major function ascribed to IFITM3 as a membrane fusion inhibitor. To further support this observation, we overexpressed the v-SNARE GS15 and determined whether this could lead to Golgi trafficking normalization despite the presence of the 85-90 IFITM3 mutant. Indeed, v-SNAREs overexpression is known to bypass membrane fusion defects between Golgi membranes 21–23 and we thus hypothesized it could relieve the defect imposed by the IFITM3 mutant. To this end, increasing levels of GS15 were expressed along with a constant amount of both 85-90 IFITM3 mutant and VSV-G, prior to the analysis of the distribution of VSV-G within triple-positive cells (Fig. 3b). Under these conditions, GS15 was able to relieve the perinuclear accumulation of the VSV-G glycoprotein induced by the IFITM3 mutant and was also able to act similarly on the 85-90 IFITM3 mutant itself, supporting our contention that a main disruptive event due to the accumulation of the 85-90 IFITM3 mutant in the Golgi is the inhibition of v- to t-SNAREs fusion.

**The 85-90 mutation in the IFITM3 CIL defines a domain that regulates IFITM3 egress from the Golgi.** To assess whether the 85-90 mutation induced retention or relocalization of IFITM3 at the Golgi, we performed a time-course analysis of both WT and mutant IFITM3 from early to late time points after ectopic DNA transfection (Fig. 4). While both proteins exhibited a predominant Golgi distribution at 6 hours post transfection, such concentration gradually diminished in the case of WT IFITM3, in agreement with its functional exit from the Golgi. On the contrary, little changes were observed over time in the case of the 85-90 IFITM3 mutant that remained in this compartment, supporting the notion that the 85-90 mutation induces the retention, rather than the redistribution, of IFITM3 in the Golgi.

In agreement with this observation, incubation of cells with the broad trafficking inhibitor Monensin induced accrued Golgi accumulation of WT IFITM3, but as expected did not modify the distribution pattern of the 85-90 mutant (Extended data Fig. 2).

Overall, these results concur in indicating that the 85-90 mutation defines a protein domain within the CIL that regulates the normal egress of IFITM3 from the cis-Golgi.

**Fine mapping of the Golgi egress domain of IFITM3 within the CIL.** To more precisely map the residues that regulated the egress of IFITM3 from the Golgi, individual amino acids spanning the entire CIL were mutated to alanine and mutants were analyzed by confocal microscopy (Fig. 5a-b and Extended data Fig. 3, alanine residues in the CIL were instead mutated to glycines). With the exception of two mutants that were barely detectable by WB (D92A and G95A), the remaining mutants were expressed to detectable levels upon WB analysis. We noticed that the D92A mutant acquired also a nuclear localization unusual for IFITM proteins, but this was not characterized further. This mutagenesis study identified a number of residues whose mutation led to accrued accumulation of IFITM3 into the Golgi (S81, V82, K83, S84, R85, D86, A96, Q97, Q98, S101, T102, A103, K104, L106 and N107), indicating that several residues within the CIL participate to this phenotype. Interestingly however, the mutations that resulted in levels of IFITM3 localization in the Golgi equivalent to those of the 85-90 mutant were essentially clustered in a patch

(from residues S81 to D86) that was posited at the boundary between the end of the intramembrane domain of IFITM3 (IMD) and the start of the CIL and that overlapped with the 85-90 stretch. Thus, the complete mutagenesis of the CIL allowed us to more precisely refine the domain responsible for the exit of IFITM3 from the Golgi (81SxKSRD86).

**A generalized Golgi egress domain is conserved among members of the dispanin/CD225 subfamily A and is functionally conserved in PRRT2, a member of the dispanin/CD225 subfamily B, genetically associated to paroxysmal kinesigenic dyskinesia (PKD).** IFITMs belong to the larger dispanin/CD225 family which is itself divided into four subfamilies (A to D, Fig. 6a)<sup>2</sup>. The A subfamily is composed of IFITM1, 2 and 3, as well as IFITM5 and IFITM10, which are not IFN regulated and exert unclear functions that in the case of IFITM5 are associated to Osteogenesis imperfecta type V, a bone-related genetic disease<sup>4</sup>. The alignment of residues spanning the IFITM3 SxKSRD domain in human IFITMs, as well as their comparison in vertebrates (Fig. 6a, aligned sequences on the left for human IFITMs and Logo on the right for vertebrate IFITMs, respectively) indicated the presence of a consensus sequence conserved across vertebrate members of the dispanin/CD225 A subfamily: S-x-K-x-R-D. This patch was not conserved at the amino acid level in the remaining subfamilies.

To determine whether this consensus domain exerted similar functions in other IFITM proteins belonging to the A subfamily, a single point mutation was introduced in the corresponding domain of IFITM1 (R64A), that contrarily to IFITM3 is essentially localized at the plasma membrane due to the lack of specific trafficking domains at its N-terminus when compared to IFITM3. Under these conditions, the introduction of a single point mutation in the IFITM Golgi egress domain was sufficient to drive the redistribution of IFITM1 from the plasma membrane to the Golgi, as observed by confocal microscopy analysis (Fig. 6b).

Thus, *in silico* and functional analyses indicate the presence of a conserved S-x-K-x-R-D domain important for the exit of members of the dispanin/CD225 A subfamily from the Golgi.

Despite the fact that the functions of certain proteins belonging to the dispanin/CD225 family remain unknown (as is the case for TMEM90A, TMEM91, TMEM233 and TMEM265), the information existing on other members (TUSC5, TMEM90B and PRRT2) indicate functions revolving around vesicular trafficking and vesicular behavior<sup>5,24,25</sup>. Among them, PRRT2 acts as a regulator of neurotransmitter vesicles in neuron cells and is genetically linked to paroxysmal kinesigenic dyskinesia (PKD, the most common type of paroxysmal movement disorder), as well as benign familial infantile seizures (BFIS). While the Golgi egress domain identified in IFITM proteins did not appear to be conserved at the amino acid level in other subfamilies, we decided to investigate whether it could be functionally conserved in PRRT2 as a prototype member of the B subfamily. Indeed, we noticed that two mutations in PRRT2 have been identified in patients affected by PKD in the same CIL region at the boundary between the IMD and the CIL (A291V and R295Q, corresponding to the underlined positions 1 and 5 of the S-x-K-x-R-D domain)<sup>26,27</sup>.

To test this hypothesis, the R295Q and I291V mutations were introduced along with a R295A alanine mutation in PRRT2 and analyzed by confocal microscopy (Fig 6c). While WT PRRT2 exhibited a predominant plasma membrane distribution, introduction of the above-mentioned mutations led to accrued redistribution of PRRT2 in the Golgi, similarly to what described for IFITM3.

Thus, these results indicate that the boundary between the IMD and the CIL of members of the dispanin/CD225 family is important for the regulation of their trafficking from the Golgi. This domain can be clearly defined in members of the dispanin/CD225 A subfamily as a consensus sequence conserved in vertebrates, and despite sequence dissimilarity, it maintains similar functions in other subfamilies, at least as appreciated in PRRT2 using *de novo* generated as well as PKD-associated genetic mutations.

## Conclusions

In the present study, we have defined a novel domain within the CIL of IFITM3 that regulates egress from the Golgi through the characterization of a novel gain-of-function IFITM3 mutant. This 81S-x-K-x-R-D86 domain is conserved at the amino acid level in vertebrate members of the dispanin/CD225 A subfamily that regroups all IFITM members. In addition, we do show here that, despite no sequence similarity, this domain is nonetheless functionally conserved in at least one member of the B subfamily (PRRT2), raising the possibility of a general functional role across all dispanin/CD225 subfamilies.

Mutations of the Golgi egress domain lead to the retention of IFITM3 in the Golgi, where IFITM3 interferes with *v*-to-t-SNARE vesicles fusion, ultimately driving macroscopic changes in the Golgi apparatus and glycoproteins trafficking defects.

The inhibitory effect of the 85-90 IFITM3 mutant on v- to t-SNARE vesicles membrane fusion is highly reminiscent of the well-described negative effects of IFITM proteins on the fusion between viral and cellular membranes after viral envelopes engage their cellular receptors and in this respect it is not surprising that increased accumulation of IFITM3 at the Golgi affects SNAREs fusion similarly. However, these results stress the importance of a controlled regulation of the exit from the Golgi of IFITM3, and possibly of other members of the family, to avoid deleterious effects on the functionality of the entire apparatus.

While ER-sorting protein domains have been identified<sup>28</sup>, similar domains have not been characterized for the Golgi and our results thus provide an important piece of the puzzle to decorticate how proteins that transit through the Golgi may be sorted out of it.

The Golgi egress domain of IFITM3 can either serve as a docking site for specific co-factors that mediate trafficking within and from the Golgi (for instance Rab proteins), it can play a regulatory role of other IFITM regions, or of course a combination of both.

The 81S-x-K-x-R-D86 domain is specially posited between the IMD and the beginning of the CIL and it is thus in close proximity with a short amphipathic helix important for antiviral functions<sup>29</sup>, with two cysteine residues that can be palmitoylated and thus affect IFITM association to membranes (C71, C72 in human IFITM3; a third cysteine C105 is also present that appears less important in IFITM3 functions<sup>30,31</sup>) and a G-x3-G domain that has been shown to be important for IFITMs oligomerization and functions<sup>32</sup>. Furthermore, the K83 residue present within the 81S-x-K-x-R-D86 domain can be itself ubiquitinated<sup>6</sup> and together with residue K104 it has been recently described to mediate PIP3 binding of IFITM3 at the plasma membrane of B cells, in a process that is required for the correct formation of a PI3K signaling platform<sup>11</sup>. Although, our confocal microscopy data suggest that the K83 IFITM3 mutant may not act as a functional PI3K platform simply because it is retained in the Golgi, the possibility of ubiquitination of the 81S-x-K-x-R-D86, at least in members of the dispanin/CD225 A subfamily, implies the potential prospect of finely tuning Golgi egress according to the dynamic status of ubiquitination of IFITM3, thus adding an additional layer of regulation to this process.

Given that the 85-90 IFITM3 mutant is a proficient membrane fusion inhibitor, we believe it unlikely that the 81S-x-K-x-R-D86 domain plays a role in IFITM oligomerization driven by the G-x3-G domain, as this would have been expected to lead to a non-functional IFITM3 mutant incapable to inhibit v- to t-SNAREs fusion.

The model we favor is that the 81S-x-K-x-R-D86 domain regulates the access of proximal domains to post translational modifications that in turn affects IFITM trafficking and more specifically access to palmitoylation at proximal cysteines. This model is in agreement with a recent one proposed by the Rothman's lab in which Golgi exit of certain proteins relies on a gradient of palmitoylation<sup>33</sup>. The model could also explain why this domain plays a conserved functional role in diverse subfamilies, despite no discernable sequence similarity, as is the case for PRRT2. The presence of two cysteines proximal to the region corresponding to the domain that regulates egress from the Golgi in the A subfamily and in PRRT2 is indeed a common feature in all members of the different dispanin/CD225 subfamilies (C276/C278 in PRRT2; C114/116 in TUSC5 as members of the B subfamily; C171/C172 in TMEM90A; C015/C106 in TMEM91 for members of the C subfamily and C152/C153 for PRRT1, member of the D subfamily).

PRRT2 is a neuronal specific protein involved in pre- and post-synaptic neurotransmitter vesicles regulation and has been genetically linked to PKD. While the majority of PKD patients suffer from mutations that result either in absent or severely truncated proteins, a few exhibit non-synonymous changes in the context of the full-length protein. Our results indicate that among them, mutations in the Golgi egress domain of PRRT2 may work by causing relocation of the protein, thus diminishing the concentration of active PRRT2 at its normal functional sites (i.e. the plasma membrane).

Although IFITMs have been predominantly studied in a viral infection context, several reports indicate that these proteins can play more pleiotropic functions: they interfere with trophoblast fusion during placental formation by affecting syncytin-mediated membrane fusion<sup>12,34</sup>; they lead to glucose-related metabolic dysfunctions in mice through unknown mechanisms<sup>35</sup> and they concur to B cell signaling<sup>11</sup>. Interestingly, ectopic expression of IFITM proteins has been in some cases reported to decrease the overall levels of viral glycoproteins and even to act more generally on translation, although the underlying mechanism(s) remain unclear<sup>36,37</sup>. In this respect, our results may provide a mechanistical explanation for the decreased levels of glycoproteins, by suggesting that the phenotype can be driven by high levels of IFITM3 accumulation in the Golgi, for instance in conditions of prolonged interferon stimulation, that in turn alter glycoproteins trafficking and stability through this secretory pathway.

More generally, our results highlight the fine line that separates the protective effects of innate defense proteins against viral aggression, from the deleterious side-effects that they may play against the cell itself. The literature provides

other examples of this ambivalence for example in the family of apolipoprotein B mRNA editing enzyme, catalytic polypeptide-like 3 proteins (APOBEC3), prototypical anti-retroviral defense proteins. While the main function of APOBEC3 members is to mutate and thus inactivate retroviral genomes thanks to their cytidine deaminase activity, this same enzymatic activity also contributes to the tumorigenic process when it is turned against the cellular genome<sup>38–40</sup>.

IFITMs are potent inhibitors of membrane fusion in the context of viral infection, but since membrane fusion is a common process in the cell, their biology (intended here as the sum of activity, dynamic location, stability etc) must be tightly regulated to avoid deleterious effects on the cell itself. Together with other examples mentioned above and recently described in the literature, our results suggest that dysregulated expression of IFITM molecules and in particular with signals that interfere with its egress from the Golgi may lead to Golgi-related dysfunctions. This may be an as yet unappreciated contribution of IFITM proteins to some pathological conditions for example in cancers or in interferonopathies in which the expression of IFITM proteins appears deregulated.

## Methods

### Cells, plasmids and antibodies

Human embryonic kidney cells (HEK293T, ATCC cat. CRL-3216) were maintained in complete DMEM media with 10% Fetal Calf Serum (Sigma cat. F7524). Untagged WT IFITM3 (gene ID: 10410) and IFITM1 (gene ID: 8519) and corresponding mutants were either previously described (85-90; 13,41), or cloned (all others) by standard mutagenesis techniques in the plasmid pQCXIP (Clontech). WT human PRRT2 (gene ID: 112476) was synthesized as N-terminal HA tag fusion protein (Genewiz) in pcDNA3 vector (ThermoFisher) and single point mutants were generated on this matrix by standard molecular biology techniques.

The HIV-1 proviral clone NL4-3 and the VSV-G expression constructs have been described elsewhere<sup>42</sup>. The mEmerald-VSV-G (mEm.-VSV-G) coding construct was a gift from Michael Davidson (Addgene, 54307); pcDNA-D1ER coding for an ER targeted enhanced CFP was a gift from Amy Palmer & Roger Tsien (Addgene cat. 36325 43). GS15-CFP and ERS24-YFP (cyanin and yellow fluorescent proteins, respectively) were obtained by Oleg Varlamov from the Oregon National Primate Research Center, USA 20. The following primary antibodies were used for WB or confocal microscopy, as indicated. Mouse monoclonals: anti- $\alpha$ -Tubulin, anti-HA and anti-VSV-G (Sigma cat. T5168, cat. H3663 and cat. V5507, respectively), anti-LAMP2 (Santa Cruz Biotechnology, cat. sc-18822), anti-CD63 and anti-GM130 (BD biosciences cat. 556019 and cat. 610823); anti-HIV-1 p24 (obtained through the NIH HIV Reagent Program, Division of AIDS, NIAID, NIH, contributed by Dr. Bruce Chesebro and Kathy Wehrly, cat. ARP-3537). Rabbit polyclonal antibodies: anti-IFITM3 (Proteintech cat. 11714-1-AP), anti-IFITM1 (Proteintech, cat. 60074) and anti-GM130 (abcam cat. Ab52649). The sheep polyclonal antibody anti-HIV-1 Env was obtained through the NIH HIV Reagent Program, Division of AIDS, NIAID, NIH (contributed by Dr. Michael Phelan, cat. ARP-288).

The following secondary antibodies were used for WB: anti-mouse, anti-rabbit and anti-sheep IgG-Peroxidase conjugated (Sigma, cat. A9044 and cat. AP188P and Dako cat. P0163); while the following ones were used for confocal microscopy: donkey anti-rabbit IgG–Alexa Fluor 594 conjugate and donkey anti-mouse IgG–Alexa Fluor 488 conjugate (cat. A-21207 and cat. A-21202; Life Technologies).

### Ectopic DNA transfections, viral production and confocal microscopy analyses

HEK293T cells were directly seeded on 0.01% poly-L-lysine-coated coverslips (Sigma, cat. P4832) and analyzed 24 hours after ectopic DNA transfection (unless otherwise specified, Lipofectamine 3000 cat. L3000008, ThermoFisher, according to the manufacturer's instructions). Cells were washed three times with PBS 1x, fixed with 4% paraformaldehyde (Euromedex, cat. 15713) for 10 min, quenched with 50 mM NH<sub>4</sub>Cl (Sigma cat. A4514) for 10 min, and permeabilized with PBS–0.5% Triton X-100 (Sigma, cat. X100) for 5 min. After a blocking step in PBS–5% milk, cells were incubated with primary antibodies for 1 hour at room temperature (dilution 1:100), washed and then incubated with fluorescent secondary antibodies (dilution 1:100). A 4',6-diamidino-2-phenylindole (DAPI)-containing mounting medium was used (ThermoFisher, cat. 62248). Images were acquired using a spectral Zeiss LSM800 confocal microscope and analyzed with Fiji software (version 2.0.0). For 3D-reconstruction, z-stack collections were analyzed with the Imaris 9.2.0 software (Oxford Instruments Group). Colocalisations were quantified using the Pearson overlap coefficient (Fiji software).

IFITMs and PRRT2 coding DNAs were routinely transfected at a concentration of 1  $\mu$ g per well of a 24 well plate along with 0.2  $\mu$ g of VSV-G or of mEm.-VSV-G. When specified, increasing doses of GS15 coding DNA were also added (0, 0.2, 0.5 and 1  $\mu$ g).

Monensin was used at a final concentration of 0.2 mM for 3 hours, prior to analysis (Sigma, cat. M5273).

Production of HIV-1 virions particles was instead carried out by calcium phosphate DNA transfection of the HIV-1 proviral clone NL4-3 (ratio 3 to 1, NL4-3 over IFITM). Virion particles released in the supernatant of transfected cells were harvested forty-eight hours post transfection, syringe-filtered (0.45  $\mu$ m filters, Minisart, cat. 146622) to remove cellular debris and purified by ultracentrifugation over a 25% sucrose cushion (28,000 rpm for 2 hours; Beckman Coulter ultracentrifuge).

In confocal microscopy experiments using the GM130 Golgi marker, IFITM or VSV-G relocalization was quantified for each cell as the ratio between the signal present at the Golgi over the signal present in the cytoplasm (Golgi/cytoplasm ratio). When the GM130 marker was not used, perinuclear accumulation was either scored visually (as in Fig 1, in light of the extremely clear phenotype; binary scoring: perinuclear or non-perinuclear), or quantified by determining the average percentage of accumulation of VSV-G at the left or right part of the nucleus (asymmetric distribution= perinuclear accumulation; symmetric distribution= non-perinuclear accumulation). To bypass artificial measurements due to differences in size between left and right portions of the cell, the avg of the signals measured at each side of the cell were used. This measurement diminishes the absolute values of the protein present at one side, but offers the advantage of making measures independent from cell size differences. Visual scoring in Fig 1 was also confirmed through this analysis.

### **Electron microscopy**

Samples were fixed in mixture of 4% paraformaldehyde (TAAB Laboratories Equipment Ltd, United Kingdom, cat. F/P001) and 1% glutaraldehyde (Electron Microscopy Science, USA, cat. 16310) in 0.1 M phosphate buffer (pH 7.4) for 24 hours, washed three  $\times$  30 min in 0.1 M of phosphate buffer, and post-fixed for one hour with 2% osmium tetroxide (Electron Microscopy Science, USA, cat. 19190) in 0.15 M of phosphate buffer. After washing in 0.1 M of phosphate buffer for 20 min and two  $\times$  20 min in distilled H<sub>2</sub>O, samples were dehydrated in a graded series of ethanol solutions (50% ethanol two  $\times$  10 min; 70% ethanol three  $\times$  15 min and last portion for 14 hours; 90% ethanol three  $\times$  20 min; and 100% ethanol three  $\times$  20 min). Final dehydration was performed by 100% propylene oxide (PrOx, ThermoFisher (Kandel) GmbH, Germany, Lot X19E013) three  $\times$  20 min. Then, samples were incubated in PrOx/EPON epoxy resin (Fluka, Switzerland) mixture in a 3:1 ratio for two hours with closed caps, 16 hours with open caps, and in 100% EPON for 24 hours at room temperature. Samples were replaced in new 100% EPON and incubated at 37 °C for 48 hours and at 60 °C for 48 hours for polymerization. Serial ultra-thin sections (thickness 70 nm) were cut with a “Leica Ultracut UCT” ultramicrotome (Leica Microsystems GmbH, Wien, Austria), placed on TEM nickel one-slot grids (Agar Scientific, Ltd. United Kingdom, cat. G2500N) coated with Formvar film and stained 20 min with 5% uranyl acetate (Merck, Darmstadt, Germany, cat. 8473) and 5 min Reynolds lead citrate. The sections were then observed at 100 kV with a Jeol 1011 TEM (JEOL, Tokyo, Japan) connected to a Gatan digital camera driven by Digital Micrograph software (GMS 3, Gatan, Pleasanton, CA, USA).

### **Fluorescence Resonance Energy Transfer (FRET) microscopy**

Analyses were performed on live cells plated on a 35 mm glass-bottom dish and transfected with 2  $\mu$ g of DNA coding the 85-90 IFITM3 mutant and 0.5  $\mu$ g each of GS15-CFP and ERS24-YFP to ensure that the majority of cells examined were IFITM3-positive. After replacing media with phenol-red MEM supplemented with 10%FCS, cells were analyzed by confocal microscopy and images were acquired at a temperature of 37°C with a spectral Zeiss LSM710 confocal microscope, equipped with an argon laser and a 63X oil immersion objective. CFP and YFP were excited with a 458 and a 514 nm lasers (emission windows set at 465-505 nm and 525-600 nm, respectively) and images were acquired with a 512x512 resolution, 8 bit line average. Photobleaching of the donor YFP was performed with 4 sequential illuminations of the selected cell (4 frames, line average 2, iterations at 400, scan speed at 8, 514 nm laser AOTF setting at 100%). Four scans were acquired after each bleaching (two before and two after). FRET efficiency was calculated from the ratio of the CFP fluorescence measured post- and pre-YFP bleaching. Analyses were performed on 15–20 individual cells per sample group. The FRET control plasmid pECFP18aaEYFP from addgene.) was used for setup (Addgene cat. 109330, gift from Gabriele Kaminski Schierle)<sup>44</sup>. Images were analyzed using the ROI manager in Fiji software.

### **Glycosidase treatment assays and WB quantification**

Cell lysates expressing IFITM3 and VSV-G proteins were collected and split in three aliquots that were either untreated, or treated with Endoglycosidase H (EndoH, NEB, P0702S) or N-glycosylase F (PNGaseF, NEB P0704S), according to the manufacturer’s instructions. Treated lysates were then analyzed by WB, images acquired using Image Lab Touch Software (version 2.0.0.27, Chemidoc Imaging System from Bio-Rad) and bands were quantified by densitometry using the volume tool in the same software.

### Softwares

Electron microscopy: Digital Micrograph software (GMS 3, Gatan, Pleasanton, CA, USA). Confocal microscopy: Fiji software (version 2.0.0), Zen (version 2.3, Zeiss) and Imaris 9.2.0 software (Oxford Instruments Group). WB: Image Lab Touch Software (version 2.0.0.27, Chemidoc Imaging System from Bio-Rad). Statistics and graphs: Graphpad Prism8 (8.4.3, Graphpad software, LLC).

### Statistical analyses

The statistical analyses used in this study were calculated with the Graphpad Prism8 software: Student t tests (unpaired, two-tailed), one-way Anova tests with either Tukey's or Dunnett's multiple comparisons, as indicated in the figure legends.

### Acknowledgements

Thanks to Delphine Muriaux for sharing insights, to Romain Appourchaux for his initial input, to Léa Picard and Lucie Etienne for help with bioinformatic analyses and evolutionary discussions and to Federico Marziali for help with FRET experiments. We are indebted to Oleg Varlamov from the Oregon National Primate Research Center, USA for v- and t-SNARE constructs as well as to the different authors of plasmids retrieved through Addgene cited in the Methods section.

LZ is the recipient of a PhD fellowship of the Chinese Scholarship Council (CSC). Work in the laboratory of AC is supported by grants from the ANRS (AO-2019-1 and AO-2021-1), as well as the ANR (ANR-20-CE15-0025-01). The funders had no role in study design, data collection and analysis, decision to publish, or preparation of the manuscript. We acknowledge the contribution of the microscopy (LYMIC-PLATIM) platform of SFR BioSciences Gerland Lyon Sud (UMS3444/US8).

### Author Contributions

L.Z. designed and performed most of the experiments. R.U. and P.R. performed and analyzed electron microscopy. A.C. supervised the research and wrote the manuscript. All authors commented on the manuscript.

### Competing Interests statement

The authors declare no competing interests.

### Data availability

Source data is provided with this paper. There is no restriction on data availability.

### References

1. Diamond, M. S. & Farzan, M. The broad-spectrum antiviral functions of IFIT and IFITM proteins. *Nat Rev Immunol* 13, 46–57 (2013).
2. Sällman Almén, M., Bringeland, N., Fredriksson, R. & Schiöth, H. B. The dispanins: a novel gene family of ancient origin that contains 14 human members. *PLoS ONE* 7, e31961 (2012).
3. Brass, A. L. et al. The IFITM proteins mediate cellular resistance to influenza A H1N1 virus, West Nile virus, and dengue virus. *Cell* 139, 1243–1254 (2009).
4. Lim, J. Y. et al. A novel Ser40Trp variant in IFITM5 in a family with osteogenesis imperfecta and review of the literature. *Clin Dysmorphol* 28, 120–125 (2019).
5. Calame, D. J. et al. Presynaptic PRRT2 Deficiency Causes Cerebellar Dysfunction and Paroxysmal Kinesigenic Dyskinesia. *Neuroscience* 448, 272–286 (2020).
6. Chesarino, N. M., McMichael, T. M., Hach, J. C. & Yount, J. S. Phosphorylation of the Antiviral Protein Interferon-inducible Transmembrane Protein 3 (IFITM3) Dually Regulates Its Endocytosis and Ubiquitination. *J. Biol. Chem.* 289, 11986–11992 (2014).
7. Yount, J. S., Karssemeijer, R. A. & Hang, H. C. S -Palmitoylation and Ubiquitination Differentially Regulate Interferon-induced Transmembrane Protein 3 (IFITM3)-mediated Resistance to Influenza Virus. *J. Biol. Chem.* 287, 19631–19641 (2012).
8. Shan, J. et al. Histone demethylase LSD1 restricts influenza A virus infection by erasing IFITM3-K88 monomethylation. *PLoS Pathog.* 13, e1006773 (2017).
9. Jia, R. et al. The N-terminal region of IFITM3 modulates its antiviral activity by regulating IFITM3 cellular localization. *J. Virol.* 86, 13697–13707 (2012).
10. Jia, R. et al. Identification of an endocytic signal essential for the antiviral action of IFITM3. *Cell. Microbiol.* 16, 1080–1093 (2014).

11. Lee, J. et al. IFITM3 functions as a PIP3 scaffold to amplify PI3K signalling in B cells. *Nature* 1–7 (2020) doi:10.1038/s41586-020-2884-6.
12. Buchrieser, J. et al. IFITM proteins inhibit placental syncytiotrophoblast formation and promote fetal demise. *Science* 365, 176–180 (2019).
13. Appourchaux, R. et al. Functional Mapping of Regions Involved in the Negative Imprinting of Virion Particle Infectivity and in Target Cell Protection by Interferon-Induced Transmembrane Protein 3 against HIV-1. *J. Virol.* 93, (2019).
14. Swanstrom, R. & Wills, J. W. Synthesis, Assembly, and Processing of Viral Proteins. in *Retroviruses* (eds. Coffin, J. M., Hughes, S. H. & Varmus, H. E.) (Cold Spring Harbor Laboratory Press, 1997).
15. Coomer, C. A., Rahman, K. & Compton, A. A. CD225 Proteins: A Family Portrait of Fusion Regulators. *Trends Genet* (2021) doi:10.1016/j.tig.2021.01.004.
16. Suddala, K. C. et al. Interferon-induced transmembrane protein 3 blocks fusion of sensitive but not resistant viruses by partitioning into virus-carrying endosomes. *PLoS Pathog.* 15, e1007532 (2019).
17. Li, K. et al. IFITM Proteins Restrict Viral Membrane Hemifusion. *PLoS Pathog* 9, (2013).
18. Malsam, J. & Söllner, T. H. Organization of SNAREs within the Golgi stack. *Cold Spring Harb Perspect Biol* 3, a005249 (2011).
19. Wang, T., Li, L. & Hong, W. SNARE proteins in membrane trafficking. *Traffic* 18, 767–775 (2017).
20. Fukasawa, M., Cornea, A. & Varlamov, O. Selective control of SNARE recycling by Golgi retention. *FEBS Lett* 587, 2377–2384 (2013).
21. Babcock, M., Macleod, G. T., Leither, J. & Pallanck, L. Genetic analysis of soluble N-ethylmaleimide-sensitive factor attachment protein function in *Drosophila* reveals positive and negative secretory roles. *J Neurosci* 24, 3964–3973 (2004).
22. Kweon, Y., Rothe, A., Conibear, E. & Stevens, T. H. Ykt6p is a multifunctional yeast R-SNARE that is required for multiple membrane transport pathways to the vacuole. *Mol Biol Cell* 14, 1868–1881 (2003).
23. Nichols, B. J. & Pelham, H. R. B. SNAREs and membrane fusion in the Golgi apparatus. *Biochimica et Biophysica Acta (BBA) - Molecular Cell Research* 1404, 9–31 (1998).
24. Beaton, N. et al. TUSC5 regulates insulin-mediated adipose tissue glucose uptake by modulation of GLUT4 recycling. *Mol Metab* 4, 795–810 (2015).
25. Kalashnikova, E. et al. SynDIG1: an activity-regulated, AMPA- receptor-interacting transmembrane protein that regulates excitatory synapse development. *Neuron* 65, 80–93 (2010).
26. Becker, F. et al. PRRT2-related disorders: further PKD and ICCA cases and review of the literature. *J Neurol* 260, 1234–1244 (2013).
27. Liu, X.-R. et al. Novel PRRT2 mutations in paroxysmal dyskinesia patients with variant inheritance and phenotypes. *Genes Brain Behav* 12, 234–240 (2013).
28. Gomez-Navarro, N. & Miller, E. Protein sorting at the ER–Golgi interface. *J Cell Biol* 215, 769–778 (2016).
29. Chesarino, N. M. et al. IFITM 3 requires an amphipathic helix for antiviral activity. *EMBO Rep* 18, 1740–1751 (2017).
30. Yount, J. S. et al. Palmitoylome profiling reveals S-palmitoylation–dependent antiviral activity of IFITM3. *Nat Chem Biol* 6, 610–614 (2010).
31. McMichael, T. M. et al. The palmitoyltransferase ZDHHC20 enhances interferon-induced transmembrane protein 3 (IFITM3) palmitoylation and antiviral activity. *J. Biol. Chem.* 292, 21517–21526 (2017).
32. Rahman, K. et al. Homology-guided identification of a conserved motif linking the antiviral functions of IFITM3 to its oligomeric state. *Elife* 9, (2020).
33. Ernst, A. M. et al. S-Palmitoylation Sorts Membrane Cargo for Anterograde Transport in the Golgi. *Dev Cell* 47, 479–493.e7 (2018).
34. Zani, A. et al. Interferon-induced transmembrane proteins inhibit cell fusion mediated by trophoblast syncytins. *J. Biol. Chem.* 294, 19844–19851 (2019).
35. Wee, Y. S., Weis, J. J., Gahring, L. C., Rogers, S. W. & Weis, J. H. Age-related onset of obesity corresponds with metabolic dysregulation and altered microglia morphology in mice deficient for Ifitm proteins. *PLoS ONE* 10, e0123218 (2015).
36. Ahi, Y. S. et al. IFITM3 Reduces Retroviral Envelope Abundance and Function and Is Counteracted by glycoGag. *mBio* 11, (2020).
37. Lee, W.-Y. J., Fu, R. M., Liang, C. & Sloan, R. D. IFITM proteins inhibit HIV-1 protein synthesis. *Sci Rep* 8, 14551 (2018).
38. Uriu, K., Kosugi, Y., Ito, J. & Sato, K. The Battle between Retroviruses and APOBEC3 Genes: Its Past and Present. *Viruses* 13, (2021).

39. Law, E. K. et al. APOBEC3A catalyzes mutation and drives carcinogenesis in vivo. *J Exp Med* 217, (2020).
40. Granadillo Rodríguez, M., Flath, B. & Chelico, L. The interesting relationship between APOBEC3 deoxycytidine deaminases and cancer: a long road ahead. *Open Biol* 10, 200188 (2020).
41. John, S. P. et al. The CD225 domain of IFITM3 is required for both IFITM protein association and inhibition of influenza A virus and dengue virus replication. *J. Virol.* 87, 7837–7852 (2013).
42. Tartour, K. et al. IFITM proteins are incorporated onto HIV-1 virion particles and negatively imprint their infectivity. *Retrovirology* 11, 103 (2014).
43. Palmer, A. E., Jin, C., Reed, J. C. & Tsien, R. Y. Bcl-2-mediated alterations in endoplasmic reticulum Ca<sup>2+</sup> analyzed with an improved genetically encoded fluorescent sensor. *Proc Natl Acad Sci U S A* 101, 17404–17409 (2004).
44. Kaminski, C. F., Rees, E. J. & Schierle, G. S. K. A quantitative protocol for intensity-based live cell FRET imaging. *Methods Mol Biol* 1076, 445–454 (2014).

### Figure Legends

**Fig. 1. A novel gain-of-function IFITM3 mutant induces secretory pathway defects that affect glycoproteins trafficking.** a) Genomic structure of IFITM3 with a highlight on amino acids of the cytoplasmic intracellular loop (CIL). In mutant 85-90, red residues have been mutated to alanine. b) Schematic representation of HIV-1 virion assembly. c) HEK293T cells were transfected with DNAs coding for the HIV-1 proviral clone NL4-3 along with control, WT or 85-90 mutant IFITM3. Cells were lysed 48 hours after transfection, while virion particles released in the supernatant were first purified by ultracentrifugation through a 25% sucrose cushion. Both cellular and viral lysates were analyzed by WB. d) HEK293T cells were ectopically transfected with DNAs coding for the indicated IFITM3s along with the G protein of the Vesicular Stomatitis virus fused to the mEmerald fluorescent reporter (mEm.-VSV-G), prior to confocal microscopy analysis twenty-four hours later. Representative confocal microscopy images and graph presenting the proportion of double-positive cells displaying perinuclear accumulation of mEm.-VSV-G (binary scoring; three independent experiments; between 50 and 100 cells scored per sample). \*, p value <0.0001 following a one-way Anova, Tukey's multiple comparison test; non-statistically significant differences, not shown. e) Lysates obtained from cells expressing VSV-G along with control, WT and mutant IFITM3 were either untreated or treated with EndoH or PNGaseF prior to WB and densitometry quantification of the EndoH-sensitive and -resistant VSV-G forms. Panels present representative results, while the graph presents the proportions of EndoH-sensitive and -resistant VSV-G obtained in 5 independent experiments. \*, p value of 0.0021 following a one-way Anova, Tukey's multiple comparison test over control. Uncropped blots and source data are provided in the relevant section.

**Fig. 2. The 85-90 IFITM3 mutant colocalizes with and induces gross morphological changes in the Golgi.** a and b) Confocal microscopy analysis and 3D-reconstruction of cells expressing the indicated IFITM3 proteins. Representative images and graph presenting phenotype proportions in at least 100 cells scored per condition (binary scoring: inflated or normal Golgi, three independent experiments). \*, p=8.3x10<sup>-9</sup> following an unpaired, two-tailed Student t test. c) Representative electron microscopy analyses of HEK293T cells expressing WT or 85-90 IFITM3 proteins. The region enlarged at the right of each panel corresponds to the red inset. Source data is provided in the relevant section.

**Fig. 3. The 85-90 IFITM3 mutant impairs fusion between v- and t-SNAREs.** a) Schematic representation of the FRET experiment and representative images pre and post ERS24-YFP bleach. FRET experiments were performed on live HEK293T cells in which an excess of DNA coding for the 85-90 IFITM3 mutant was used over GS15-CFP and ERS24-YFP (five-fold excess) to ensure that the majority of cells analyzed were also IFITM3-positive. The boxes and whiskers plot presents the normalized decrease and values distribution in FRET observed in control and 85-90 IFITM3 expressing cells from three independent experiments and >20 cells examined. \*, p value of 0.0008, following an unpaired two-tailed Student t test. b) HEK293T cells expressing constant amounts of 85-90 IFITM3 and VSV-G were co-transfected with increasing amounts of GS15-CFP coding DNA, prior to confocal microscopy analysis (GS15/85-90 ratios of 0.2 and 0.5). Given that VSV-G accumulation in the Golgi leads to its asymmetrical perinuclear distribution in the cell, VSV-G fluorescence was determined for each cell according to the presented scheme. The fluorescence measured over distance in the cell was used to calculate the proportion of VSV-G protein present at one side (the left side was set as the side with higher protein accumulation). Representative pictures and graph presenting the distribution of VSV-G at one side of the cell in triple-positive cells (n=2 with 20 to 31 cells analyzed per condition). White circles highlight example cells of increased FRET (a) and of phenotypic differences in the perinuclear accumulation of VSV-

G (b), respectively. \*\*\*\*, p value of <0.0001 following a one-way Anova, Tukey's multiple comparison test over 85-90 IFITM3 condition with no GS15-CFP. Source data is provided in the relevant section.

**Fig. 4. Time course confocal microscopy analysis indicates that the 85-90 IFITM3 mutation affects the normal egress of IFITM3 from the Golgi.** HEK293T cells were examined by confocal microscopy at different times post ectopic DNA transfection to determine the localization of IFITM3 proteins over time. Representative pictures and graph presenting the distribution of IFITM3 in the Golgi (calculated as a Golgi/cytoplasm ratio on 39 to 62 cells per time point and per condition in two independent experiments, AVG, SEM and individual values). The table presents p values obtained after a one-way Anova, Tukey's multiple comparison test between the indicated conditions: ns: non significant; \*, p value <0.05; \*\*\*\*, p value <0.0001. Source data is provided in the relevant section.

**Fig. 5. Mutagenesis of the entire CIL of IFITM3 finely maps the domain involved in the egress of IFITM3 from the Golgi.** a) Individual amino acid of the CIL were changed to alanine or to glycine when alanine residues were present, prior to confocal microscopy analysis. Representative pictures are shown here (IFITM3 only) while their colocalization with the cis-Golgi marker GM130 is shown in the extended data Figure 3. b) Quantification of the IFITM3 proportion in Golgi is provided as a Golgi/cytoplasm ratio in the box and whisker plot (20 cells per mutant in two to three independent experiments analyzed). Asterisks and lines within the box indicate averages and median values, respectively. Yellow boxes indicate mutants with Golgi/cytoplasm IFITM3 ratios equivalent to the 85-90 IFITM3 mutant and non-statistically significant when compared to 85-90 following an ordinary one-way Anova, Dunnett's multiple comparison test. c) Representative WB analysis of mutant proteins. Uncropped blots and source data are provided in the relevant section.

**Fig. 6. The Golgi egress domain of IFITM3 is conserved across vertebrate members of the dispanin/CD225 subfamily A and is functionally conserved in PRRT2, a member of the B subfamily as shown by genetic mutations associated to PKD.** a) Alignment of the indicated portions of human members of the different dispanin/CD225 subfamilies. The relevant domain is circled in red. The position of the first amino acid of each sequence is shown within parentheses. Left, logo files obtained after alignment of vertebrate orthologues of the indicated genes for each subfamily, except D. b) Single point mutation and confocal microscopy analysis of the Golgi egress domain of IFITM1. c) Point mutations and confocal microscopy analysis of PRRT2 mutants in the region corresponding to the Golgi egress domain of IFITM3. R295Q and A291V are genetic mutations associated to PKD. Representative pictures are shown for each protein, while separated channels are provided in the extended data Fig. 4. Whiskers and boxes plots of the quantification of the proportion of each protein in the Golgi as a Golgi/cytoplasm ratio (25-75 percentiles with individual cells represented as dots; group average indicated by an asterisk, n=20 in three independent experiments). Colored boxes represent statistical significant differences after a two-tailed Student t test or a One-way Anova Dunnett's multiple comparison test (b and c, respectively) of the examined mutant over WT. \*\*, p value of 0.0019; \*\*\*\*, p value <0.0001. Source data is provided in the relevant section.

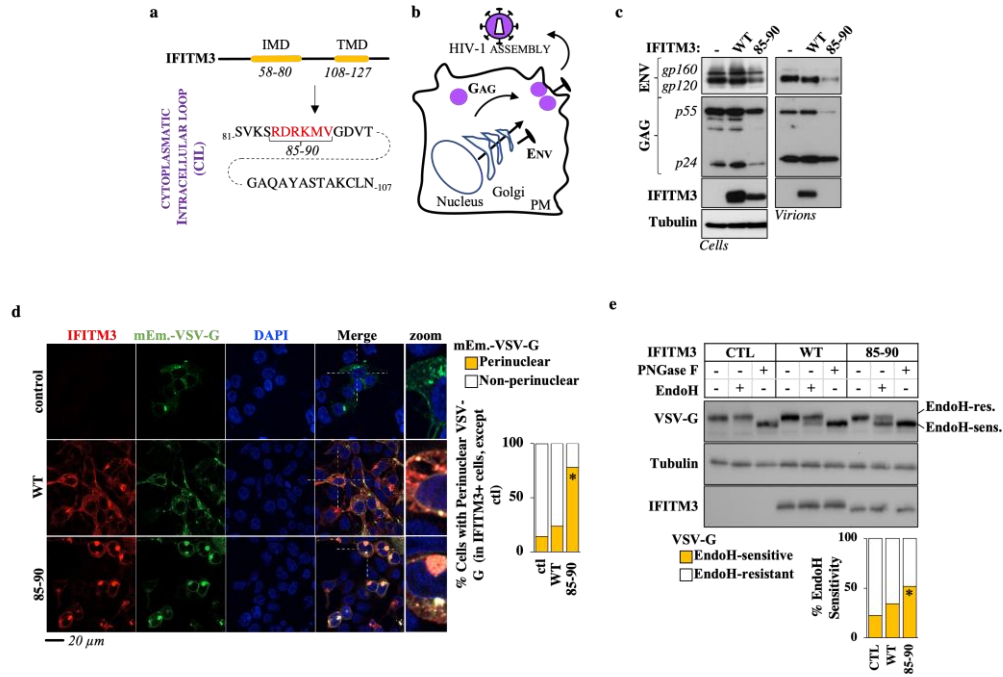
**Extended data. Figure 1. The 85-90 IFITM3 mutant does not colocalize with CD63, LAMP2 nor with the ER.** HEK293T cells ectopically expressing the indicated IFITM3s, or co-transfected with the ER reporter D1ER were analyzed by confocal microscopy with the indicated markers. Whiskers and boxes plot of the Pearson's colocalization coefficients (25-75 percentiles with individual cells represented as dots; n=16 to 38 per condition in three independent experiments). A one-way Anova with Tukey's multiple comparison test was applied for each marker to evaluate differences in localization between WT and 85-90 IFITM3 mutant (non statistical significant differences are represented by white boxes; p <0.0001 by colored ones). Source data is provided in the relevant section.

**Extended data. Figure 2. The broad trafficking inhibitor Monensin affects the egress from the Golgi of WT IFITM3, but not of the 85-90 mutant.** Cells expressing the indicated IFITM3 protein were either treated or untreated with Monensin for 3 hours at 0.2 mM, prior to confocal microscopy analysis. Panels present typical staining, while the graph presents the proportion of IFITM3 in the Golgi as an IFITM3 Golgi/cytoplasmic ratio (AVG= lines and individual values displayed as dots). The lower table presents the result of the indicated statistical analyses: ns, non significant; \*\* p values < 0.006. Source data is provided in the relevant section.

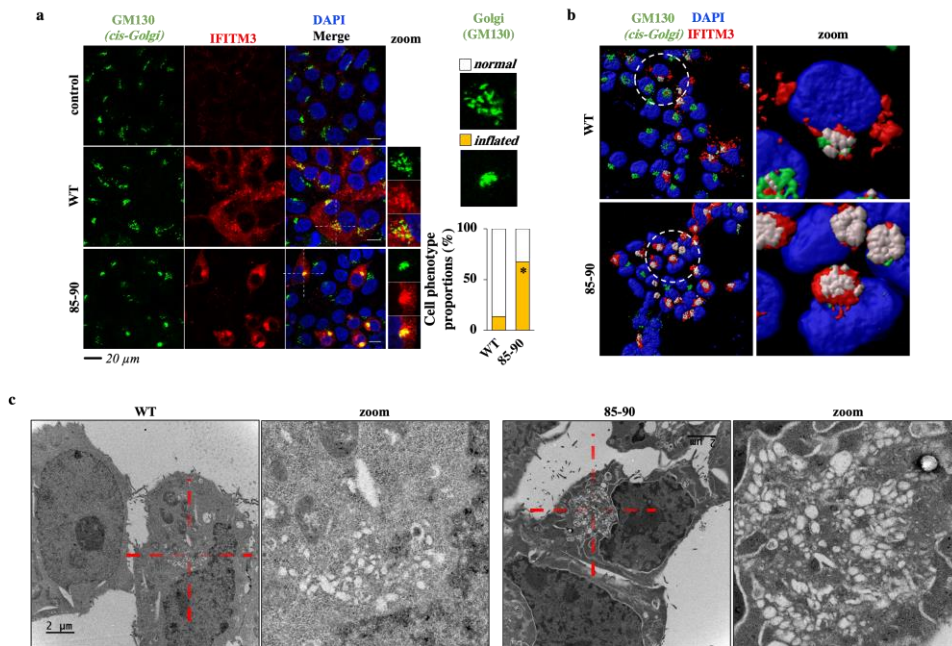
**Extended data. Figure 3. Complete confocal microscopy analyses of the individual point mutants of the CIL of IFITM3.** This figure presents the entire panel of confocal microscopy analyses (i.e. IFITM3, GM130 and DAPI staining) of the mutants presented in Figure 5, which for lack of space presents only IFITM3 staining panels. Source data is provided in the relevant section of Figure 2.

**Extended data. Figure 4. Complete confocal microscopy analyses of the individual point mutants of IFITM1 and PRRT2.** This figure presents the entire panel of confocal microscopy analyses (i.e. PRRT2, IFITM1, GM130 and DAPI staining) of the mutants presented in Figure 6b and 6c, which for lack of space presents only overlays but not separated channels. Source data is provided in the relevant section of Figure 6.

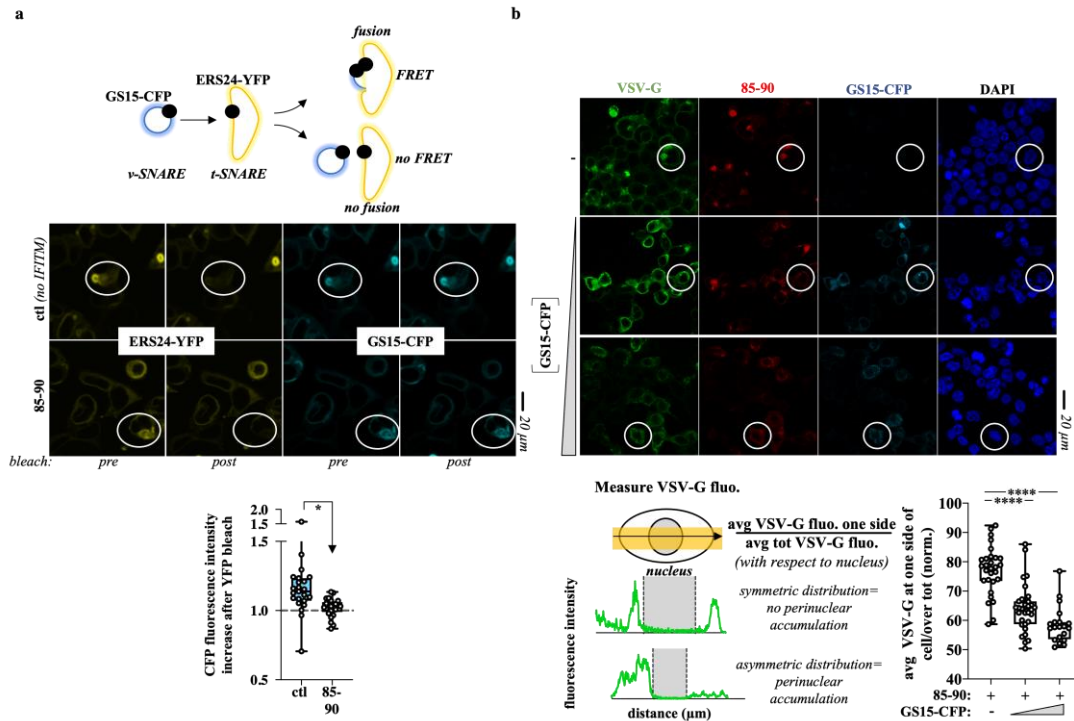
Li et al, Figure 1



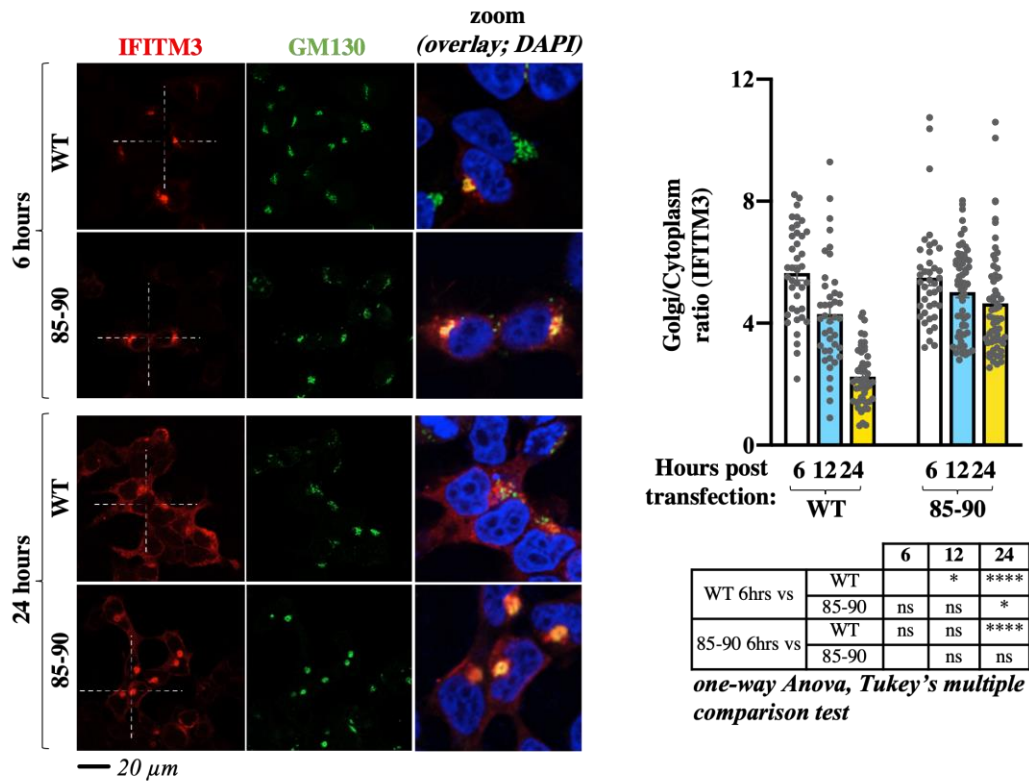
Li et al, Figure 2



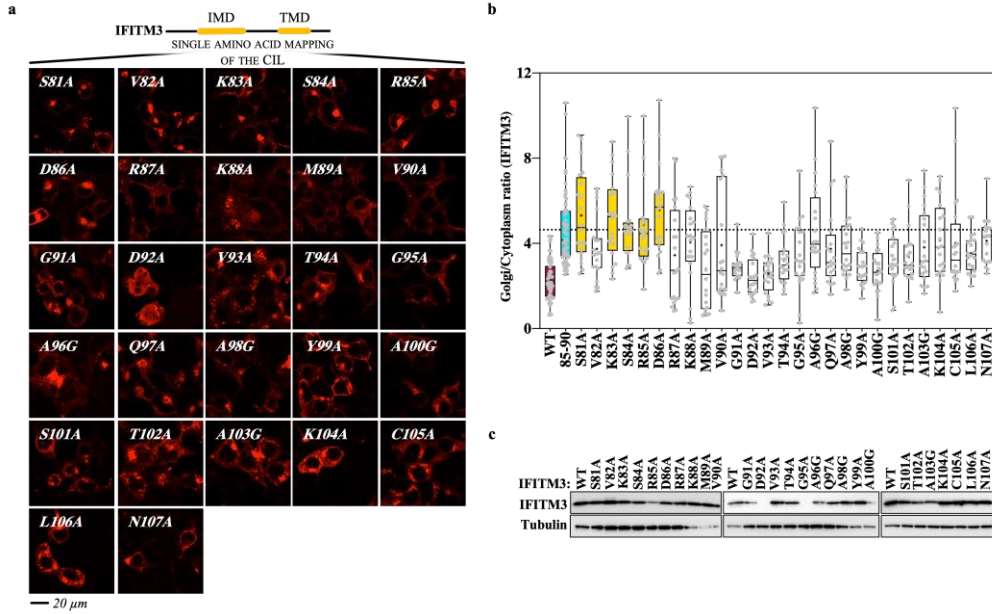
Li et al, Figure 3



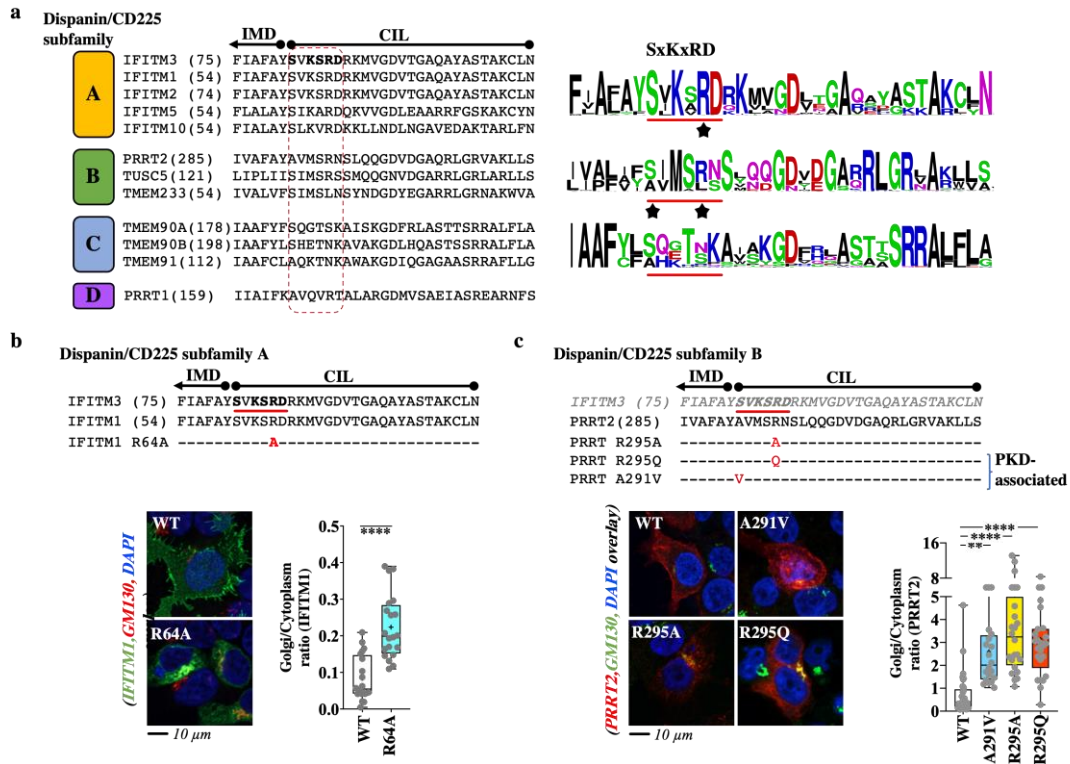
Li et al, Figure 4



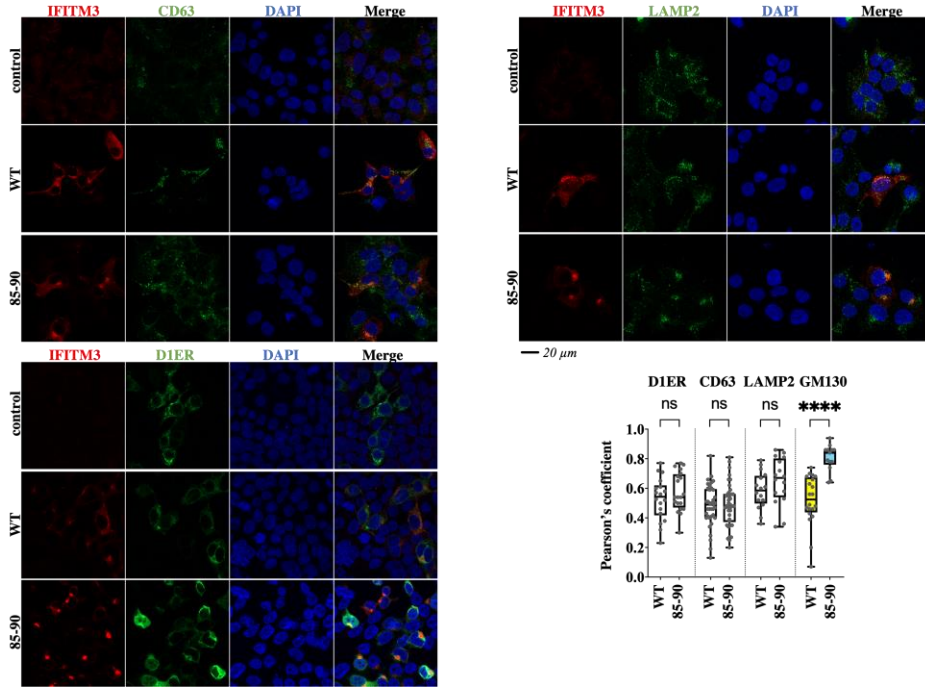
Li et al, Figure 5



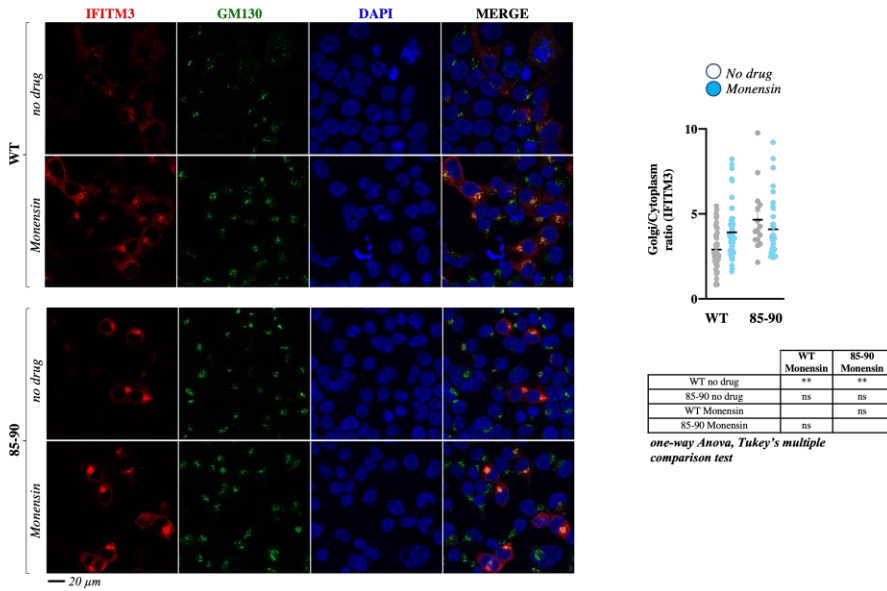
Li et al, Figure 6



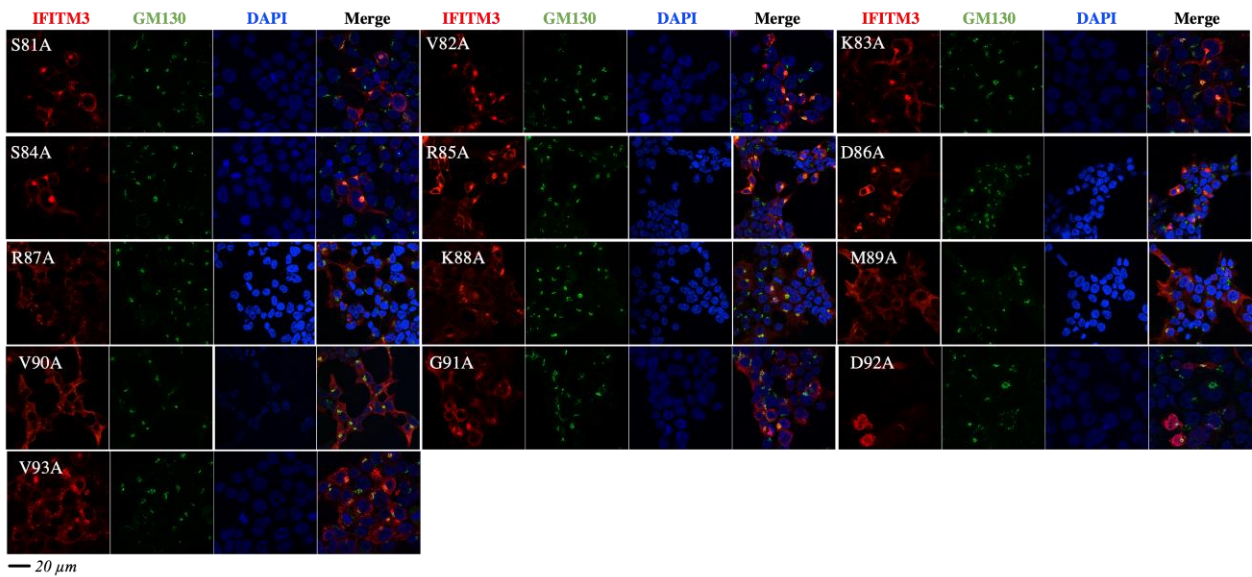
Li et al, Extended Data. Figure 1



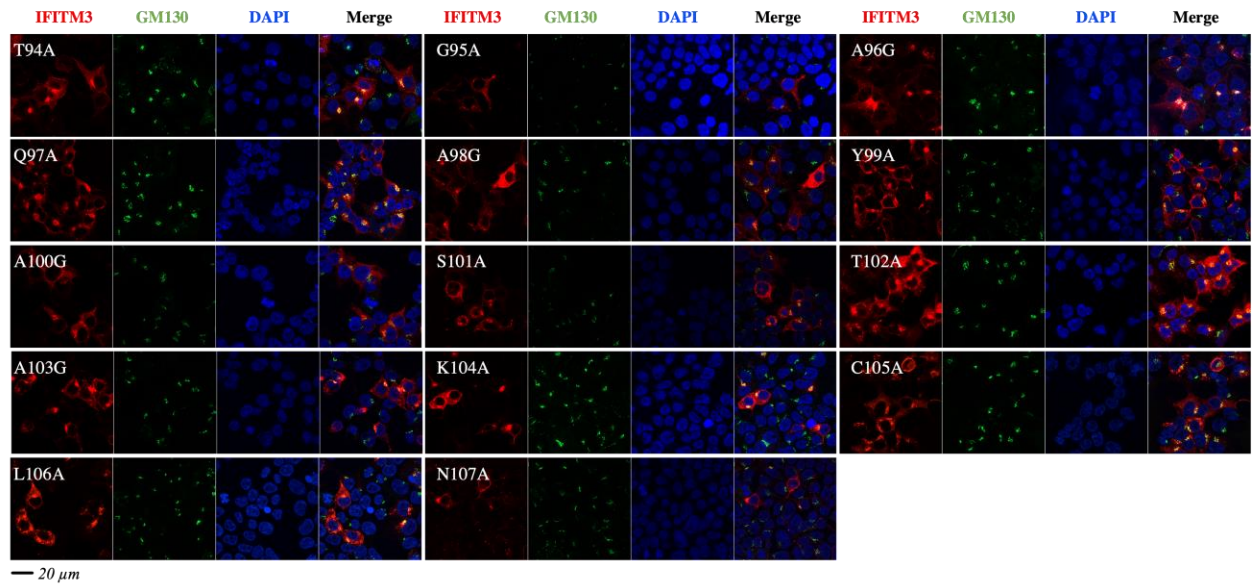
Li et al, Extended Data. Figure 2



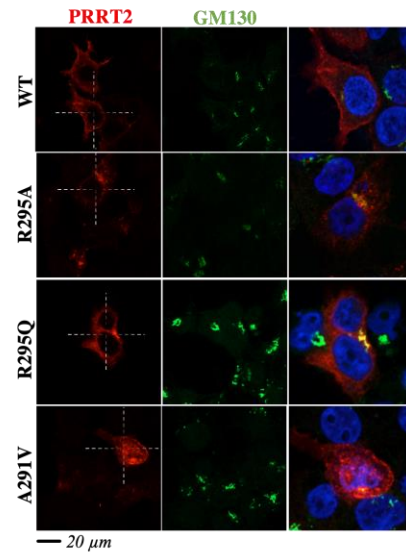
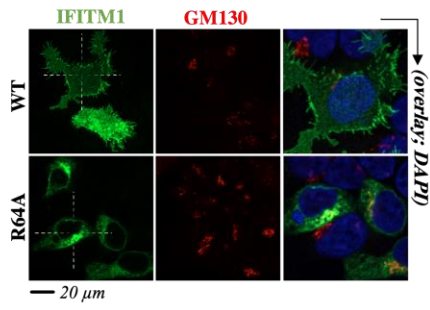
Li et al, Extended Data. Figure 3



Li et al, Extended Data. Figure 3 continued



Li et al, Extended Data. Figure 4



## **Appourchaux et al 2019, JVI, Summary**

In this work, a large panel of IFITM3 mutants was analyzed to identify domains that could affect either the negative imprinting of virion particles or the target cell abilities of IFITM3. The mutants were also examined for their intracellular distribution and stability to also identify domains required for these properties. The results obtained allowed us to conclude that the two antiviral properties linked to IFITM3 were specified by the same domains although we were not able to identify a mutant that completely lost its antiviral properties.

In this larger study, I conducted some of the analyses of the IFITM3 mutants that were presented in the manuscript. These results were then used as the basis of my own PhD project aimed at a more cellular characterization of the behavior of IFITM3.



# Functional Mapping of Regions Involved in the Negative Imprinting of Virion Particle Infectivity and in Target Cell Protection by Interferon-Induced Transmembrane Protein 3 against HIV-1

Romain Appourchaux,<sup>a</sup> Mathilde Delpeuch,<sup>a</sup> Li Zhong,<sup>a</sup> Julien Burlaud-Gaillard,<sup>b</sup> Kevin Tartour,<sup>a</sup> George Savidis,<sup>c,d</sup> Abraham Brass,<sup>c,d</sup>  Lucie Etienne,<sup>a</sup> Philippe Roingeard,<sup>b,e</sup> Andrea Cimorelli<sup>a</sup>

<sup>a</sup>Centre International de Recherche en Infectiologie, Inserm U1111, Université Claude Bernard Lyon 1, CNRS, UMR5308, Ecole Normale Supérieure de Lyon, Université Lyon, Lyon, France

<sup>b</sup>Plateforme IBISA de Microscopie Electronique, Université de Tours et CHU de Tours, Tours, France

<sup>c</sup>Department of Microbiology and Physiological Systems, University of Massachusetts Medical School, Worcester, Massachusetts, USA

<sup>d</sup>Gastroenterology Division, Department of Medicine, University of Massachusetts Medical School, Worcester, Massachusetts, USA

<sup>e</sup>INSERM U1259, Université de Tours et CHU de Tours, Tours, France

**ABSTRACT** The interferon-induced transmembrane proteins (IFITMs) are a family of highly related antiviral factors that affect numerous viruses at two steps: in target cells by sequestering incoming viruses in endosomes and in producing cells by leading to the production of virions that package IFITMs and exhibit decreased infectivity. While most studies have focused on the former, little is known about the regulation of the negative imprinting of virion particle infectivity by IFITMs and about its relationship with target cell protection. Using a panel of IFITM3 mutants against HIV-1, we have explored these issues as well as others related to the biology of IFITM3, in particular virion packaging, stability, the relation to CD63/multivesicular bodies (MVBs), the modulation of cholesterol levels, and the relationship between negative imprinting of virions and target cell protection. The results that we have obtained exclude a role for cholesterol and indicate that CD63 accumulation does not directly relate to an antiviral behavior. We have defined regions that modulate the two antiviral properties of IFITM3 as well as novel domains that modulate protein stability and that, in so doing, influence the extent of its packaging into virions. The results that we have obtained, however, indicate that, even in the context of an IFITM-susceptible virus, IFITM3 packaging is not sufficient for negative imprinting. Finally, while most mutations concomitantly affect target cell protection and negative imprinting, a region in the C-terminal domain (CTD) exhibits a differential behavior, potentially highlighting the regulatory role that this domain may play in the two antiviral activities of IFITM3.

**IMPORTANCE** IFITM proteins have been associated with the sequestration of incoming virions in endosomes (target cell protection) and with the production of virion particles that incorporate IFITMs and exhibit decreased infectivity (negative imprinting of virion infectivity). How the latter is regulated and whether these two antiviral properties are related remain unknown. By examining the behavior of a large panel of IFITM3 mutants against HIV-1, we determined that IFITM3 mutants are essentially packaged into virions proportionally to their intracellular levels of expression. However, even in the context of an IFITM-susceptible virus, IFITM3 packaging is not sufficient for the antiviral effects. Most mutations were found to concomitantly affect both antiviral properties of IFITM3, but one CTD mutant exhibited a divergent behavior, possibly highlighting a novel regulatory role for this domain. These findings

**Citation** Appourchaux R, Delpeuch M, Zhong L, Burlaud-Gaillard J, Tartour K, Savidis G, Brass A, Etienne L, Roingeard P, Cimorelli A. 2019. Functional mapping of regions involved in the negative imprinting of virion particle infectivity and in target cell protection by interferon-induced transmembrane protein 3 against HIV-1. *J Virol* 93:e01716-18. <https://doi.org/10.1128/JVI.01716-18>.

**Editor** Frank Kirchhoff, Ulm University Medical Center

**Copyright** © 2019 American Society for Microbiology. All Rights Reserved.

Address correspondence to Andrea Cimorelli, [acimarel@ens-lyon.fr](mailto:acimarel@ens-lyon.fr).

M.D. and L.Z. contributed equally to this work.

**Received** 28 September 2018

**Accepted** 19 October 2018

**Accepted manuscript posted online** 24 October 2018

**Published** 4 January 2019

thus advance our comprehension of how this class of broad antiviral restriction factors acts.

**KEYWORDS** IFITM, IFITM3, interferon, restriction factor, human immunodeficiency virus, viral resistance

The interferon-induced transmembrane proteins (IFITMs) are a family of highly related proteins characterized by the presence of two hydrophobic transmembrane domains (TM1 and TM2) separated by a conserved intracellular loop (CIL) and variable N- and C-terminal domains (NTD and CTD, respectively) (1, 2). In humans, this family is composed of five expressed members (IFITM1, -2, -3, -5, and -10), three of which are interferon regulated and endowed with broad antiviral properties (IFITM1, -2, and -3 [collectively referred to as IFITMs in the present manuscript]) (3–5).

A number of studies have firmly established that IFITMs target a large spectrum of distinct viral families (5–33), although viruses that resist IFITMs, or use them as cofactors, such as human coronavirus OC43, have been identified (6, 34–36).

For viruses, such as HIV-1, that are susceptible to these restriction factors, IFITMs appear to act according to a bimodal inhibition mode, with which they are able to target two different steps of the viral life cycle (15, 36, 37).

The first and most studied antiviral mechanism described for IFITMs takes place in target cells, where IFITMs arrest incoming virion particles in endosomes, leading to their subsequent degradation (6, 11, 12, 16, 18, 20–22, 24, 26, 31, 38). This inhibition mode targets pH-dependent viruses that undergo viral-to-cellular membrane fusion after endosomal internalization but also pH-independent viruses that either fuse directly at the plasma membrane or, as for HIV-1, appear to use endosomes as an additional, nonmandatory entry pathway. The second mechanism, first described for HIV-1 by our and other laboratories (15, 23, 37) and more recently extended to other viruses (36), occurs in virion-producing cells. In this setting, IFITMs coalesce with viral structural proteins at sites of assembly, leading to the production of virion particles that package IFITMs and display reduced infectivity. We refer to the latter property as the negative imprinting of virion particle infectivity by IFITMs (23, 36).

At present, it is unknown whether this decrease in infectivity is due to the physical incorporation of IFITMs in virion particles or if it is the result of an action of IFITMs on unknown cellular functions that in turn influence virion assembly. Over the years, several studies raised the possibility that IFITM3 could act by either modulating the intracellular content of cholesterol (during target cell protection) (39) or commandeering a decrease in the amount of mature envelope glycoproteins incorporated into HIV-1 virions (37). However, both of these findings remain debated, as further studies failed to obtain evidence of changes in either intracellular cholesterol levels (31, 40) or glycoprotein incorporation upon IFITM expression (16, 23, 36, 41, 42).

Despite the fact that the exact molecular mechanism through which IFITMs act remains unclear, virions produced in the presence of IFITMs exhibit an impaired ability to undergo fusion with cellular membranes, the same step that hinders fusion between the membranes of incoming virions and IFITM-decorated endosomes during target cell infection (15, 23, 37, 40, 43–45). In the case of HIV-1, partial to complete resistance to this antiviral effect has been shown to be conferred by R5-tropic envelope proteins that use the CCR5 chemokine receptor to access target cells (16, 46, 47). It appears, therefore, that the antiviral effects that IFITMs have on membrane fusion can be countered through the use of specific envelope glycoproteins or through the engagement of specific coreceptors on target cells.

A number of studies have revealed domains that have important regulatory functions on the antiviral properties of the different IFITM members, influencing their ability to recruit multiple cellular partners and to mediate protection of target cells from viral challenge (19, 33, 43, 48–55). However, little is known about domains that specify the negative imprinting properties of IFITMs.

In this study, we have directly addressed this question by analyzing the behavior of

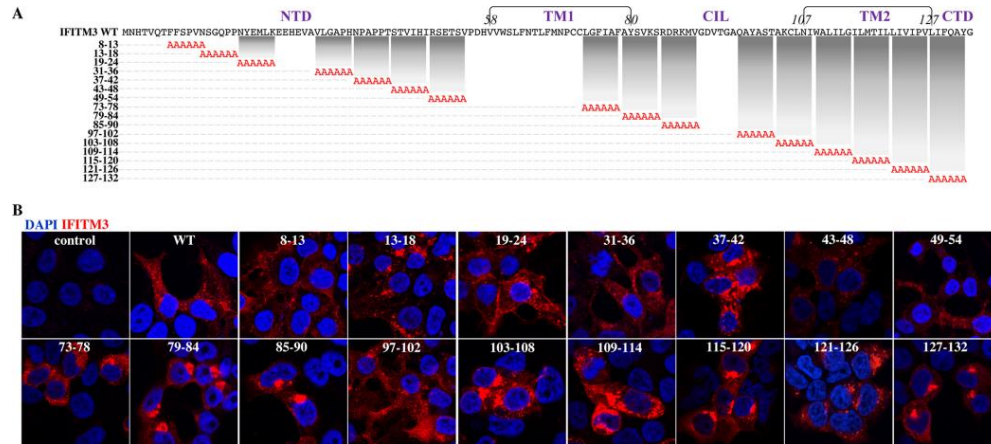


**FIG 1** IFITM3 mutants used here. (A) IFITM3 mutants used in this study. Mutants that could not be reliably detected upon transient DNA transfection of HEK293T cells were excluded from our study and are not presented here. FACS, fluorescence-activated cell sorter. (B) The intracellular localization of these mutants was analyzed by confocal microscopy, and representative pictures are displayed. Of note, this analysis is meant to provide a qualitative assessment of the intracellular distribution of the different IFITM3 mutants and does not reflect their relative expression levels, which instead were quantified by WB.

a panel of 16 different mutants spanning the entire length of IFITM3 against HIV-1 (19). The relatively large number of mutants examined allowed us to also explore the functional relationship between antiviral behavior and several parameters that have been associated with the biology of IFITM3, including their incorporation into virions, their stability, their reported ability to increase the levels of formation of CD63-positive vesicles and multivesicular bodies (MVBs) in the cell, as well as their ability to affect cholesterol levels. To complete these analyses, we have also determined the antiviral activities of these mutants during target cell protection, establishing for the first time a comprehensive analysis of the relationship between these two antiviral properties.

The data that we have obtained in our study highlight novel regions of IFITM3 that modulate the negative imprinting properties of IFITM3, its ability to mediate target cell protection, as well as its stability in the cell. The latter parameter seems to be the main driver of IFITM3 incorporation into virions, as most mutants were found to be incorporated into virions proportionally to their level of expression in the cell. The extent of IFITM3 incorporation into virions, however, does not correlate with the antiviral phenotype, allowing us to conclude that IFITM3 virion packaging is not sufficient for its antiviral functions. Finally, we noted that mutations throughout IFITM3 exerted a concomitant modulation of both target cell protection and negative imprinting of virions. Only two domains made an exception to this rule, the first located in the CIL that we believe to be a novel gain-of-function IFITM3 mutant and the second located in the CTD that may represent a region involved in the differential regulation of the two antiviral properties ascribed to IFITM3.

## RESULTS

**Presentation of the IFITM3 mutants used in this study.** To comprehensively identify domains regulating the negative effects of IFITM3 against HIV-1, we took advantage of a collection of mutants spanning the entire length of IFITM3 (6 amino acids changed to alanines per mutant, named by the number of the first and last substituted residues) (19) (Fig. 1A). A few mutants were excluded from the analysis due to unreliable expression or a lack of detection with the antibodies used here, leaving a total of 16 mutants. Given that only seven of these mutants had been previously examined by confocal microscopy (19), a complete qualitative analysis was carried out

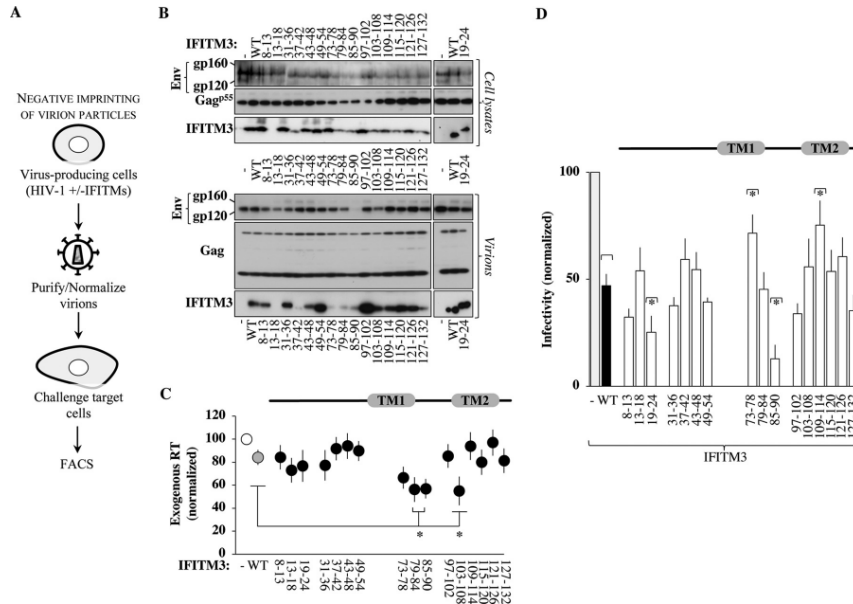


**FIG 2** Effects of the expression of the different IFITM3 mutants on the production and infectivity of HIV-1 virion particles. (A) Experimental scheme used to further characterize the antiviral effects of IFITM3 mutants during the negative imprinting of virion particle infectivity. Briefly, HIV-1 virion particles were produced by transient DNA transfection of HEK293T cells with DNAs coding for the different IFITM3 mutants along with the NL4-3 proviral clone and an HIV-1-based miniviral genome bearing a self-inactivating LTR and an expression cassette for GFP. Two days afterwards, cells were lysed, and virion particles were purified by ultracentrifugation through a 25% sucrose cushion, prior to normalization by exo-RT activity and further analyses. (B) Western blot panels presenting typical results obtained for both cell and viral lysates. Mutant 19-24 was the sole mutant whose detection required hybridization with a distinct anti-IFITM3 antibody compared to the remaining mutants. (C) Quantification of the amounts of virion particles produced in the presence of the different IFITM3 mutants by exo-RT. The graph presents data obtained from 6 experiments. \*,  $P < 0.05$  as determined by a Student  $t$  test upon comparison to WT IFITM3 (two tailed, unpaired). (D) Normalized amounts of virions were used to challenge target HeLaP4 cells, and the extent of infection was measured 2 to 3 days afterwards by flow cytometry. The graph presents data obtained with 4 to 8 independent experiments. \*,  $P < 0.05$  as determined by a Student  $t$  test for comparisons between the indicated mutant and WT IFITM3 (two tailed, unpaired). All mutants displayed statistically significant differences over the control according to the same test (not displayed on the graph for simplicity).

for all of them (Fig. 1B). Several of the IFITM3 mutants were found to exhibit a more peripheral (mutants 8-13 and 19-24) or a more internal (mutants 79-84, 85-90, 103-108, 115-120, and 127-132) distribution than the wild type (WT) after confocal microscopy analysis. A more restricted analysis of the colocalization of relevant IFITM3 mutants with the endosomal marker CD63 is provided below.

#### Identification of mutations that modulate the ability of IFITM3 to negatively imprint the infectivity of HIV-1 virion particles.

In previous studies, we determined that the effects of IFITMs on the infectivity of virion particles derived from HIV-1, but also from many other viruses, are apparent in all cell types tested, ranging from primary macrophages and blood lymphocytes to established cell lines (23, 36). As such, we used HEK293T cells as a validated model cell line in which to comprehend the roles of distinct regions of IFITM3 in HIV-1 infectivity. IFITM3 mutants were expressed transiently at levels that we have previously shown to be comparable to those observed in primary dendritic cells stimulated with interferon alpha (IFN- $\alpha$ ) (as schematically presented in Fig. 2A) (23, 36). Cells were cotransfected with DNAs encoding the IFITM3 variants, the NL4-3 proviral clone, and a miniviral HIV-1-based genome bearing the green fluorescent protein (GFP) reporter and a self-inactivating long terminal repeat

(LTR). This setup allowed us to examine replication-competent HIV-1 virions (in which all viral proteins are expressed at natural levels from their cognate promoter) on the basis of a single round of infection, as the GFP-bearing viral genome can be mobilized only once during infection, from virus-producing cells to target ones. Virion particles were purified by ultracentrifugation through a 25% sucrose cushion and then normalized by the exogenous reverse transcriptase (exo-RT) activity, which in our hands provides results identical to those of p24-based normalization (23). Cellular and viral lysates were then analyzed by Western blotting (WB), and the amounts of Gag, Env, and IFITM3 proteins were quantified by densitometry (see Fig. 2B for a representative example). All IFITM3 mutants were detectable in cell lysates albeit with notable variations that required enhancement of the signal in the case of the most drastically affected mutant (8-13 [this mutant was retained due to its interesting phenotype {see below}]). The structural viral proteins Gag p55 and Env gp160 were also detected at similar levels, although small variations could be observed across experiments. Upon purification, the amounts of virion particles produced under the different conditions varied little in comparison to the control, with the exception of a small yet significant decrease upon the expression of the IFITM3 mutants 79-84, 85-90, and 103-108 (55 to 56% of the total) (Fig. 2C). Given that virions were normalized for further analyses, these differences were not investigated further. When exo-RT-normalized virion particles were analyzed by WB, no major variations were observed in the levels of mature Env gp120 incorporated in virions produced in the presence of the different IFITM3 mutants, with the exception of mutant 85-90, whose expression resulted in a near loss of Env detection (Fig. 2B). The expression of WT IFITM3 had been previously associated with the loss of mature Env incorporation in HIV (37). However, this finding remains controversial, as other studies have not observed such changes in the HIV-1 glycoprotein (16, 23, 41, 42) or for other viral glycoproteins (36), so at present, the reasons for this discrepancy remain unclear. Given that under the experimental conditions used here, no major changes were observed in the amounts of mature Env incorporated into HIV-1 virions upon the expression of the WT or of most IFITM3 mutants, we believe that 85-90 most likely represents a gain-of-function mutant.

All IFITM3 mutants copurified with HIV-1 virions, although to widely different extents (including mutant 13-18 after enhancement of the WB signal), indicating that none of the mutations analyzed here prevented the incorporation of IFITM3 into HIV-1 virions.

The infectivity of normalized virion particles was then measured upon viral challenge of target HeLaP4 cells, prior to flow cytometry analysis 2 to 3 days afterwards (Fig. 2D). Under conditions in which the expression of wild-type IFITM3 resulted in a 55% decrease in infectivity in single-round infection assays, all IFITM3 mutants tested exerted measurable and variable effects on the infectivity of virion particles with respect to the control, and four exhibited substantially distinct behaviors with respect to the WT (Fig. 2D). Specifically, the 19-24 and the 85-90 IFITM3 mutants imparted greater infectivity defects (70% and 85% lower infectivity than the control, respectively), while the 73-78 and the 109-114 mutants displayed less infectivity defects (29% and 25%). Among these four mutants, the infectivity defect of IFITM3 mutant 85-90 was expected in light of the major impairment in gp120 incorporation observed upon its expression, and the one of the 19-24 mutant was also expected due to previous studies (41). In search of mutants that could completely relieve the antiviral effects of IFITM3 on the production of infectious virion particles, the two relevant mutations were combined (73-78/109-114) (Fig. 3). However, this double mutant was still proficient in altering virion infectivity (exhibiting wild-type antiviral activities rather than decreased ones), indicating that the effects of these mutations cannot be functionally combined into a single IFITM3 molecule. The reasons why the combination of two relieving mutations in TM1 and TM2 result in the reacquisition of the antiviral phenotype remain unclear.

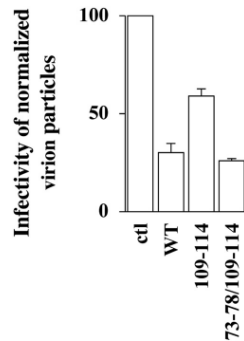


**FIG 3** Two mutations that individually relieve the negative imprinting properties of IFITM3 on virion particles fail to cooperatively alleviate the antiviral phenotype. The antiviral activity of the double IFITM3 mutant 73-78/109-114 was assessed as described in the legend to Fig. 2. The graph presents the infectivity of normalized amounts of virion particles produced in the presence of this mutant during the challenge of target HeLaP4 cells (averages and standard errors of the means [SEM] from two independent experiments).

**Several conserved domains in IFITM3 influence the protein's stability.** Differently from an approach based on stable expression and selection of IFITM3-expressing cells (19), transient transfection allowed us to more directly appreciate differences in IFITM3 protein levels and therefore to highlight novel domains that affected the steady-state levels of accumulation of IFITM3 (Fig. 4A). Several mutations led to a statistically significant decrease in the accumulation of IFITM3 in the cell: in the NTD (13-18 and 37-42), in TM1 (73-78 and 79-84), and in the CIL (85-90 and 103-108). The involvement of these amino acid stretches in the stability of IFITM3 has not been appreciated previously, with the exception of mutant 13-18 ( $_{13}$ NSGQPP $_{18}$ ) adjacent to the region  $_{17}$ PPNYEML $_{23}$ , which acts as a docking site for E3 ubiquitin ligase neural precursor cell expressed developmentally downregulated protein 4 (NEDD4), adaptor protein 2 (AP2), as well as the Fyn kinase (10, 18, 51, 54, 55). Mining of public databases for “immune IFITMs” (i.e., IFITM1, -2, and -3) indicated that the TM1-CIL region and in particular amino acids 72 to 91 and 103 to 108, which affect the protein's stability, have been strictly conserved during million years of primate evolution (Fig. 4B), while, as expected from previous studies, the NTD exhibited higher variability (30, 41, 56–58). In contrast to mutants 72-91 and 103-108, the evolutionary history of the domains spanning residues 13 to 18 and 37 to 42 (both contained within the NTD and affecting protein stability) shows signs of divergence within different primate clades, given that the region spanning residues 37 to 42 is well conserved among New and Old World monkeys, while the one spanning residues 13 to 18 has undergone more-dramatic diversification.

**Determinants of IFITM3 incorporation into virion particles.** Our mutagenesis study failed to reveal a single mutation that completely abrogated the ability of IFITM3 to be incorporated into virion particles. However, several mutations were identified that decreased the absolute levels of IFITM3 molecules incorporated into normalized amounts of virion particles, in particular 13-18, 37-42, 73-78, 79-84, and 127-132 (Fig. 4C). To determine whether this decrease was due to the loss of a specific virion-packaging signal, or whether it was linked to lower levels of expression in the cell, we compared the levels of accumulation of the different IFITM3 mutants in cells and in purified virions (Fig. 4D [the normalized protein levels in virions and cells as well as their ratio, defined here as an IFITM3 virion incorporation index, are displayed]). This analysis strongly indicated that IFITM3 mutants were incorporated into virions proportionally to their levels of expression in the cell. The sole exception was represented by mutant

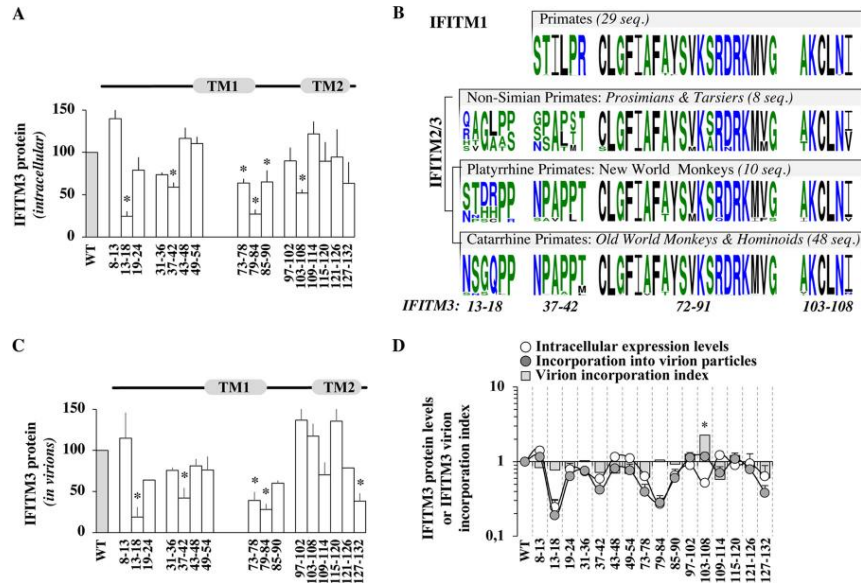


**FIG 4** Identification of conserved IFITM3 domains that influence the intracellular levels of accumulation of IFITM3 and modulate the extent of IFITM3 incorporation into virions. (A) Domains influencing the intracellular levels of accumulation of IFITM3. The amounts of IFITM3 mutants present in intracellular lysates were determined after WB analysis following densitometry-based quantification and normalization to WT values. (B) Evolutionary conservation of domains influencing IFITM3 levels. Shown are primate IFITM1, -2, and -3 with sequence logos showing amino acids (probability is plotted on the y axis) corresponding to the different domains of interest for each primate gene clade. The number of sequences used for the analysis is indicated (seq, sequences) (see Materials and Methods for details). Color-coding is the default in WebLogo3. (C) Domains influencing IFITM3 incorporation into virion particles (as in panel A), after quantification of the levels of IFITM3 mutants present in exo-RT-normalized virion particles. (D) Comparison between the intracellular levels of expression and virion incorporation of the different IFITM3 mutants (log scale) following densitometry-based quantification and normalization to WT values. The graph also displays the ratio of the amount of IFITM3 protein incorporated into virion particles with respect to their intracellular levels of expression as a virion incorporation index, after normalization to WT IFITM3. \*,  $P < 0.05$  as determined by a Student  $t$  test for comparison between the indicated mutant and the WT (two tailed, unpaired).

103-108, which was less stable than the wild type in cells yet was incorporated as well as WT IFITM3 into virions (therefore displaying a virion incorporation index of 2.25). This result indicates that mutation of the corresponding amino acid stretch ( $_{103}AKCLNI_{108}$ ) at the border between the CIL and TM2 somehow exerts a double effect, by reducing the protein's stability on one hand and by leading to higher levels of incorporation into virions on the other.

Overall, the results obtained here indicate (i) that several regions control the stability of IFITM3 in the cell that, based on their evolutionary conservation/divergence across primates, may act by influencing the overall structural conservation of IFITMs (TM1-CIL) or more-specific regulatory functions (NTD) and (ii) that an important determinant of IFITM3 incorporation into virions is the intracellular level of its expression.

**The levels of incorporation of IFITM3 into virions do not correlate with their ability to negatively affect HIV-1 virion infectivity.** Given that an open question in the field is to determine whether the physical presence of IFITM3 in virion particles is instrumental for their ability to decrease virion infectivity, we used our results to determine the possible existence of a correlation between incorporation levels of IFITM3 and the potency of the antiviral phenotype (Fig. 5). Overall, the results that we have obtained indicate no correlation between antiviral properties of virion particle infectivity and either the extent of IFITM3 incorporation into virions or intracellular levels of expression. These data therefore suggest that the incorporation of IFITM3 into

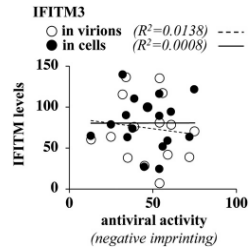


**FIG 5** The antiviral activities of the different IFITM3 mutants do not correlate with their intracellular expression levels or with the extent of their incorporation into virion particles. Shown are correlative analyses between the levels of accumulation of the different IFITM3 mutants in the cell, their incorporation into virions, and their antiviral activity in the negative imprinting of HIV-1 virion particles.

HIV-1 particles is not sufficient for the negative imprinting phenotype, as previously suggested by other studies (16), as well as by the existence of viruses that resist IFITMs despite robust incorporation (for instance, Rift Valley fever virus) (36). The question of whether IFITM3 incorporation is necessary for the antiviral phenotype remains open at present due to the fact that we could not isolate an IFITM3 mutant completely excluded from virion particles. In light of the fact that approximately one-third of IFITM3 is composed of transmembrane regions, such a mutant may be difficult to obtain.

**The ability of IFITM3 to decrease virion particle infectivity does not correlate with the accumulation of CD63-positive vesicles in cells, and IFITM3 does not affect cholesterol homeostasis.** A commonly observed phenotype associated with the expression of IFITM3 is an increase in the levels of the endosomal marker CD63, which may be indicative of increased vesicular trafficking or multivesicular body (MVB) formation (11, 20, 38, 39, 48, 59) and, by extension, of higher lysosomal activity, which may be pertinent for the antiviral effects of IFITM3, at least during viral entry. However, it is unclear whether this observation is functionally linked to the antiviral functions of IFITM3. The expression of WT IFITM3 was clearly accompanied by an increase in the proportion of CD63-positive cells (from 35% to 70%) (Fig. 6A and B), in agreement with previous studies. When a similar analysis was conducted on a restricted number of IFITM3 mutants, the proportion of cells displaying higher-level accumulation of CD63<sup>+</sup> vesicles varied across mutants. Under the same experimental conditions, IFITM3-expressing cells displayed higher proportions of discernible MBVs following electron microscopy than did control cells (from 9% to 25%) (Fig. 6C presents MBVs from WT IFITM3-expressing cells), and similarly to CD63, this proportion varied among the different IFITM3 mutants (Fig. 6C, graph). Supporting the notion that higher CD63 positivity relates to higher MVB activity, a near-perfect correlation was observed between these two parameters for the different mutants analyzed (Fig. 6D). However, neither correlated with the antiviral behavior of IFITM3 mutants (Fig. 6E [CD63 accumulation]), indicating that this phenotype does not directly relate to the ability of IFITM3 to decrease virion particle infectivity.

An increase in the intracellular levels of cholesterol in A549 cells was previously hypothesized to be at the basis of the defect imparted by IFITM3 at membrane fusion. However, the role of cholesterol homeostasis in IFITM3-mediated restriction remains controversial (31, 39, 40, 60). To explore this issue, we measured the amount of cholesterol-laden lipid droplets after Nile Red staining by confocal microscopy in HEK293T cells expressing or not expressing WT IFITM3 (see Fig. 7A for representative pictures and Fig. 7B for averages of data from multiple experiments). Given that the antiviral effects of IFITM3 are manifest in this cell type, changes in cholesterol levels should also appear here if they are functionally relevant. Cells treated with either methyl- $\beta$ -cyclodextrin (m $\beta$ CD) or oleic acid (OA) presented low to undetectable and

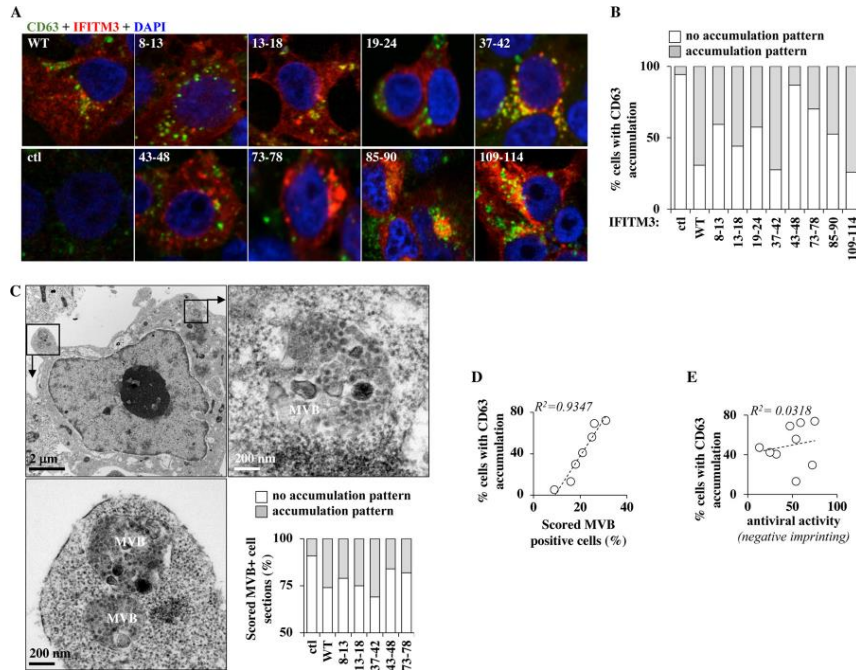


**FIG 6** IFITM3 mutants modulate the extent of accumulation of CD63-positive vesicles as well as MVBs in cells, but these properties do not correlate with their antiviral behaviors. (A and B) Cells expressing or not expressing a short list of IFITM3 mutants were analyzed by confocal microscopy using the endosomal marker CD63. (C) Same as above, but cells were analyzed by electron microscopy. A representative picture of a cell expressing WT IFITM3 is displayed, while the number of scored MVB-positive cell sections in the different mutants is presented in the graph (please note the different scale). (D and E) Correlative analyses, as indicated. The graphs present data obtained in 2 independent experiments (electron microscopy) or 3 independent experiments (immunofluorescence analysis) with over 100 scored cells under each condition.

increased intracellular cholesterol levels, respectively, as measured by Nile Red staining and in agreement with their well-known effects on cholesterol homeostasis.

Instead, when control cells were compared to cells expressing WT IFITM3, no qualitative or quantitative differences were observed. Similarly, no differences in median fluorescence intensities (MFIs) were observed when the extent of Nile Red accumulation was assessed through a distinct assay (flow cytometry) (Fig. 7C).

While these results indicate that IFITM3 is unlikely to affect cholesterol homeostasis in the cells tested in this study, they do not formally exclude the possibility that the infectivity defect of virion particles produced in the presence of IFITM3 could be due to a specific enrichment of cholesterol in virion particle membranes. To address this issue, HIV-1 virions were produced and purified by ultracentrifugation through a 25% sucrose cushion from cells expressing or not expressing IFITM3. The virion preparations were then normalized by either exo-RT activity or total lipid contents (using R18, a fluorescent lipophilic dye that intercalates linearly in membranes and allows their quantification, prior to the quantification of cholesterol).

Under these conditions, no changes were observed in the amounts of cholesterol under the two conditions (Fig. 7D). Despite the fact that this purification procedure cannot separate bona fide virion particles from exosomal vesicles, these data, in addition to the lack of changes in cholesterol levels in cells, strongly suggest that the membrane fusion defect ascribed to IFITM3 does not involve cholesterol changes. Due

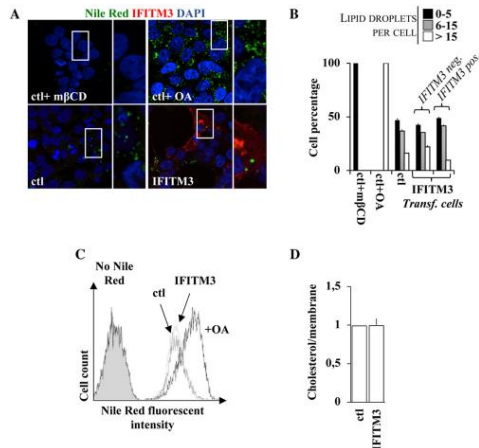


**FIG 7** IFITM3 does not affect cholesterol levels in cells or in purified virion particles. (A and B) HEK293T cells were analyzed by confocal fluorescence microscopy following staining of intracellular lipid droplets by Nile Red (0.25  $\mu$ g/ml). Control cells were treated with either methyl- $\beta$ -cyclodextrin (1 mM) or oleic acid (100  $\mu$ M), well known to either deplete or increase the intracellular levels of cholesterol. Representative pictures are presented in panel A, while the number of lipid droplets per cell is presented in panel B for over 75 cells analyzed under each condition. (C) Same as panel A, but the accumulation of Nile Red was quantified by flow cytometry. (D) Virions produced in the presence or absence of WT IFITM3 were produced and purified as described above. In this case, viral preparations were normalized by their membrane content upon R18 labeling. Cholesterol levels were measured according to the cholesterol/cholesteryl ester quantification kit (Abcam). The graph presents averages and SEM of data from three independent experiments.

to these results, the extent of cholesterol modification for the different mutants was not explored further.

**Identification of mutations that modulate the ability of IFITM3 to protect target cells from HIV-1 infection.** Although the IFITM3 mutants used in this study have been analyzed against other viruses during target cell protection (19), their activities against HIV-1 have not been explored. To directly compare the antiviral activities of IFITM3 mutants at entry and in virion particle imprinting, HEK293T cells were transiently transfected with the different IFITM3 mutants along with CD4 and CXCR4, and their respective expression levels were assessed by WB and flow cytometry, respectively (as schematically presented in Fig. 8A, with typical results shown in Fig. 8B). No notable differences were observed in the cell surface expression of both CD4 and CXCR4 in the presence of the different IFITM3 mutants (Fig. 8B). These cells were used as targets for viral challenge (NL4-3-pseudotyped HIV-1 encoding GFP used at multiplicities of infection [MOIs] of between 0.1 and 0.5), and the extent of infection was measured 2 to 3 days afterwards by flow cytometry (Fig. 8C). As expected, cells expressing WT IFITM3 displayed increased resistance to viral challenge (70% decrease in infection rates, compared to control cells). The susceptibility of cells expressing the different IFITM3 mutants varied from 85 to 15% (all statistically significant compared to control cells [not marked in Fig. 8]), but despite variations in target cell susceptibility, only two mutants significantly relieved the antiviral properties of IFITM3 compared to the wild type, mutant 13-18 and mutant 37-42, both located in the protein N terminus (Fig. 8C). The partial loss of the antiviral activity of these mutants may be related to their lower expression levels than the WT, although on a more global scale, the intracellular levels of expression of the different IFITM3 mutants did not correlate with their antiviral activity in target cell protection (Fig. 8D).

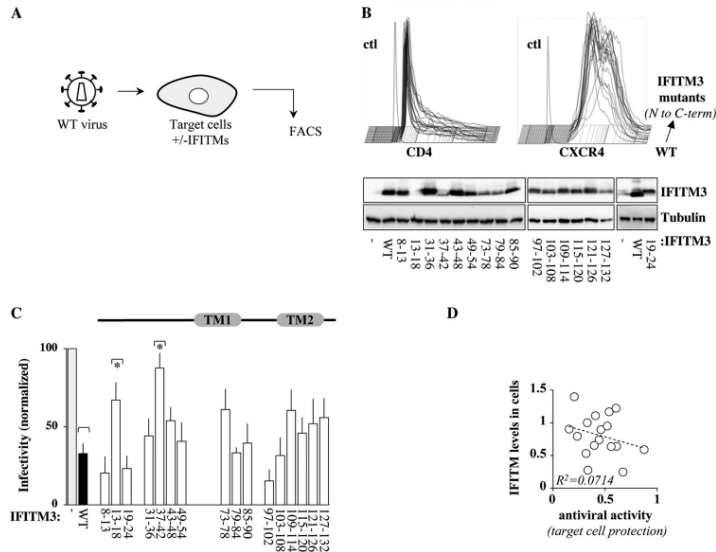


**FIG 8** Behaviors of the different IFITM3 mutants during target cell protection. (A) Experimental scheme used here to evaluate the abilities of the different IFITM3 mutants to protect target cells from HIV-1 infection. HEK293T cells were used as target cells due to their efficient transfection rates, following transient transfection with DNAs coding for the different IFITM3 mutants along with CD4 and CXCR4. (B) Two days after transfection, cells were analyzed by either WB or flow cytometry to determine the levels of expression of the different proteins. (C) Cells were then challenged with an equal dose of GFP-encoding HIV-1 (NL4-3 at an MOI of between 0.1 and 0.5), prior to flow cytometry analysis 2 to 3 days afterwards. The panels present typical results obtained, while the graph presents averages and SEM obtained from 5 to 7 independent experiments. \*,  $P < 0.05$  as determined by a Student  $t$  test for comparisons between the indicated mutant and WT IFITM3 (two tailed, unpaired). All mutants display  $P$  values of  $< 0.05$  when the same test is carried out in comparison to control cells (asterisks are not displayed for simplicity). (D) Correlative analysis between the extent of incorporation of the different IFITM3 mutants into virion particles and their levels of expression in cells.

**Overall comparison of the behaviors of IFITM3 mutants with respect to their ability to mediate negative imprinting of virion particles and target cell protection and to affect protein stability.** To reveal potential links between the abilities of the different IFITM3 mutants to act at both steps of the viral life cycle, as well as to appreciate the relationship between these antiviral properties and IFITM3 stability, the effects of individual mutations on these three parameters were normalized to those of the WT and compared (Fig. 9), as indicated.

On a general level, with two exceptions that are discussed in more detail below, most mutants presented similar trends in their ability to influence negative imprinting of virion particles and target cell protection. The magnitudes of such variations were generally similar for both antiviral phenotypes, with the exception of mutants 13-18 and 37-42, in which target cell protection was relieved 2-fold more than negative imprinting. These two IFITM3 mutants are less stable than the WT, which would suggest that target cell protection is more sensitive than negative imprinting to the intracellular levels of IFITM3. However, although protein stability can influence the behavior of specific mutants, this parameter does not simply explain the protein's phenotypes, because no correlation could be drawn between the protein levels of the different IFITM3 mutants and their antiviral phenotypes.

Although the concomitant variations observed for most IFITM3 mutants in their two antiviral properties could suggest a common antiviral mechanism, mutants 85-90 and 127-132 display a divergent behavior, a finding that may support a model in which two

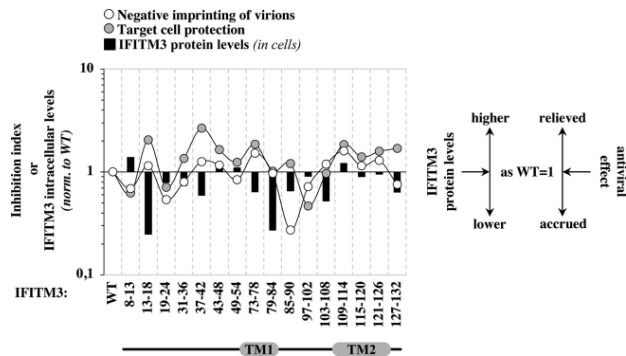


**FIG 9** Overall comparison of the activities of individual mutants to affect negative imprinting of virion particles, target cell protection, as well as the intracellular levels of accumulation. (A) The two antiviral activities of the different IFITM3 mutants as well as their relative stability were normalized to those of WT and overlaid to highlight the behavior of individual mutants that deviated from the wild type, as indicated.

distinct antiviral mechanisms are at play. Mutant 85-90 behaves as the WT during target cell protection, but its expression in virion-producing cells leads to a drastic decrease in Env incorporation into virions, which readily explains their accrued infectivity defect.

Interference with Env maturation and incorporation has been reported previously for WT IFITM3. However, this finding remains controversial, and similarly to other studies, here we have not observed changes in Env incorporation for WT IFITM3 as well as most mutants. As a consequence, we believe that mutant 85-90 gained a novel function, and as such, it is unlikely to represent a protein domain that can disconnect the two antiviral properties. Instead, the behavior of IFITM3 mutant 127-132 in the CTD may suggest that this region differentially regulates target cell protection and negative imprinting of virions.

## DISCUSSION

In this study, we have systematically examined the behavior of a large panel of IFITM3 mutants with respect to their ability to interfere with the production of infectious HIV-1 virions. We have done so in a widely used model cell line that reproduces the infectivity defects imparted by IFITMs on different viruses and in different cell types (both primary and established). This approach allowed us to gather novel insights into the mechanisms regulating the negative imprinting properties of IFITM3 as well as to explore their relationship with other issues of interest in the biology of this antiviral factor. For the sake of clarity, these topics are described in separate subsections, below.

**Novel domains that regulate IFITM3 stability.** Making use of stable cell lines, a previous study identified regions of IFITM3 that strongly influenced protein stability, and accordingly, these mutants could not be used here (19). However, the use of transient transfection allowed us to identify additional domains involved in protein stability: mutants 13-18 and 37-42 in the NTD; 73-78 in TM1; and 79-84, 85-90, and 103-108 in the CIL. The behavior of mutant 13-18 ( $_{13}$ NSGGQPP $_{18}$ ) is not unexpected, as it overlaps a region that acts as a docking site for several proteins ( $_{17}$ PPNYEML $_{23}$ ): the E3 ubiquitin ligase Nedd4 (PPNY), AP2 (YEML), and the tyrosine kinase Fyn (Y) (10, 18, 51, 54, 55). Mutation of the two proline residues in mutant 13-18 may favor the association with AP2, leading to higher levels of internalization of IFITM3 (this mutant indeed displays an increased intracellular distribution) and higher levels of lysosomal degradation. Instead, the destabilizing role of mutations in the CIL is of high interest because this region is extremely conserved among members of the IFITM family, and its role in the biology of IFITM3 remains relatively less well studied than other regions.

Our results therefore suggest that the CIL plays a novel regulatory role in IFITM3 protein stability and/or trafficking that deserves further investigation.

**IFITM3 incorporation in and negative imprinting properties on HIV-1 virion particles.** Perhaps unsurprisingly for a protein composed for one-third of transmembrane regions, our analysis did not reveal a single 6-amino-acid-stretch mutation capable of excluding IFITM3 from virions. However, the comparison between IFITM3 levels in cells and in virions allowed us to appreciate that the main driver of the incorporation of mutant into virion particles seems to be their degree of expression, in agreement with similar findings obtained with endogenous IFITMs in primary macrophages undergoing spreading HIV-1 infection. Under the experimental conditions used here, differences in the localization of IFITM3 mutants did not have a major influence, in line with similar findings for IFITM1, -2, and -3, which were also equally well incorporated into virion particles despite distinct intracellular distributions (15, 16, 23, 36). Although we have extensively determined in previous studies that IFITMs copurifying with viral fractions are packaged into virions and not in exosomes in cells undergoing active virion assembly (by CD45 depletion and immunogold electron microscopy [23, 36]), it can be argued that IFITMs could in principle also be incorporated into virion particles in other cellular vesicles (for instance, CD45-negative cells).

The results obtained here allow us to determine that IFITM3 incorporation is not sufficient for its effect on virions and that the potency of the antiviral phenotype can be disconnected from the levels of IFITM3 packaging. Indeed, several mutants endowed with wild-type antiviral activities are incorporated at low to undetectable levels in virion particles, as best illustrated by the mutant 13-18, which is barely detectable in HIV-1 virion particles. However, our results do not allow us to determine whether the physical presence of IFITM3 in virion particles is absolutely necessary for the antiviral phenotype, because we have not identified a single IFITM3 mutant completely excluded from HIV-1 virions (this mutant may be impossible to obtain without disrupting most of the protein structure). Hence, two possibilities still exist to explain how IFITM3 may influence virion infectivity: either very low levels of IFITM3 are sufficient to impart a negative effect on virion infectivity or the physical presence of IFITM3 in virion particles is not important for the antiviral phenotype. At present, we favor the latter hypothesis, as it would explain not only the lack of a correlation between the antiviral activities of several IFITM3 mutants and their degree of incorporation into particles but also a previous observation from our laboratory indicating that IFITM1 can decrease the infectivity of Dugbe virus (DUGV) (a member of the *Bunyaviridae* family) without being detectably incorporated into virion particles (36). An important corollary of this hypothesis would be that IFITM3 acts on the cell during virion assembly to modify an important component of virion particles that results in the membrane fusogenicity defect.

**Relationship between antiviral phenotypes, accumulation of CD63-positive vesicles, and cholesterol.** In agreement with previous studies, we also found here that the expression of several IFITM3 mutants leads to higher CD63 and MVB contents (11, 19, 20, 38, 39, 48, 59). However, the analysis of a number of IFITM3 mutants indicated that this parameter does not correlate with antiviral activities, as, for instance, mutant 43-48 retained robust antiviral activities despite a clear inability to induce CD63 vesicle accumulation. Therefore, our analysis does not grant a direct functional relevance to this widely observed phenotype during the antiviral activities of IFITM3, although it remains possible that qualitative rather than quantitative differences in the induction of CD63-MVBs may have been missed in our analyses.

The data that we have obtained here also exclude a role of cholesterol changes in the antiviral effects of IFITM3, as we have observed no modulation of this lipid in either cells or virion particles expressing or not expressing this restriction factor using different techniques. However, cholesterol is only one of the many lipids present in membranes, and it remains possible that IFITM3 acts by affecting the homeostasis of other lipids (for instance, phospholipids) that in turn affect the behavior of membranes in a more functional manner.

**Mechanistic insights into the bimodal inhibitory activity of IFITM3.** Our analysis reveals that two regions in the NTD (spanning residues 13 to 18 and 37 to 42) are important for the antiviral effects of IFITM3 against HIV-1 during target cell protection. These regions do not play major roles in the case of influenza A virus (IAV) and dengue virus (DENV), viruses that are instead influenced by nonoverlapping regions in the NTD as well as by mutations in TM1 and the CIL (19). The fact that different viruses display distinct susceptibilities to the same IFITM3 mutant had been noted previously after comparison of IAV and DENV. If such differences exist in the case of viruses that at least share a pH-dependent mechanism to enter target cells, it is highly plausible that other portions of IFITM3 regulate HIV-1 entry, as this virus uses a pH-independent mechanism to fuse at the plasma membrane and likely also in endosomes (61). In this respect, it will be of interest to determine whether other pH-independent viruses display susceptibility to specific mutations in IFITM3 similar to that of HIV-1 or not.

In contrast to target cell protection, no exhaustive study has examined the abilities of different regions of IFITM3 to modulate virion particle infectivity, so the results that we have obtained in the case of HIV-1 cannot be directly compared to those of other studies. Our analysis highlights four modulatory regions in IFITM3: two regions in TM1 and TM2 (residues 73 to 78 and 109 to 114) that partially relieve the infectivity defect on newly produced virion particles and two in the NTD and CIL that interestingly increase it (residues 19 to 24 and 85 to 90).

At first sight, therefore, the domains involved in the two antiviral properties of IFITM3 do not overlap each other. However, when the respective activities of each mutant are normalized, an interesting link between these antiviral effects becomes more readily apparent, in that most IFITM3 mutations that alter negative imprinting concomitantly affect target cell protection albeit with slightly different magnitudes. This would therefore indicate that the antiviral activities against HIV-1 ascribed to IFITM3 may be similarly modulated by the same regions. While the decreased stability of certain IFITM3 mutants could be called into play to explain the behavior of certain mutants, on a more global scale, IFITM3 stability is not the main parameter influencing the antiviral activities.

At present, only two mutants diverge from this common trend, and at least one of them (127-132) may represent a region that differentially controls target cell protection over negative imprinting. Mutant 85-90 in the CIL represents in our view a gain-of-function mutant that interferes with the trafficking and/or incorporation of HIV-1 envelope glycoproteins into virions. Env modulation by IFITM3 remains a controversial subject (16, 23, 36, 37, 41), and it remains possible that the relative expression levels of both IFITM3 and HIV-1 Env determine whether this effect is observable or not. However, under the experimental conditions used here, IFITM3 variants exerted their antiviral effects without modulating the extent of HIV-1 Env incorporation into virions. As such, the 85-90 mutant should be considered to have a gain-of-function phenotype. How this unique activity occurs has not been further investigated here, but it is intuitive that this mechanism would affect more deeply the infectivity of newly produced virion particles rather than target cell protection.

Instead, mutant 127-132 presents wild-type behavior with respect to virion particle infectivity but is less active during target cell protection. The CTD underwent strong diversifying evolution between members of the IFITM family (30, 41, 56–58), and given that this region has been described to insert into lysosomal membranes where it is processed (1), it is possible that mutations in this domain affect more strongly their ability to sequester incoming virion particles in endolysosomal vesicles during target cell infection rather than the production of infectious virion particles.

In conclusion, the results that we have gathered here provide novel insights into the regions of IFITM3 that intervene in the production of infectious virion particles, in target cell protection, as well as in IFITM3 protein stability. More specifically, our study highlighted the role of two regions of interest supporting the need for further inves-

tigations on the role of the CIL and CTD in the stability and antiviral inhibition associated with this broad antiviral restriction factor.

## MATERIALS AND METHODS

**Cells, plasmids, antibodies, and reagents.** HEK293T and HeLaP4 cells (stably expressing the CD4/CXCR4 receptors in addition to an HIV-1-LTR- $\beta$ -galactosidase reporter cassette) were maintained in complete Dulbecco's modified Eagle's medium (DMEM) supplemented with 10% fetal calf serum (both cell lines were obtained from the Cellulon repository of SFR Biosciences in Lyon-Gerland). The different IFITM3 mutants were described previously (19). IFITM3 variants are expressed in the context of the QCXIP vector (Clontech) in the absence of any epitope tag. Double mutants were engineered in the same backbone using standard molecular biology techniques. HIV-1 virion particles were produced by transient DNA cotransfection of HEK293T cells in the presence of IFITM3, the proviral clone NL4-3, and an HIV-1-based miniviral genome bearing a self-inactivating LTR and coding for GFP (pRRL-CMV-GFP) (23, 36). This allowed us to precisely quantify the infectivity of otherwise replication-competent virion particles on the basis of a single cycle of infection. CD4- and CXCR4-encoding DNAs were obtained from the AIDS Reagent and Reference Program of the NIH. Antibodies were as follows: antitubulin (Sigma), anti-Gag/p24 (clone 183-H12-5C from the AIDS Reagents Program of the NIH), antiserum to HIV-1 gp120 (clone 288 from the AIDS Reagents Program of the NIH), anti-NTD IFITM3 (catalog number AP1153a; Abgent) or anti-IFITM3 (rabbit polyclonal) (catalog number 11714-1-AP; Proteintech), anti-CD63 (catalog number 556019; BD Biosciences), and anti-CD4 and anti-CXCR4 (catalog numbers 551980 and 551968, respectively; Becton, Dickinson). Nile Red, methyl- $\beta$ -cyclodextrin (M $\beta$ CD), and oleic acid (OA) were purchased from Sigma (catalog numbers 19123, C4555, and O1008, respectively). The 19-24 mutant did not cross-react with the anti-NTD antibody, so this mutant was quantified separately using the polyclonal anti-IFITM3 antibody mentioned above.

Quantification of the different proteins analyzed here was carried out after densitometric analysis of results obtained after WB (ImageJ software). For IFITM3 mutants expressed at low levels, quantifications were carried out on overexpressed signals. Pilot comparative experiments were carried out with digital-fluorescence-based WB quantification (Odyssey CLx imaging system; LiCor), but given the high level of concordance of the results, Odyssey quantification was not used further.

To measure the amount of cholesterol in virion-associated membranes, supernatants obtained after transient DNA transfection of HEK293T cells were divided into two aliquots and either left untreated or incubated with 1  $\mu$ g/ml of octadecyl rhodamine B chloride (R18; Invitrogen), a fluorescent lipophilic dye that intercalates linearly in membranes (62). Virions were then purified for both R18-labeled and unlabeled aliquots by ultracentrifugation through a 25% (wt/vol) sucrose cushion. The R18 fluorescence incorporated into viral membranes was quantified on a Tecan plate reader and used to normalize for cholesterol levels measured on the specular aliquot of virion particles (cholesterol/cholesteryl ester quantification kit, catalog number ab65359; Abcam). Cholesterol levels are therefore normalized here for the total amount of lipids present in each sample.

**Viral production and infection.** HIV-1 virion particles were produced by calcium phosphate DNA transfection of HEK293T cells in the presence of the different IFITM3 mutants or control DNAs with a DNA ratio of 8:4:3 for NL4-3, pRRL-CMV-GFP, and IFITM3, respectively (for a total of 15  $\mu$ g of DNA per 10-cm plate). We had previously determined that these concentrations of IFITM3 were comparable to those measured in primary dendritic cells stimulated with type I interferons. Forty-eight hours after DNA transfection, cells were lysed, supernatants were filtered through a 0.45- $\mu$ m syringe filter, and virions were then purified by ultracentrifugation at 28,000 rpm for 75 min through a 25% (wt/vol) sucrose cushion. After ultracentrifugation, the pellet was resuspended in 1  $\times$  phosphate-buffered saline (PBS) and normalized by exo-RT activity. Viral infectivity was determined 2 to 3 days after challenge of HeLaP4 cells by flow cytometry. To measure the effects of the different IFITM3 mutants on target cell protection, HEK293T cells were transiently transfected with DNAs coding for CD4 and CXCR4 along with IFITM3 mutants (ratio of 0.2:0.2:1, respectively, for a total of 1.4  $\mu$ g DNA per well of a 6-well plate). Two days after transfection, cells were used as targets for infection with WT GFP-HIV-1, prior to flow cytometry analysis 2 to 3 days afterwards.

**Confocal microscopy.** HEK293T cells were grown on 0.01% poly-L-lysine-coated coverslips and analyzed 36 h after transfection with DNAs coding for wild-type IFITM3 or mutants. For DNA transfections, Lipofectamine 2000 (Invitrogen) was used according to the manufacturer's instructions. Cells were fixed with 4% paraformaldehyde for 20 min, quenched with 50 mM NH<sub>4</sub>Cl for 10 min, and permeabilized with PBS-0.5% Triton X-100 for 5 min. After a blocking step in PBS-5% milk, cells were incubated with primary antibodies overnight, followed by incubation for 2 h with a donkey anti-rabbit IgG-Alexa Fluor 594 conjugate (catalog number A-21207; Life Technologies) and/or a donkey anti-mouse IgG-Alexa Fluor 488 conjugate (catalog number A-21202; Life Technologies). A 4',6-diamidino-2-phenylindole (DAPI)-containing mounting medium was used (Southern Biotech). Images were acquired using a spectral Zeiss LSM710 confocal microscope and analyzed with Fiji software. Where indicated, Nile Red was added during the last three 5-min washes with PBS at 0.25  $\mu$ g/ml before mounting of the coverslips (confocal microscopy) or added directly to the medium at the same concentration during the last 30 min of culture, prior to cell harvest.

**Electron microscopy.** HEK293T cells transfected as described above were fixed for 24 h in 4% paraformaldehyde (PFA) and 1% glutaraldehyde in 0.1 M phosphate buffer (pH 7.2). Samples were then washed in PBS and postfixed by incubation with 2% osmium tetroxide for 1 h. Samples were then fully dehydrated in a graded series of ethanol solutions and propylene oxide. The impregnation step was performed with a mixture (1:1) of propylene oxide-Epon resin, and the samples were then left overnight

in pure resin. Cells were then embedded in Epon resin, which was allowed to polymerize for 48 h at 60°C. Ultrathin sections (90 nm) of these blocks were obtained with an EM UC7 ultramicrotome (Leica Microsystems, Wetzlar, Germany). Sections were stained with 2% uranyl acetate and 5% lead citrate, and observations were made with a transmission electron microscope (catalog number 1011; JEOL, Tokyo, Japan).

**Host phylogenetic analyses.** Homologous sequences of the primate IFITM1 to -3 genes were retrieved from publicly available databases using NCBI tBLASTn with human IFITM1 or human IFITM3 as the query. Multiple duplication events in ancient and recent times during primate evolution make phylogenetic analyses of the IFITM1 to -3 genes in primates challenging (41). For this study, a conservative approach was used in which all sequences annotated as being noncoding (XR/NR identification) in the NCBI database were discarded so that the analysis was performed on the following sequences: 29× for IFITM1, corresponding to 24 species; 8× for nonsimian primate IFITM3, corresponding to 4 species; 10× for New World monkey IFITM3, corresponding to 4 species; and 48× for hominoid and New World monkey (*Catarrhini*) IFITM2/3, corresponding to 25 species. Amino acid sequences were aligned with Muscle. The motifs of interest were subsequently isolated and separated according to gene phylogeny. A sequence logo was then produced for each motif and each group using WebLogo3 (<http://weblogo.threeplusone.com>).

**Data availability.** All relevant data are within the paper.

#### ACKNOWLEDGMENTS

We thank the NIH AIDS Reagent Program for DNAs and antibodies. We are also indebted to the CelluloNet and PLATIM facilities of UMS3444 Biosciences Gerland. We thank all the contributors of freely available genome sequences.

Work in the laboratory of A.C. received the support of grants from the Agence Nationale de Recherche sur le Sida (ANRS), Sidaction, Finovi, and the ENS-L. L.E. is supported by the CNRS and by grants from amfAR (Mathilde Krim phase II fellowship 109140-58-RKHF), the Fondation pour la Recherche Médicale (FRM) (Projet Innovant, ING20160435028), Finovi ("recently settled scientist" grant), the ANRS (ECTZ19143), and the ANR LABEX ECOFECT (ANR-11-LABX-0048 of Université de Lyon, within the program Investissements d'Avenir [ANR-11-IDEX-0007] operated by the French National Research Agency). G.S. and A.B. were supported by the Burroughs Wellcome Investigators in the Pathogenesis of Infectious Disease Fund, the Bill and Melinda Gates Foundation, and Gilead Sciences, Inc. The funders had no role in study design, data collection and analysis, decision to publish, or preparation of the manuscript.

#### REFERENCES

- Bailey CC, Kondur HR, Huang IC, Farzan M. 2013. Interferon-induced transmembrane protein 3 is a type II transmembrane protein. *J Biol Chem* 288:32184–32193. <https://doi.org/10.1074/jbc.M113.514356>.
- Weston S, Czieso S, White IJ, Smith SE, Kellam P, Marsh M. 2014. A membrane topology model for human interferon inducible transmembrane protein 1. *PLoS One* 9:e104341. <https://doi.org/10.1371/journal.pone.0104341>.
- Friedman RL, Manly SP, McMahon M, Kerr IM, Stark GR. 1984. Transcriptional and posttranscriptional regulation of interferon-induced gene expression in human cells. *Cell* 38:745–755. [https://doi.org/10.1016/0092-8674\(84\)90270-8](https://doi.org/10.1016/0092-8674(84)90270-8).
- Farber CR, Reich A, Barnes AM, Becerra P, Rauch F, Cabral WA, Bae A, Quinlan A, Glorieux FH, Clemens TL, Marini JC. 2014. A novel IFITM5 mutation in severe atypical osteogenesis imperfecta type VI impairs osteoblast production of pigment epithelium-derived factor. *J Bone Miner Res* 29:1402–1411. <https://doi.org/10.1002/jbmr.2173>.
- Perreira JM, Chin CR, Feeley EM, Brass AL. 2013. IFITMs restrict the replication of multiple pathogenic viruses. *J Mol Biol* 425:4937–4955. <https://doi.org/10.1016/j.jmb.2013.09.024>.
- Brass AL, Huang IC, Benita Y, John SP, Krishnan MN, Feeley EM, Ryan BJ, Weyer JL, van der Weyden L, Fikrig E, Adams DJ, Xavier RJ, Farzan M, Elledge SJ. 2009. The IFITM proteins mediate cellular resistance to influenza A H1N1 virus, West Nile virus, and dengue virus. *Cell* 139:1243–1254. <https://doi.org/10.1016/j.cell.2009.12.017>.
- Schoggins JW, Wilson SJ, Panis M, Murphy MY, Jones CT, Bieniasz P, Rice CM. 2011. A diverse range of gene products are effectors of the type I interferon antiviral response. *Nature* 472:481–485. <https://doi.org/10.1038/nature09907>.
- Anafu AA, Bowen CH, Chin CR, Brass AL, Holm GH. 2013. Interferon-inducible transmembrane protein 3 (IFITM3) restricts reovirus cell entry. *J Biol Chem* 288:17261–17271. <https://doi.org/10.1074/jbc.M112.438515>.
- Everitt AR, Clare S, McDonald JU, Kane L, Harcourt K, Ahras M, Lall A, Hale C, Rodgers A, Young DB, Haque A, Billker O, Tregoning JS, Dougan G, Kellam P. 2013. Defining the range of pathogens susceptible to Ifitm3 restriction using a knockout mouse model. *PLoS One* 8:e80723. <https://doi.org/10.1371/journal.pone.0080723>.
- Everitt AR, Clare S, Pertel T, John SP, Wash RS, Smith SE, Chin CR, Feeley EM, Sims JS, Adams DJ, Wise HM, Kane L, Goulding D, Digard P, Anttila V, Baillie JK, Walsh TS, Hume DA, Palotie A, Xue Y, Colonna V, Tyler-Smith C, Dunning J, Gordon SB, GenSIS Investigators, MOSAIC Investigators, Smyth RL, Openshaw PJ, Dougan G, Brass AL, Kellam P. 2012. IFITM3 restricts the morbidity and mortality associated with influenza. *Nature* 484:519–523. <https://doi.org/10.1038/nature10921>.
- Huang IC, Bailey CC, Weyer JL, Radoshitzky SR, Becker MM, Chiang JJ, Brass AL, Ahmed AA, Chi X, Dong L, Longobardi LE, Boltz D, Kuhn JH, Elledge SJ, Bavari S, Denison MR, Choe H, Farzan M. 2011. Distinct patterns of IFITM-mediated restriction of filoviruses, SARS coronavirus, and influenza A virus. *PLoS Pathog* 7:e1001258. <https://doi.org/10.1371/journal.ppat.1001258>.
- Lu J, Pan Q, Rong L, He W, Liu SL, Liang C. 2011. The IFITM proteins inhibit HIV-1 infection. *J Virol* 85:2126–2137. <https://doi.org/10.1128/JVI.01531-10>.
- Mudhasani R, Tran JP, Retterer C, Radoshitzky SR, Kota KP, Altamura LA, Smith JM, Packard BZ, Kuhn JH, Costantino J, Garrison AR, Schmaljohn CS, Huang IC, Farzan M, Bavari S. 2013. IFITM-2 and IFITM-3 but not IFITM-1 restrict Rift Valley fever virus. *J Virol* 87:8451–8464. <https://doi.org/10.1128/JVI.03382-12>.
- Bailey CC, Huang IC, Kam C, Farzan M. 2012. Ifitm3 limits the severity of

- acute influenza in mice. *PLoS Pathog* 8:e1002909. <https://doi.org/10.1371/journal.ppat.1002909>.
15. Compton AA, Bruel T, Porrot F, Mallet A, Sachse M, Euvrard M, Liang C, Casartelli N, Schwartz O. 2014. IFITM proteins incorporated into HIV-1 virions impair viral fusion and spread. *Cell Host Microbe* 16:736–747. <https://doi.org/10.1016/j.chom.2014.11.001>.
  16. Foster TL, Wilson H, Iyer SS, Coss K, Doores K, Smith S, Kellam P, Finzi A, Borrow P, Hahn BH, Neil SJD. 2016. Resistance of transmitted founder HIV-1 to IFITM-mediated restriction. *Cell Host Microbe* 20:429–442. <https://doi.org/10.1016/j.chom.2016.08.006>.
  17. Gorman MJ, Poddar S, Farzan M, Diamond MS. 2016. The interferon-stimulated gene *Ifitm3* restricts West Nile virus infection and pathogenesis. *J Virol* 90:8212–8225. <https://doi.org/10.1128/JVI.00581-16>.
  18. Jia R, Xu F, Qian J, Yao Y, Miao C, Zheng YM, Liu SL, Guo F, Geng Y, Qiao W, Liang C. 2014. Identification of an endocytic signal essential for the antiviral action of IFITM3. *Cell Microbiol* 16:1080–1093. <https://doi.org/10.1111/cmi.12262>.
  19. John SP, Chin CR, Ferreira JM, Feeley EM, Aker AM, Savidis G, Smith SE, Elia AE, Everitt AR, Vora M, Pertel T, Elledge SJ, Kellam P, Brass AL. 2013. The CD225 domain of IFITM3 is required for both IFITM protein association and inhibition of influenza A virus and dengue virus replication. *J Virol* 87:7837–7852. <https://doi.org/10.1128/JVI.00481-13>.
  20. Muñoz-Moreno R, Cuesta-Gejijo MA, Martínez-Romero C, Barrado-Gil L, Galindo I, García-Sastre A, Alonso C. 2016. Antiviral role of IFITM proteins in African swine fever virus infection. *PLoS One* 11:e0154366. <https://doi.org/10.1371/journal.pone.0154366>.
  21. Narayana SK, Helbig KJ, McCartney EM, Eyre NS, Bull RA, Eltahla A, Lloyd AR, Beard MR. 2015. The interferon-induced transmembrane proteins, IFITM1, IFITM2, and IFITM3 inhibit hepatitis C virus entry. *J Biol Chem* 290:25946–25959. <https://doi.org/10.1074/jbc.M115.657346>.
  22. Savidis G, Ferreira JM, Portmann JM, Meraner P, Guo Z, Green S, Brass AL. 2016. The IFITMs inhibit Zika virus replication. *Cell Rep* 15:2323–2330. <https://doi.org/10.1016/j.celrep.2016.05.074>.
  23. Tartour K, Appourchaux R, Gaillard J, Nguyen XN, Durand S, Turpin J, Beaumont E, Roch E, Berger G, Mahieux R, Brand D, Roingard P, Cimarelli A. 2014. IFITM proteins are incorporated onto HIV-1 virion particles and negatively imprint their infectivity. *Retrovirology* 11:103. <https://doi.org/10.1186/s12977-014-0103-y>.
  24. Weston S, Czesio S, White IJ, Smith SE, Wash RS, Diaz-Soria C, Kellam P, Marsh M. 2016. Alphavirus restriction by IFITM proteins. *Traffic* 17:997–1013. <https://doi.org/10.1111/tra.12416>.
  25. Zhang W, Zhang L, Zan Y, Du N, Yang Y, Tien P. 2015. Human respiratory syncytial virus infection is inhibited by IFN-induced transmembrane proteins. *J Gen Virol* 96:170–182. <https://doi.org/10.1099/vir.0.066555-0>.
  26. Poddar S, Hyde JL, Gorman MJ, Farzan M, Diamond MS. 2016. The interferon-stimulated gene *IFITM3* restricts infection and pathogenesis of arthrogenic and encephalitic alphaviruses. *J Virol* 90:8780–8794. <https://doi.org/10.1128/JVI.00655-16>.
  27. Qian J, Le Duff Y, Wang Y, Pan Q, Ding S, Zheng YM, Liu SL, Liang C. 2015. Primate lentiviruses are differentially inhibited by interferon-induced transmembrane proteins. *Virology* 474:10–18. <https://doi.org/10.1016/j.virol.2014.10.015>.
  28. Warren CJ, Griffin LM, Little AS, Huang IC, Farzan M, Pyleon D. 2014. The antiviral restriction factors IFITM1, 2 and 3 do not inhibit infection of human papillomavirus, cytomegalovirus and adenovirus. *PLoS One* 9:e96579. <https://doi.org/10.1371/journal.pone.0096579>.
  29. Weidner JM, Jiang D, Pan XB, Chang J, Block TM, Guo JT. 2010. Interferon-induced cell membrane proteins, IFITM3 and tetherin, inhibit vesicular stomatitis virus infection via distinct mechanisms. *J Virol* 84:12646–12657. <https://doi.org/10.1128/JVI.01328-10>.
  30. Wilkins J, Zheng YM, Yu J, Liang C, Liu SL. 2016. Nonhuman primate IFITM proteins are potent inhibitors of HIV and SIV. *PLoS One* 11:e0156739. <https://doi.org/10.1371/journal.pone.0156739>.
  31. Wrensch F, Winkler M, Pohlmann S. 2014. IFITM proteins inhibit entry driven by the MERS-coronavirus spike protein: evidence for cholesterol-independent mechanisms. *Viruses* 6:3683–3698. <https://doi.org/10.3390/v6093683>.
  32. McMichael TM, Zhang Y, Kenney AD, Zhang L, Zani A, Lu M, Chemudupati M, Li J, Yount JS. 15 June 2018. IFITM3 restricts human metapneumovirus infection. *J Infect Dis* <https://doi.org/10.1093/infdis/jiy361>.
  33. Chesarina NM, Compton AA, McMichael TM, Kenney AD, Zhang L, Soewarna V, Davis M, Schwartz O, Yount JS. 2017. IFITM3 requires an amphipathic helix for antiviral activity. *EMBO Rep* 18:1740–1751. <https://doi.org/10.15252/embr.201744100>.
  34. Zhao X, Guo F, Liu F, Cuconati A, Chang J, Block TM, Guo JT. 2014. Interferon induction of IFITM proteins promotes infection by human coronavirus OC43. *Proc Natl Acad Sci U S A* 111:6756–6761. <https://doi.org/10.1073/pnas.1320856111>.
  35. Zhao X, Sehgal M, Hou Z, Cheng J, Shu S, Wu S, Guo F, Le Marchand SJ, Lin H, Chang J, Guo JT. 2018. Identification of residues controlling restriction versus enhancing activities of IFITM proteins on entry of human coronaviruses. *J Virol* 92:e01535-17. <https://doi.org/10.1128/JVI.01535-17>.
  36. Tartour K, Nguyen XN, Appourchaux R, Assil S, Barateau V, Bloyet LM, Burlaud Gaillard J, Confort MP, Escudero-Perez B, Gruffat H, Hong SS, Moroso M, Reynard O, Reynard S, Decembre E, Ftaich N, Rossi A, Wu N, Arnaud F, Baize S, Dreux M, Gerlier D, Paranhos-Baccala G, Volchkov V, Roingard P, Cimarelli A. 2017. Interference with the production of infectious viral particles and bimodal inhibition of replication are broadly conserved antiviral properties of IFITMs. *PLoS Pathog* 13:e1006610. <https://doi.org/10.1371/journal.ppat.1006610>.
  37. Yu J, Li M, Wilkins J, Ding S, Swartz TH, Esposito AM, Zheng YM, Freed EO, Liang C, Chen BK, Liu SL. 2015. IFITM proteins restrict HIV-1 infection by antagonizing the envelope glycoprotein. *Cell Rep* 13:145–156. <https://doi.org/10.1016/j.celrep.2015.08.055>.
  38. Feeley EM, Sims JS, John SP, Chin CR, Pertel T, Chen LM, Gaiha GD, Ryan BJ, Donis RO, Elledge SJ, Brass AL. 2011. IFITM3 inhibits influenza A virus infection by preventing cytosolic entry. *PLoS Pathog* 7:e1002337. <https://doi.org/10.1371/journal.ppat.1002337>.
  39. Amini-Bavil-Olyaei S, Choi YJ, Lee JH, Shi M, Huang IC, Farzan M, Jung JU. 2013. The antiviral effector IFITM3 disrupts intracellular cholesterol homeostasis to block viral entry. *Cell Host Microbe* 13:452–464. <https://doi.org/10.1016/j.chom.2013.03.006>.
  40. Desai TM, Marin M, Chin CR, Savidis G, Brass AL, Melikyan GB. 2014. IFITM3 restricts influenza A virus entry by blocking the formation of fusion pores following virus-endosome hemifusion. *PLoS Pathog* 10:e1004048. <https://doi.org/10.1371/journal.ppat.1004048>.
  41. Compton AA, Roy N, Porrot F, Billet A, Casartelli N, Yount JS, Liang C, Schwartz O. 2016. Natural mutations in IFITM3 modulate post-translational regulation and toggle antiviral specificity. *EMBO Rep* 17:1657–1671. <https://doi.org/10.15252/embr.201642771>.
  42. Shi G, Schwartz O, Compton AA. 2017. More than meets the I: the diverse antiviral and cellular functions of interferon-induced transmembrane proteins. *Retrovirology* 14:53. <https://doi.org/10.1186/s12977-017-0377-y>.
  43. Li K, Markosyan RM, Zheng YM, Golfetto O, Bungart B, Li M, Ding S, He Y, Liang C, Lee JC, Gratton E, Cohen FS, Liu SL. 2013. IFITM proteins restrict viral membrane hemifusion. *PLoS Pathog* 9:e1003124. <https://doi.org/10.1371/journal.ppat.1003124>.
  44. Gerlach T, Hensen L, Matrosovich T, Bergmann J, Winkler M, Peteranderl C, Klenk HD, Weber F, Herold S, Pohlmann S, Matrosovich M. 2017. pH optimum of hemagglutinin-mediated membrane fusion determines sensitivity of influenza A viruses to the interferon-induced antiviral state and IFITMs. *J Virol* 91:e00246-17. <https://doi.org/10.1128/JVI.00246-17>.
  45. Desai TM, Marin M, Mason C, Melikyan GB. 2017. pH regulation in early endosomes and interferon-inducible transmembrane proteins control avian retrovirus fusion. *J Biol Chem* 292:7817–7827. <https://doi.org/10.1074/jbc.M117.783878>.
  46. Wang Y, Pan Q, Ding S, Wang Z, Yu J, Finzi A, Liu SL, Liang C. 2017. The V3 loop of HIV-1 Env determines viral susceptibility to IFITM3 impairment of viral infectivity. *J Virol* 91:e02441-16. <https://doi.org/10.1128/JVI.02441-16>.
  47. Yu J, Liu SL. 2018. The inhibition of HIV-1 entry imposed by interferon inducible transmembrane proteins is independent of co-receptor usage. *Viruses* 10:E413. <https://doi.org/10.3390/v10080413>.
  48. Yount JS, Karssemeijer RA, Hang HC. 2012. S-palmitoylation and ubiquitination differentially regulate interferon-induced transmembrane protein 3 (IFITM3)-mediated resistance to influenza virus. *J Biol Chem* 287:19631–19641. <https://doi.org/10.1074/jbc.M112.362095>.
  49. Shan J, Zhao B, Shan Z, Nie J, Deng R, Xiong R, Tsun A, Pan W, Zhao H, Chen L, Jin Y, Qian Z, Lui K, Liang R, Li D, Sun B, Lavillette D, Xu K, Li B. 2017. Histone demethylase LSD1 restricts influenza A virus infection by erasing IFITM3-K88 monomethylation. *PLoS Pathog* 13:e1006773. <https://doi.org/10.1371/journal.ppat.1006773>.
  50. McMichael TM, Zhang L, Chemudupati M, Hach JC, Kenney AD, Hang HC, Yount JS. 2017. The palmitoyltransferase ZDHHC20 enhances interferon-induced transmembrane protein 3 (IFITM3) palmitoylation and antiviral activity. *J Biol Chem* 292:21517–21526. <https://doi.org/10.1074/jbc.M117.800482>.

51. Chesarino NM, McMichael TM, Hach JC, Yount JS. 2014. Phosphorylation of the antiviral protein interferon-inducible transmembrane protein 3 (IFITM3) dually regulates its endocytosis and ubiquitination. *J Biol Chem* 289:11986–11992. <https://doi.org/10.1074/jbc.M114.557694>.
52. Wu WL, Grotefend CR, Tsai MT, Wang YL, Radic V, Eoh H, Huang IC. 2017. Delta20 IFITM2 differentially restricts X4 and R5 HIV-1. *Proc Natl Acad Sci U S A* 114:7112–7117. <https://doi.org/10.1073/pnas.1619640114>.
53. Jia R, Ding S, Pan Q, Liu SL, Qiao W, Liang C. 2015. The C-terminal sequence of IFITM1 regulates its anti-HIV-1 activity. *PLoS One* 10:e0118794. <https://doi.org/10.1371/journal.pone.0118794>.
54. Jia R, Pan Q, Ding S, Rong L, Liu SL, Geng Y, Qiao W, Liang C. 2012. The N-terminal region of IFITM3 modulates its antiviral activity by regulating IFITM3 cellular localization. *J Virol* 86:13697–13707. <https://doi.org/10.1128/JVI.01828-12>.
55. Chesarino NM, McMichael TM, Yount JS. 2015. E3 ubiquitin ligase NEDD4 promotes influenza virus infection by decreasing levels of the antiviral protein IFITM3. *PLoS Pathog* 11:e1005095. <https://doi.org/10.1371/journal.ppat.1005095>.
56. Sällman Almén M, Bringeland N, Fredriksson R, Schiöth HB. 2012. The dispanins: a novel gene family of ancient origin that contains 14 human members. *PLoS One* 7:e31961. <https://doi.org/10.1371/journal.pone.0031961>.
57. Zhang Z, Liu J, Li M, Yang H, Zhang C. 2012. Evolutionary dynamics of the interferon-induced transmembrane gene family in vertebrates. *PLoS One* 7:e49265. <https://doi.org/10.1371/journal.pone.0049265>.
58. Hickford D, Frankenberg S, Shaw G, Renfree MB. 2012. Evolution of vertebrate interferon inducible transmembrane proteins. *BMC Genomics* 13:155. <https://doi.org/10.1186/1471-2164-13-155>.
59. Wee YS, Roundy KM, Weis JJ, Weis JH. 2012. Interferon-inducible transmembrane proteins of the innate immune response act as membrane organizers by influencing clathrin and v-ATPase localization and function. *Innate Immun* 18:834–845. <https://doi.org/10.1177/1753425912443392>.
60. Lin TY, Chin CR, Everitt AR, Clare S, Perreira JM, Savidis G, Aker AM, John SP, Sarlah D, Carreira EM, Elledge SJ, Kellam P, Brass AL. 2013. Amphotericin B increases influenza A virus infection by preventing IFITM3-mediated restriction. *Cell Rep* 5:895–908. <https://doi.org/10.1016/j.celrep.2013.10.033>.
61. Miyauchi K, Kim Y, Latinovic O, Morozov V, Melikyan GB. 2009. HIV enters cells via endocytosis and dynamin-dependent fusion with endosomes. *Cell* 137:433–444. <https://doi.org/10.1016/j.cell.2009.02.046>.
62. Mangeot PE, Dollet S, Girard M, Ciancia C, Joly S, Peschanski M, Lotteau V. 2011. Protein transfer into human cells by VSV-G-induced nanovesicles. *Mol Ther* 19:1656–1666. <https://doi.org/10.1038/mt.2011.138>.